PATCHINESS: ZOOPLANKTON BEHAVIOR IN FINESCALE VERTICAL SHEAR LAYERS

A Thesis
Presented to
The Academic Faculty

by

Aaron Conway True

In Partial Fulfillment
of the Requirements for the Degree
Master of Science in the
School of Civil and Environmental Engineering

Georgia Institute of Technology
December 2011

PATCHINESS: ZOOPLANKTON BEHAVIOR IN FINESCALE VERTICAL SHEAR LAYERS

Approved by:

Dr. Donald R. Webster, Advisor
School of Civil and Environmental Engineering
Georgia Institute of Technology

Dr. Jeannette Yen
School of Biology
Georgia Institute of Technology

Dr. Marc J. Weissburg
School of Biology
Georgia Institute of Technology

Date Approved: 14 November 2011

ACKNOWLEDGEMENTS

To my Lord and Savior Jesus Christ, the joy, strength, wisdom, and revelation you give me by your Holy Spirit are as much a part of this thesis as the work of my own hands! Thank you for true life.

To my advisor Dr. Donald R. Webster, I could not hope to find a more knowledgeable, committed, motivating, down-to-earth advisor, thank you! To my committee members, Dr. Jeannette Yen and Dr. Marc Weissburg, I admire your pure curiosity about the natural world around us, thank you for your invaluable contributions.

Ellen, you're amazing, you're gorgeous, I love you, you have vastly improved the quality of this work, I look forward to life together!

To my own flesh and blood, I love you all, thank you for instilling in me a love of life, God, and people.

To the friends too numerous to list (unfortunately), thanks for loving me and reminding me that there is, in fact, life being lived outside academia, ha ha!

To my funders, the National Science Foundation (Grant NSF-BIO OCE), you enabled this work and will ensure that the results are put to use! Thank you.

"Then he led me back to the bank of the river... And he said to me, 'This water flows toward the eastern region and goes down into the Arabah, and enters the sea; when the water flows into the sea, the water will become fresh. **And wherever the river goes, every living creature that swarms will live, and there will be very many fish**. For this water goes there, that the waters of the sea may become fresh; so everything will live where the river goes. Fishermen will stand beside the sea ... It's fish will be of very many kinds...'

$\sim$ From Ezekiel 47:6-10

TABLE OF CONTENTS

LIST OF TABLES

LIST OF FIGURES

SUMMARY

Regions containing gradients of vertical flow are often associated with sharp changes in hydrographic and biochemical water properties in coastal marine ecosystems. Often these are sites of dense plankton aggregations of critical ecological importance. This study is concerned with the behavioral response of various ecologically-important species of zooplankton to finescale gradients of vertical velocity in an effort to determine the extent to which individual behavioral responses to physical cues on the finescale ($< 1\ m$) have the potential to drive ecological processes in the coastal ocean on the submesoscale ($< 1\ km$). Extrapolating from individual behavior to population scale phenomena helps shed light on the factors regulating the spatiotemporal distribution of coastal marine ecosystem productivity. The ability to resolve and predict the spatiotemporal distribution of productivity in the highly dynamic coastal marine environment provides a crucial tool for accurately modeling and managing sustainable fisheries for generations to come.

A recirculating flume apparatus with a laminar, planar free jet (the Bickley jet) was used to create finescale gradients of fluid velocity (shear) in both upwelling and downwelling configurations for zooplankton behavioral assays. Particle image velocimetry (PIV) was used to fully resolve the velocity fields allowing us to fine-tune experimental parameters to match fluid mechanical conditions commonly measured in the field. Zooplankton behavioral assays with two tropical calanoid copepods, *Acartia negligens* and *Clausocalanus furcatus*, an estuarine mysid, *Neomysis americana*, and the larvae of an estuarine mud crab, *Panopeus herbstii*, were conducted in control (stagnant), upwelling, and downwelling flow configurations. Finally, statistical

analyses (ANOVA) of individual zooplankton trajectories revealed the potential for individual behavioral responses to persistent finescale vertical shear layers to produce population scale aggregations, which is proposed here as a mechanism of patchiness in coastal marine ecosystems.

Results from behavioral analyses reveal species-specific threshold shear strain rates that trigger individual behavioral responses. Furthermore, results show statistically significant changes in behavior (relative swimming speed, turn frequency, heading) for all species tested in response to a coherent shear structure in the form of finescale upwelling and downwelling jets. The results show that changes in individual behavior can increase Proportional Residence Time (PRT = percent time spent in the jet structure). On a population scale, the increase in PRT can lead to dense aggregations around persistent flow features, which is consistent with numerous field studies. These dense, patchy aggregations of zooplankton have profound trickle-up ecological consequences in coastal marine ecosystems.

In summary, the results of this study indicate that shear-triggered depth-keeping behavior and aggregation around persistent vertical flow structures by individual zooplankters is likely a ubiquitous behavior among the zooplankton. These behaviors, at a variety of spatiotemporal scales and for a variety of ecological reasons, may act as mechanisms which produce considerable patchiness both vertically (by depth-keeping behavior) and horizontally (by aggregation around frontal features) in estuarine and coastal marine ecosystems. It is likely that gradients of vertical velocity may act as an initial mechanosensory cue for zooplankters to optimize habitat partitioning and locate high-density food, nutrient, and mate patches.

CHAPTER I

INTRODUCTION

The patchy nature of primary and secondary productivity in coastal marine ecosystems has been well known and documented for the past 50 years. From the ocean basin scale ($\sim 10,000\ km$) to the viscous damping range ($\sim 1\ mm$), physical forcing and individual plankton behavior synergize to produce spatially and temporally coherent regions of extreme productivity engulfed in a vast marine desert, which is commonly referred to as *patchiness*. Coral reefs have a unique ability to retain high concentrations of phytoplankton, zooplankton and nutrients (Yahel et al. 1998) as oases of intense diversity, productivity, and dynamism (Odum and Odum 1955) in the marine landscape. Similarly, oceanographic fronts have long been known as ecological hotspots of enhanced productivity, with cascading ecological effects (Largier 1993). Finally, recent advances in acoustic and optical instrumentation have revealed vertically-thin, high-density plankton layers which are most often associated with hydrographic structure (pycnocline, thermocline, etc.), dubbed *thin layers* (Cowles et al. 1993, Dekshenieks et al. 2001, McManus et al. 2003). In all cases, it is the unique coupling of physical forcing and individual plankton behavior across vast spatiotemporal scales that interact to create highly patchy plankton distributions and govern spatiotemporal productivity dynamics. Patchiness in coastal marine ecosystems has profound ecological consequences, and thus quantifying basic mechanisms that have the potential to generate patchiness is fundamental to modeling and managing marine fishery resources.

Biophysical coupling refers generically to the coupling of biological (and/or related chemical) effects and physical forcing that produces patchiness across a wide range

of spatial scales in coastal marine ecosystems. Physical forcing mechanisms may include turbulent mixing, stratification, pycnocline/thermocline dynamics, internal wave processes, free shear flows, mesoscale currents, Langmuir circulation, and upwelling dynamics. Similarly, biological and chemical mechanisms at work may include differential phytoplankton growth and zooplankton grazing, ontogenetic and diel vertical migrations, passive settling of phytoplankton along isopycnals, cue sensing, and foraging behavior among zooplankton. Quantifying the individual and interactive effects of the various physical and biochemical factors at work at the *correct spatial and temporal scales* is fundamentally important to accurately assessing the full ecological implications of patchy productivity.

Major advances in acoustic and optical instrumentation in the past 15 years (Cowles et al. 1998, Holliday et al. 1998, Jaffe et al. 1998, Holliday et al. 2003) have greatly increased our ability to detect, observe, and resolve patchy productivity *in situ*. This has enabled laboratory investigations to isolate possible mechanisms of patchiness and quantify their effects on plankton behavior. With care, these results can be accurately scaled and extrapolated to the ecosystem-level with relevance, specifically through the linkage of finescale ($< 1\ m$) individual behavioral processes and submesoscale (10s to 100s m) forcing mechanisms that underlay the spatiotemporal distribution of marine fishery productivity (Figure 1.1).

The present study has employed various tools from experimental fluid mechanics to build a fully-resolved laboratory model of a finescale upwelling/downwelling jet (vertical shear layer). Behavioral assays have allowed us to quantify the effect of persistent shear layers, common features in coastal marine ecosystems, on zooplankton behavior. Results indicate this is likely a mechanism of patchiness *in situ*.

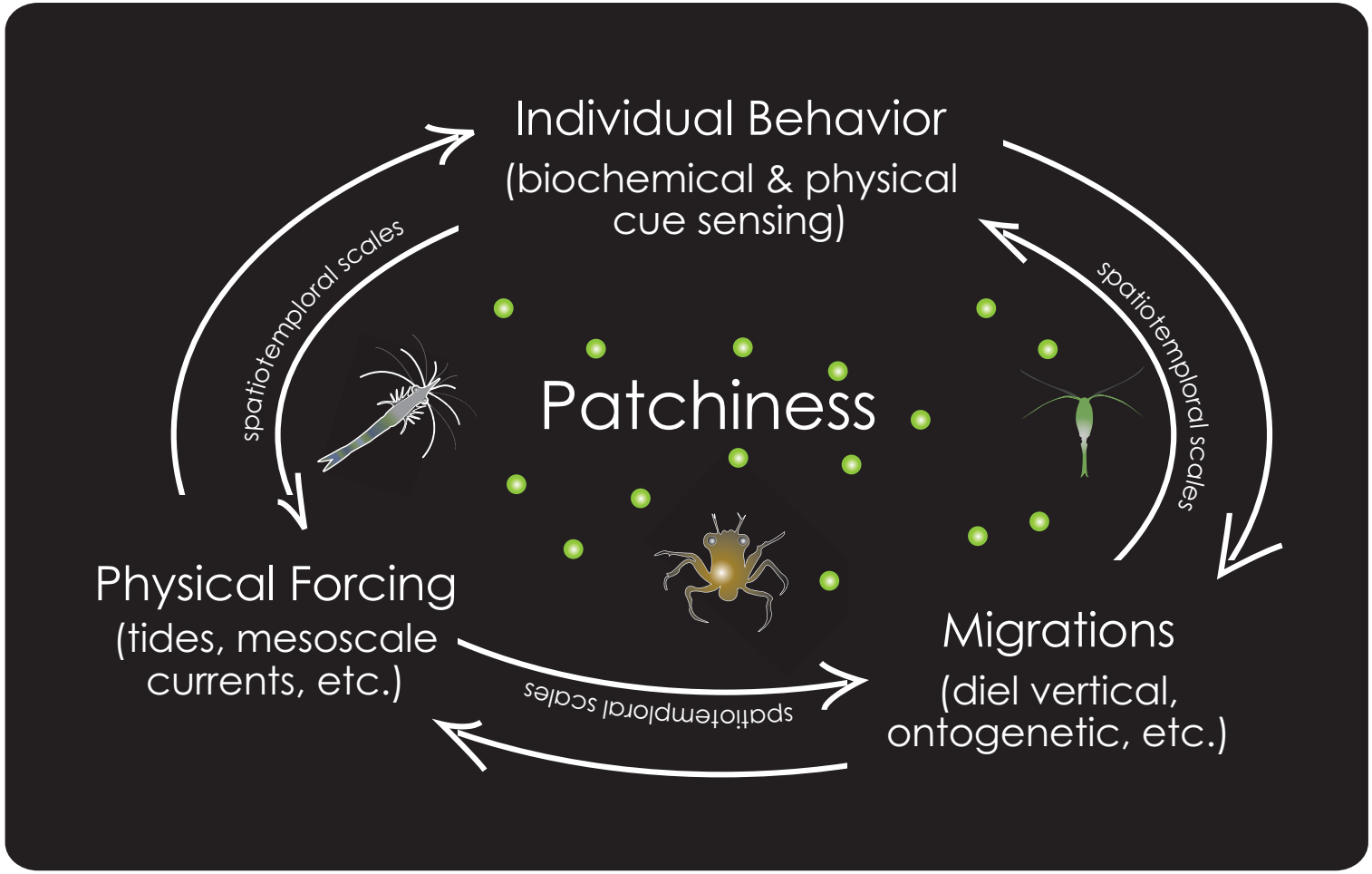

Figure 1.1: Biophysical Mechanisms of Patchiness

CHAPTER II

LITERATURE REVIEW

The present study is concerned with the behavioral response of various species of zooplankton to finescale gradients of vertical velocity in an effort to determine the extent to which individual behavioral responses to physical cues on the finescale ($< 1\ m$) have the potential to drive ecological processes in the coastal ocean on the submesoscale ($< 1\ km$). Extrapolating from individual behavior to population scale phenomena will ultimately shed light on the factors regulating the spatiotemporal distribution of coastal marine productivity. The ability to resolve and predict the spatiotemporal distribution of productivity in the highly dynamic coastal marine environment provides a crucial tool for accurately modeling and managing sustainable fisheries for generations to come.

Thus, the topics reviewed here are chosen to provide the necessary physical and biological background as well as the relevant ecological context: patchiness in coastal marine ecosystems, zooplankton sensory ecology, and some useful concepts from fluid mechanics.

2.1 A Case Study in Patchiness: Thin Layers

Thin layers are one of the most ecologically significant and research-inspiring subjects that have risen out of the interdisciplinary study of oceanographic processes in the past 15 years. The term *thin layer* in the context of biological and physical oceanography is more or less synonymous with biophysical coupling and has come to be defined as spatially coherent plankton patches (marine snow, bacteria, phytoplankton, zooplankton, icthyoplankton) in which biomass can be several orders of magnitude greater than the water column immediately above or below the layer. Thin

layers range in thickness from a few centimeters to a few meters vertically, span up to square kilometers horizontally, and can persist for days. Thin layers most often correspond with structure in the ocean associated with vertical gradients of physical, chemical and biological properties in the water column (Dekshenieks et al. 2001). They are a widespread phenomenon occurring in virtually all marine environments where conditions are favorable including fjords, river mouths, continental shelves, and shelf basins (McManus et al. 2003). The extremely dense aggregation of biomass in thin layers has profound implications on the health and vitality of marine ecosystems, specifically through its linkage of fine scale ($< 1\ m$) individual behavioral processes and submesoscale (10s to 100s m) processes that underlay the spatiotemporal distribution of marine fishery productivity. The coupling of biochemical effects and physical forcing that drives thin layer dynamics are qualitatively applicable to many other regions of patchy productivity, from coral reefs to estuarine fronts to classical upwelling systems.

Major advances in acoustic and optical instrumentation in the past 15 years (Cowles et al. 1998, Holliday et al. 1998, Jaffe et al. 1998, Holliday et al. 2003) have greatly increased our ability to detect, observe, and resolve thin layer structures *in situ*. Quantifying the various convergent and divergent processes driving thin layer dynamics will help to ultimately evaluate the full ecological importance of these marine oases.

2.1.1 Formation, Maintenance, and Dispersion

In order to quantify thin layer dynamics, it is helpful to apply a control volume approach when considering the physical, chemical, and biological factors that regulate the formation, maintenance, and dissipation of thin layers. In general, these factors can be considered convergent (they encourage layer formation) or divergent (they

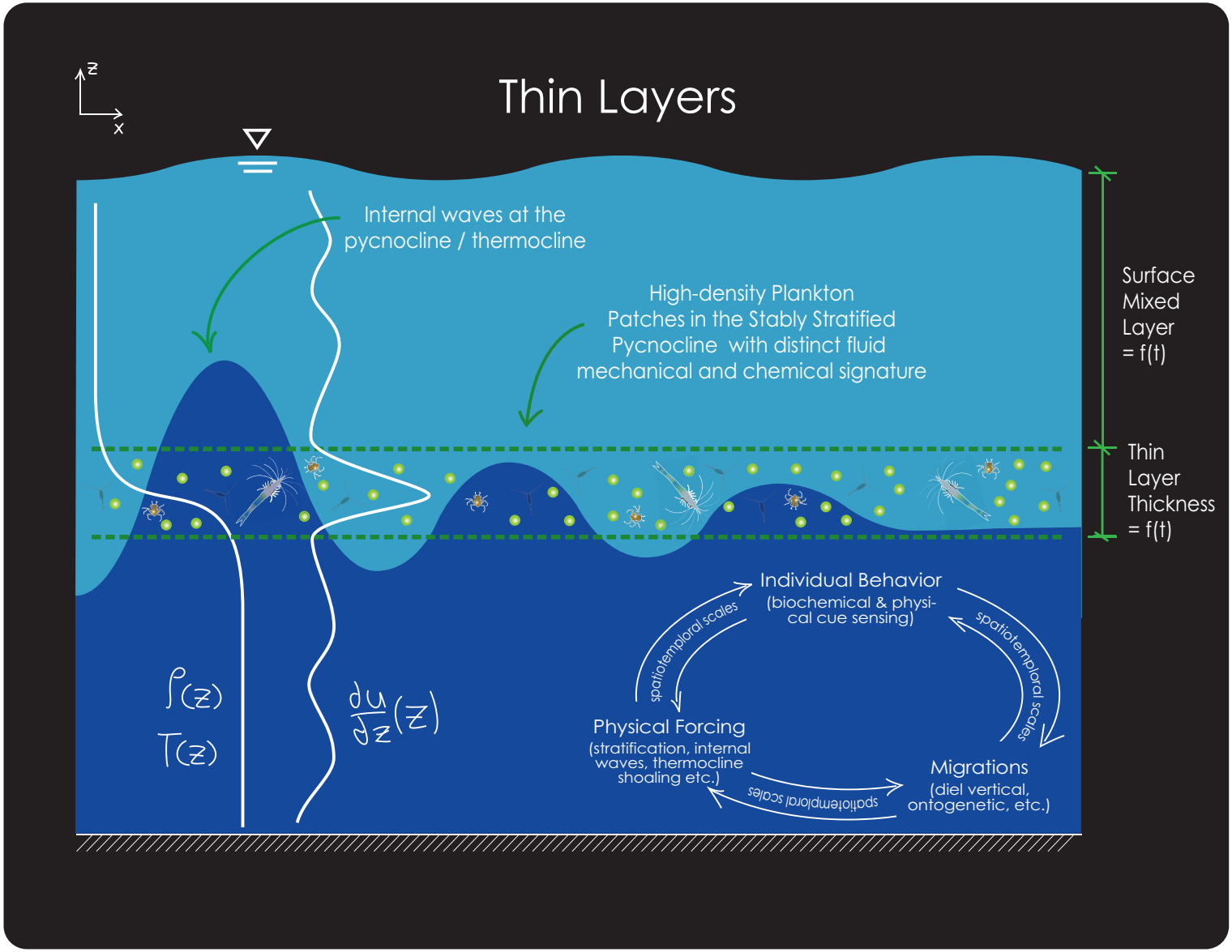

Figure 2.1: Thin Layers: Biophysical Coupling in the Production of High-density Plankton Patches

encourage dispersion), and conditions are considered favorable for thin layer development if the convergent mechanisms outweigh the divergent mechanisms (Sullivan et al. 2010, McManus et al. 2003, Stacey et al. 2007). Similarly, thin layers will be maintained when convergence and divergence are in balance, and they can be either locally or entirely dispersed when divergence outweighs convergence (Birch et al. 2008, Stacey et al. 2007).

Generally speaking, physical processes (vertical shear, turbulent mixing, stratification, internal wave packets) set the stage for the formation of thin layers, and biological and chemical processes (passive settling of phytoplankton along isopycnals, active migration and swimming behavior, behavioral responses to chemical and physical cues, foraging) are increasingly seen as the regulators of maintenance and dispersion. For these reasons and considering that thin layers almost without exception form in the pycnocline (Dekshenieks et al. 2001, McManus et al. 2003), the Richardson number has arisen as a baseline indicator of whether thin layer formation is feasible or not given the present *in situ* hydrographic conditions. The Richardson number, Ri, is defined as follows:

$$Ri = \frac{N^2}{\left(\frac{\partial u}{\partial z}\right)^2} \tag{2.1}$$

where the Brunt-Väisälä or buoyancy frequency, N, is defined as:

$$N = \sqrt{-\frac{g}{\rho_o}\frac{\partial \rho}{\partial z}} \tag{2.2}$$

Ri represents the ratio of the stabilizing effect of vertical density stratification characterized by N to the destabilizing effect of vertical shear (Kundu and Cohen 2004). Field studies indicate that thin layers do not exist when Ri is less than 0.25 (Dekshenieks et al. 2001, Velo-Suarez et al. 2010). Somewhat unsurprisingly, the critical value of the Richardson number for a continuously stratified flow with vertical shear as derived from the normal modes linear stability analysis is 0.25 (Drazin and

Reid 1981). Thus, we see close biophysical coupling in the necessity of turbulent mixing to be suppressed and stratification maintained ($Ri > 0.25$) to promote thin layer formation.

Various convergence mechanisms can act in concert to encourage the formation of a thin layer when the Richardson number criteria for the formation of a thin layer ($Ri > 0.25$) is met. For a comprehensive overview of proposed thin layer formation mechanisms summarized below, see Cheriton et al. (Cheriton et al. 2009). Several authors have highlighted the importance of the ability of phytoplankton to self-regulate buoyancy and thus maintain vertical position along a given isopycnal in the formation of thin layers (Derenbach et al. 1979, Franks 1992, Alldredge et al. 2002). Additionally, various mechanisms that generate vertical shear such as current jets, the passage of internal waves, and horizontal intrusions can act to vertically compress and thin an existing plankton layer (Franks 1995, Ryan et al. 2008). More recently, Durham et al. (Durham et al. 2009) proposed a biophysical mechanism by which the combination of phytoplankton motility and vertical shear can trigger thin layer formation in what they termed *gyrotactic trapping*. A major biophysical/biochemical mechanism important in thin layer formation is motile plankton actively aggregating in response to physical and chemical cues in the ecological context of foraging, mate-seeking, and predator-avoidance (Leising 2001, Dekshenieks et al. 2001, McManus et al. 2003, Woodson et al. 2005, Woodson et al. 2007, Benoit-Bird et al. 2010, Moline et al. 2010). Finally, purely biological mechanisms such as *in situ* phytoplankton blooms, differential grazing, and swimming behavior can also play important roles in thin layer formation (Cowles et al. 1998, Alldredge et al. 2002, Holliday et al. 2003).

Once a thin layer is formed, a complex balance between the competing convergent and divergent physical, biological, and chemical processes plays out across a wide range of spatiotemporal scales. Gallager et al. (Gallager et al. 2004) found that plankton aggregations were sustained only when the Motility Number ($Mn =$

U_{swim}/U_{rms} = plankton swimming speed / RMS of turbulent velocity fluctuations) was greater than 3, which essentially shows that plankton swimming behavior must dominate physical forcing for thin layers to be maintained. Similarly, Steinbuck et al. (Steinbuck et al. 2009) found that high dinoflagellate swimming speed was required to overcome the effects of turbulent mixing during thin layer formation, but once the layer was formed reduced swimming speed was required for layer maintenance. Benoit-bird et al. (Benoit-Bird et al. 2009, Benoit-Bird et al. 2010) showed the importance of predation on shaping thin layer thickness, edge shape, and intensity. Finally, Cheriton et al. (Cheriton et al. 2009) document the importance of internal wave propagation in the convergence (thinning) and divergence (thickening) of an existing thin layer structure. Thus, it is clear that biophysical interactions in thin layer maintenance are complex and diverse, and a holistic understanding of these internal linkages can only be gained through systematic laboratory studies that isolate and quantify the effects of various interactions over the correct spatial and temporal scales.

Organism behavior and turbulent mixing act together to dissipate a thin layer structure at some point. Shoaling and vertical displacement of the thermocline/pycnocline, animal migration out of the layer, turbulent mixing, and intense predation can bring about the end of a thin layer structure. Additionally, large scale changes in water column shear and stratification, as well as smaller scale events such as the passage of internal wave packets can act to partially or entirely dissipate a thin layer (Sullivan et al. 2010). Various modeling studies have sought to quantify the dynamic balance between convergent and divergent mechanisms (Stacey et al. 2007, Birch et al. 2008).

In summary, formation, persistence, and dispersion of thin layers lie at the intersection of physical forcing and plankton behavioral responses to discontinuities in the water column associated with physical and chemical gradients. High-resolution, biologically-physically coupled field studies documenting various aspects of thin layer

structures *in situ* abound in the literature (Derenbach et al. 1979, Cowles et al. 1998, Dekshenieks et al. 2001, McManus et al. 2003, Sutor et al. 2005, Cheriton et al. 2007, Cheriton et al. 2009, Benoit-Bird et al. 2009, Moline et al. 2010), and have highlighted the importance of understanding the correct biological (growth, predation, cue sensing, foraging, etc.) and physical (thermocline and pycnocline dynamics, internal waves, vertical shear, turbulent mixing) mechanisms at the *correct spatial and temporal scales*. However, there is still a decided lack of well-designed laboratory studies that have the potential to extrapolate the ecological implications of thin layer phenomena to the fisheries scale.

2.1.2 Ecological Implications

Well-designed laboratory studies isolate various biological and physical factors important in thin layer dynamics and quantify the potential of these effects to ripple up through the trophic system. Quantifying zooplankton behavioral responses to individual and combined factors such as velocity gradients (shear strain rate), density gradients (salinity, temperature), and chemical gradients (phytoplankton, chemical exudates, etc.) typical of *in situ* conditions is undoubtedly fundamental to our understanding of thin layer dynamics. This information provides the crucial connection between individual behavioral processes and ecological processes on the submesoscale, which drive marine ecosystem productivity. A few key studies, which have highlighted the ecological importance of thin layer dynamics, are considered below.

Early work by Tiselius (Tiselius 1992) utilized weak density stratification to create finescale patches of a diatom, *Thalassiosira weissflogii*, and to assess behavioral responses of a calanoid copepod, *Acartia tonsa*. He found that *A. tonsa* can utilize density differences and/or phytoplankton chemical exudates to perform area-restricted searches and remain in the high density phytoplankton patch.

Bochdansky and Bollens (Bochdansky and Bollens 2004) investigated changes in

the spatial distribution and physiological processes of the calanoid copepod *Acartia hudsonica* in response to differing spatial and temporal distributions of a thin layer of the diatom *Skeletonema costatum*. The study found that the distribution of copepods showed a significant, but ephemeral change in response to thin diatom layers. The copepods, given a choice, will preferentially swim through the layer of diatoms rather than around. Also, the thin layer significantly influenced the depth at which the copepods were distributed. The authors note that the aggregative force of the thin layers on the copepods could be the result of an area-restricted search strategy where the copepods increase their turn angles and decrease their hop size to maintain their position in the food patch, which is consistent with previous research (Tiselius 1992). These experimental results further established that copepod behavioral responses toward food patchiness are species-, food type-, and feeding history-dependent.

The same laboratory setup was used by Clay et al. (Clay et al. 2004) to determine if the vertical distributions of 5 and 10 day old Pacific herring (*Clupea pallasi*) larvae are affected by thin layers of highly concentrated rotifers (*Brachionus plicatilis*) and density stratification. They found that the peak abundance of herring larvae occurred at the thin layer when density stratification was present. This result suggests that thin layers, which by nature include a physical signature (density jump, shear strain rate, etc.), drive the vertical distribution of larvae rather than just food patches in general.

Both of the previous two studies suggested further laboratory modeling over relevant spatial and temporal scales, in which individual and combined biological, chemical, and physical cues can be presented with the resulting zooplankton behavioral responses quantified. Further laboratory studies should specifically investigate how organisms orient themselves within thin layers, specific environmental cues, and individual behavioral responses that act as mechanisms for the formation of, and the aggregation at, thin layers.

Ignoffo et al. (Ignoffo et al. 2005) examined the effect of food patches and stratification on the behavior of the rotifer *Brachionus plicatilis*. They found that the rotifers aggregated around food patches and dispersed once the patch was depleted. Furthermore, rotifers selectively chose thin layers based the type of food present and aggregated at density gradients without food presence. Again, this suggests the importance of not only biological cues (food) but physical cues in producing zooplankton aggregations, the combination of which is found in thin layers.

Perhaps the most exhaustive and quantitative thin layer laboratory study to date was conducted by Woodson et al. (Woodson et al. 2005, Woodson et al. 2007). Using a laminar planar jet in a recirculating flume, the behavioral effects of isolated and combined velocity and density gradients, and thin layers of phytoplankton (cells and/or metabolic exudates) were quantified for two calanoid copepods, *Acartia tonsa* and *Temora longicornis*. Copepods were exposed to both isolated and combined cues and the behavioral responses of the copepods to each treatment scenario were quantified in terms of relative swimming speed and turn frequency pre- and post-contact with the treatment layer, as well as proportional residence time (PRT = time spent in the treatment layer / total time of observation). In both species, sharp density gradients acted as barriers to vertical migration. Additionally, they found that both species increased swimming speed and turn frequency for the velocity gradient and chemical exudate treatments in order to remain in the thin layer, thus increasing PRT. The presence of chemicals (cells or exudates) was shown to enhance the behavioral response induced by the velocity gradient alone. These results are consistent with an excited area-restricted search mechanism found in previous studies (e.g., Tiselius 1992). Thus, a cue hierarchy can be established where velocity gradients act as an initial cue for decreasing search area, and additional cues such as chemical exudates increase the aggregative effect. The fully quantified, interactive effects of various physical and biological cues in this study on a species-specific basis make

it particularly useful in understanding the complex biophysical interactions in thin layers, and in extrapolating these results to the ecosystem level with relevance.

In summary, it is the unique combination of biochemical gradients and physical structure in thin layers that combine to produce these high-biomass drivers of coastal marine productivity. Individual organisms exploiting the highly concentrated, coincident sensory information can produce population scale aggregations with profound trickle up trophic consequences.

2.2 Zooplankton Life History, Morphology, and Sensory Ecology

Zooplankton, like all plankton, live in an aquatic environment in which their primary goals are three-fold: to eat, to not be eaten, and to reproduce, each being mediated by fluid mechanical and chemical sensory cues. Thus, the ability of an organism to detect and respond to the highly dynamic transport of momentum, heat, and chemicals in the ocean over various spatial and temporal scales will dictate the life success of that organism.

The aim of the present study is to quantify behavioral responses of a diverse group of zooplankters to a single physical sensory cue (shear strain rate) in the form of ecologically-relevant gradients of vertical flow. Thus, the subjects reviewed in this section give a brief overview of zooplankton mechanosensing, as well as a few illustrative examples in the zooplankton. Finally, the life histories and morphology of each animal from the present study, two calanoid copepods, a mysid shrimp, and a mud crab larvae, will be considered before special attention is given to the sensory ecology; that is, what is known about the way that these organisms gather and respond to physical (fluid mechanical) cues in their marine environments.

2.2.1 Mechanosensing: The Velocity Gradient Tensor

There are multiple fluid mechanical cues a zooplankter could sense in any flow field, namely acceleration, vorticity, and deformation (e.g. Kundu and Cohen 2004). A general three-dimensional velocity gradient, $\partial u_i/\partial x_j$, can be decomposed into rotational and irrotational components, the strain rate tensor, e_{ij}, and the rotation tensor, r_{ij}, where i and j are the three coordinate directions, as:

$$\frac{\partial u_i}{\partial x_j} = e_{ij} + \frac{1}{2} r_{ij} \tag{2.3}$$

with the strain rate tensor given as

$$e_{ij} = \frac{1}{2}\left(\frac{\partial u_i}{\partial x_j} + \frac{\partial u_j}{\partial x_i}\right) = \begin{vmatrix} \frac{\partial u_1}{\partial x_1} & \frac{1}{2}\left(\frac{\partial u_2}{\partial x_1} + \frac{\partial u_1}{\partial x_2}\right) & \frac{1}{2}\left(\frac{\partial u_3}{\partial x_1} + \frac{\partial u_1}{\partial x_3}\right) \\ \frac{1}{2}\left(\frac{\partial u_2}{\partial x_1} + \frac{\partial u_1}{\partial x_2}\right) & \frac{\partial u_2}{\partial x_2} & \frac{1}{2}\left(\frac{\partial u_3}{\partial x_2} + \frac{\partial u_2}{\partial x_3}\right) \\ \frac{1}{2}\left(\frac{\partial u_3}{\partial x_1} + \frac{\partial u_1}{\partial x_3}\right) & \frac{1}{2}\left(\frac{\partial u_3}{\partial x_2} + \frac{\partial u_2}{\partial x_3}\right) & \frac{\partial u_3}{\partial x_3} \end{vmatrix} \tag{2.4}$$

and the rotation tensor given as

$$r_{ij} = \frac{\partial u_i}{\partial x_j} - \frac{\partial u_j}{\partial x_i} = -\varepsilon_{ijk}\omega_k = \begin{vmatrix} 0 & -\left(\frac{\partial u_2}{\partial x_1} - \frac{\partial u_1}{\partial x_2}\right) & -\left(\frac{\partial u_3}{\partial x_1} - \frac{\partial u_1}{\partial x_3}\right) \\ \left(\frac{\partial u_2}{\partial x_1} - \frac{\partial u_1}{\partial x_2}\right) & 0 & -\left(\frac{\partial u_3}{\partial x_2} - \frac{\partial u_2}{\partial x_3}\right) \\ \left(\frac{\partial u_3}{\partial x_1} - \frac{\partial u_1}{\partial x_3}\right) & \left(\frac{\partial u_3}{\partial x_2} - \frac{\partial u_2}{\partial x_3}\right) & 0 \end{vmatrix} \tag{2.5}$$

The strain rate tensor can be thought of as the relative velocity due to pure deformation and can itself be decomposed into the normal strain rate terms (diagonal terms) and the shear strain rate terms (twice the off-diagonal terms). The rotation tensor can be thought of as the relative velocity due to fluid rotation, which can be succinctly described by the vorticity vector ω_k as in Equation 2.5. Thus, any three-dimensional velocity field can be thought of as the superposition of rotational and

deformational flow components, and the ability of a zooplankter to distinguish between flow components allows it to distinguish say the suction force from a predator (Holzman and Wainwright 2009) versus the fluid mechanical signature of a phytoplankton cell entrained in its own feeding current (Strickler and Balazsi 2007). The type of flow component most important in triggering behavioral responses in various zooplankton species is an important piece of quantitative data that allows for the coupling of hydrodynamically-characterized environments and individual and population scale zooplankton behavior.

Copepods, and many crustacean zooplankton, are able to sense spatial gradients of flow via an array of mechanosensory hairs, or setae, which are located along the entire body but are most highly concentrated on the antennules (Yen et al. 1992, Fields et al. 2002) (see Figure 2.2). Bending or deformation of setae caused by fluid flow relative to the body generates neural signals, providing the bridge between hydromechanical signal and behavioral response (Fields et al. 2002). Thus, for a copepod to gain useful information about the hydrodynamic environment around it there must be relative fluid motion around the copepod (i.e. it cannot be simply passively advected in uniform flow). The morphological similarities between calanoid copepods and other crustacean zooplankton, such as decapod crab larvae and mysids, as well as the overwhelming circumstantial evidence in the literature, make a strong case for the generalization of *qualitative* findings from the copepod mechanosensory literature to other crustacean zooplankton.

Early work by Yen et al. (Yen et al. 1992) laid the foundation for quantifying the effects of fluid mechanical cues on zooplankton behavior. The calanoid copepods *Labidocera madurae* and *Acartia fossae* were exposed to controlled mechanical stimuli via a waveform generator. Via monitoring neural activity, both copepods were found to be extremely sensitive to small displacements and sensitivity increased with

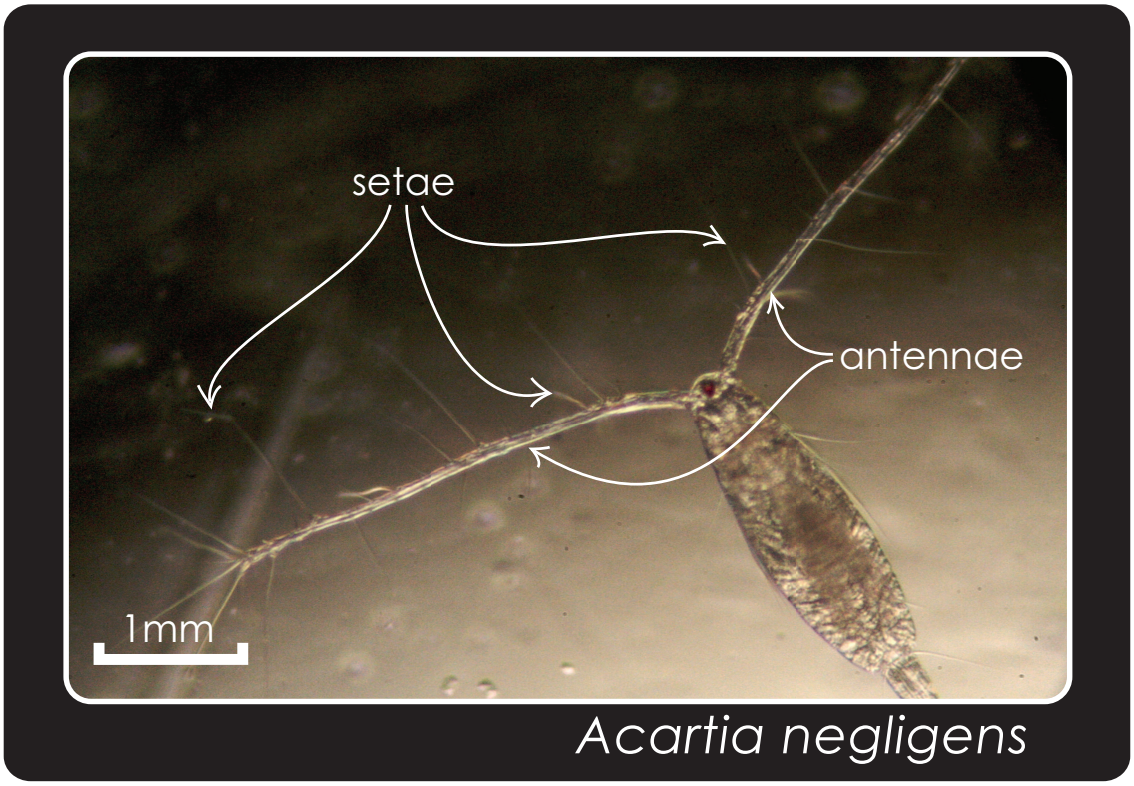

Figure 2.2: Mechanosensitive Setae Distributed Along the Anntennae of *Acartia negligens*

increasing stimuli frequency. Displacements as small as 10 nm and displacement velocities as small as 20 $\mu m/s$ were enough to trigger neural responses. They concluded that copepod setae may be explicit velocity sensors, they are capable of sensing closely spaced stimuli, responses are dependent upon stimuli frequency and duration, and receptors can supply directional information. Since this foundational study, much effort has gone into understanding the bridge between neural and behavioral thresholds as well as identifying the most behaviorally important fluid mechanical cue.

In detailed experiments by Kiørboe et al. (Kiørboe and Visser 1999, Kiørboe et al. 1999), the copepod *Acartia tonsa* was systematically exposed to each isolated fluid mechanical cue (deformation rate, vorticity, and accelartion) and behavioral responses were gauged. Acceleration and vorticity were determined to be largely unimportant cues, with more intense focus warranted for the importance of deformation rate in eliciting behavioral responses from copepods. Threshold escape behavioral responses to pure deformation ranged from 1.19 to 2.49 s^{-1}. These studies largely focused the ensuing literature to investigations of the effects of threshold fluid deformation rates in eliciting escape responses. Table 2.1 summarizes quantitative threshold deformation rates that elicit copepod escape responses reported in the literature.

The threshold deformation rates reported in Table 2.1 elicit *escape* responses in copepods. Behavioral responses other than escapes have also been observed in a few studies. Strickler and Balazsi (Strickler and Balazsi 2007) found that copepods were capable of distinguishing the source of a hydrodynamic disturbance (prey, predator, mate, etc.) based on the strength of the hydrodynamic disturbance. This suggests that different types of behavioral responses to different types and magnitudes of various hydrodynamic signals are likely in the zooplankton. Manifestations of other behavioral responses to a threshold deformation rate could include increased turn frequency and swimming speed consistent with area-restricted foraging behavior. This

Table 2.1: Threshold Deformation Rates Reported for Escape Response in Various Copepod Species

Species	Threshold Deformation Rate(s^{-1})	Study
Calanus finmarchicus	0.40	Haury et al. (Haury et al. 1980)
Polyathra remata, Rotifer	2.0 – 3.1	Kirk and Gilbert (Kirk and Gilbert 1988)
Acartia hudsonica	0.80	Yen and Fields (Yen and Fields 1992)
Euchaeta rimana	2.4	Fields and Yen (Fields and Yen 1997)
Pleuromamma xiphias	4.6	Fields and Yen (Fields and Yen 1997)
Labidocera madurae	6.3	Fields and Yen (Fields and Yen 1997)
Acartia tonsa, Adult	0.38	Fields and Yen (Fields and Yen 1997)
Acartia tonsa, Nauplii	0.38	Fields and Yen (Fields and Yen 1997)
Oithona spp.	3.8	Fields and Yen (Fields and Yen 1997)
Eurytemora affinis	1.9	Viitasalo et al. (Viitasalo et al. 1998)
Acartia tonsa	1.19 – 2.49	Kiørboe et al. (Kiørboe et al. 1999)
Temora longicornis, Nauplii	2.78 – 3.96	Titelman (Titelman 2001)
Eurytemora affinis, Nauplii	1.88 – 2.65	Titelman and Kiørboe (Titelman and Kiørboe 2003)
Euterpina acuftifrons, Nauplii	1.92 – 4.25	Titelman and Kiørboe (Titelman and Kiørboe 2003)
Calanus helgolandicus, Nauplii	0.52 – 3.24	Titelman and Kiørboe (Titelman and Kiørboe 2003)
Centropages typicus, Nauplii	2.60 – 2.79	Titelman and Kiørboe (Titelman and Kiørboe 2003)

was shown by Woodson et al. (Woodson et al. 2005) with species-specific behavioral strain thresholds ranging from 0.015 - 0.06 s^{-1} for the calanoid copepods *Acartia tonsa* and *Temora longicornis*. Importantly, these threshold values are one to two orders of magnitude lower than thresholds that induce escape responses and one to two orders of magnitude higher than neural response thresholds (Yen et al. 1992).

Other important findings in the copepod mechanosensory literature have highlighted the effects of animal size and setal sensitivity (Kiørboe et al. 1999), the importance of resolving fluid signals at the *setal* location (Jiang et al. 2002), and the effects of body orientation with respect to the fluid mechanical signal (Fields 2010).

2.2.2 A Closer Look at a Few Zooplankters

A theme in the sensory ecology literature is the idea of a cue hierarchy in triggering changes in behavior (Tumlinson et al. 1993, Vet 1999). A cue hierarchy explains the relative importance of various types of sensory cues (physical and chemical) in triggering behavioral responses in relation to one another. For example, Woodson et al. (Woodson et al. 2007) found that velocity gradients (shear) act as an initial cue to restrict search area in a foraging copepod. The addition of chemical cues enhances the response and allows the copepod to hone in on a particular resource patch with greater effectiveness. The idea of a cue hierarchy is ever present in the life cycle of a zooplankter and is particularly helpful when considering zooplankton sensory ecology. The three zooplankters considered below are particularly relevant to the present study and illustrate the use of cue hierarchies in a variety of habitats as a means of adaptive life strategy.

2.2.2.1 Calanoid Copepods: Life History and Morphology

Crustaceans of the subclass Copepoda are collectively the most numerous multicellular organisms on earth, ranging in size from 0.5 - 12 *mm*. There are ten orders of

copepods with 200 families, 1650 genera, and some 11,500 known species (Mauchline 1998). Perhaps the best-known and most studied family is Calanoida, primarily pelagic marine copepods.

Calanoid copepods reproduce sexually before hatching from eggs and going through a series of larval stages that culminate in the final adult stage. Almost all calanoid copepods hatch into the first nauplius stage (NI) and molt five times into the NVI stage. Following the NVI stage, calanoids enter the initial copepodid juvenile stage (CI), which, after five more molts, results in the adult stage (CVI) (Mauchline 1998). Adult calanoid copepods have bodies that are made up of three main regions: the urosome (tail), the five-segmented metasome (body), and the cephalosome (head). Paired appendages along the body aid swimming, prey detection and capture, and mating, whereas antennae and antennules emanating from the head region are covered in mechanosensitive setae responsive to displacements on the *nm* scale (Yen et al. 1992, Mauchline 1998). Additionally, chemosensors are distributed along the cephalic appendages (Paffenhöfer 1998). Various species of calanoids can be distinguished by differences in body and appendage morphology and swimming behavior as illustrated in Figures 2.3 and 2.4.

As the largest collective of multicellular organisms on earth and direct consumers of primary producers, copepods are an integral component of the marine ecosystem and are critical in understanding the spatiotemporal distribution of productivity in the world's oceans.

2.2.2.2 Calanoid Copepod Sensory Ecology

"The Paradox of the Plankton" as proposed by G.E. Hutchinson (Hutchison 1961) asked how a number of similar species competing for similar, limited resources in an isotropic, homogeneous environment could survive. The answer is: they do not.

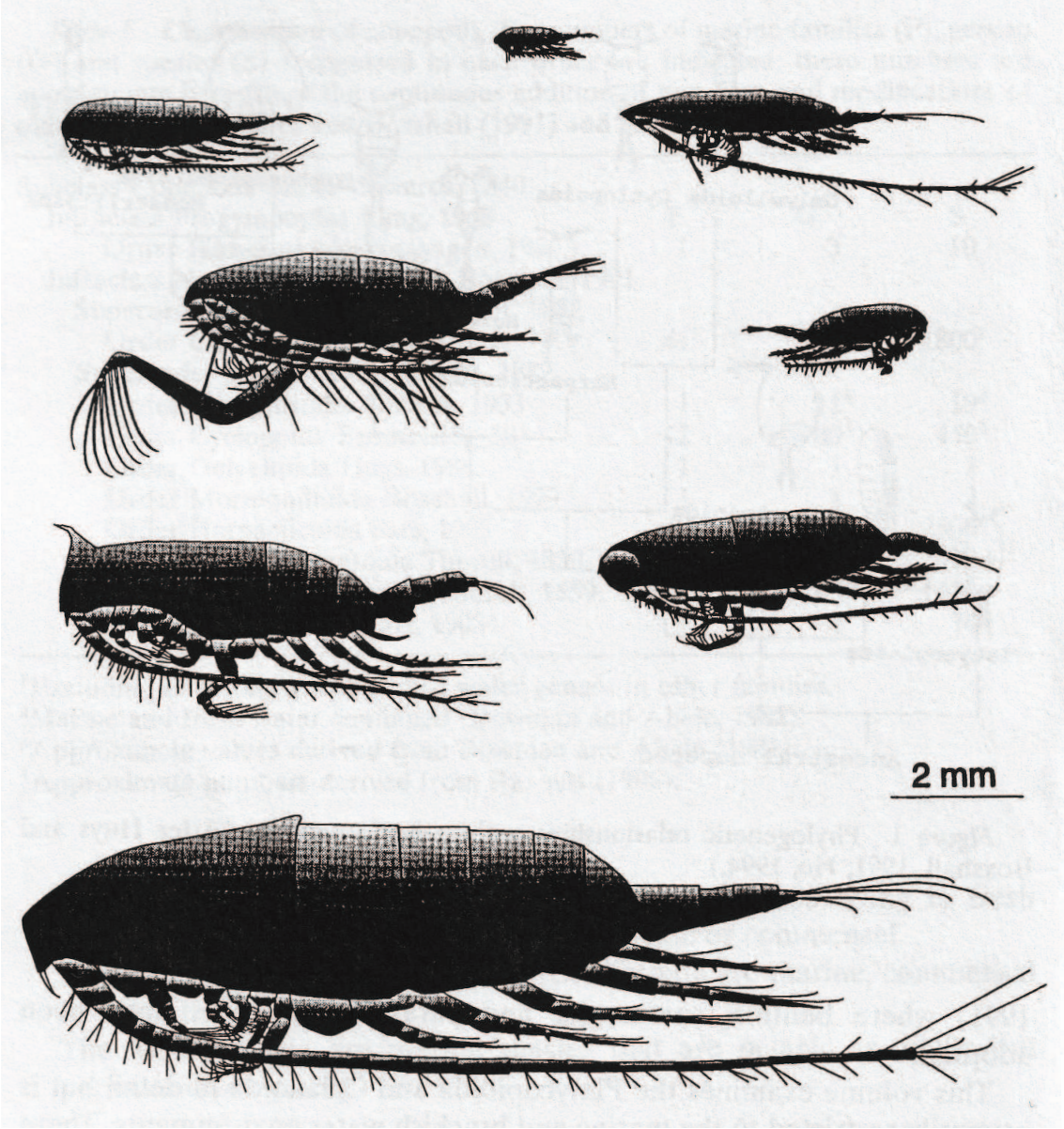

Figure 2.3: Various Calanoid Morphologies from Mauchline (Mauchline 1998)

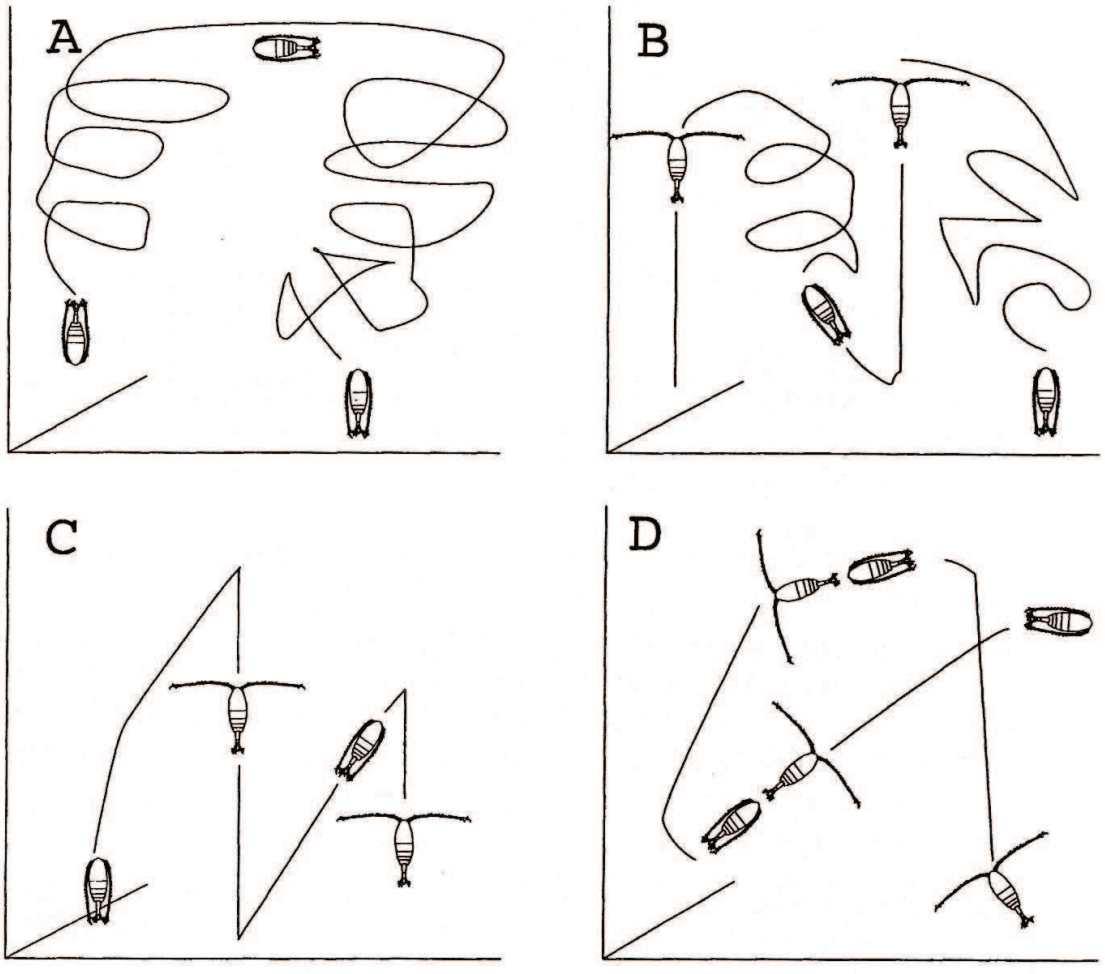

Figure 2.4: Various Calanoid Swimming Styles from Mauchline (Mauchline 1998)

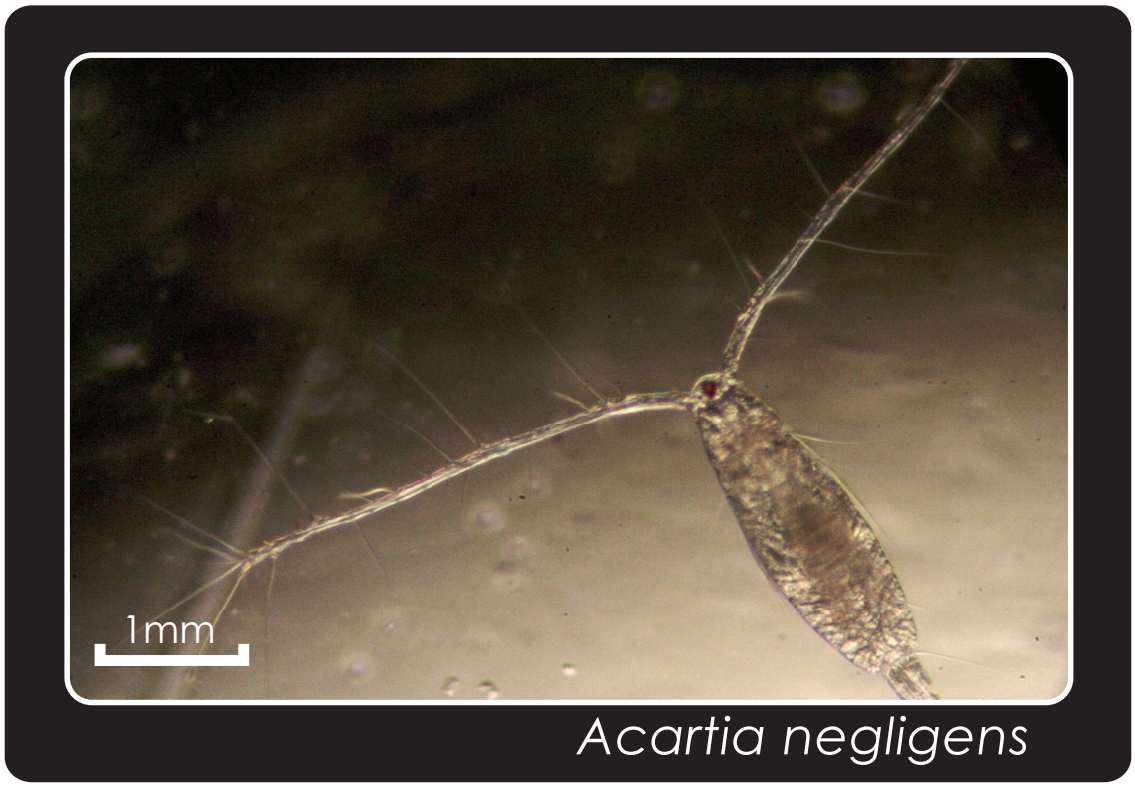

Figure 2.5: *Acartia negligens* collected in the Gulf of Aqaba, Red Sea, near Eilat, Israel (photo by Ellen True)

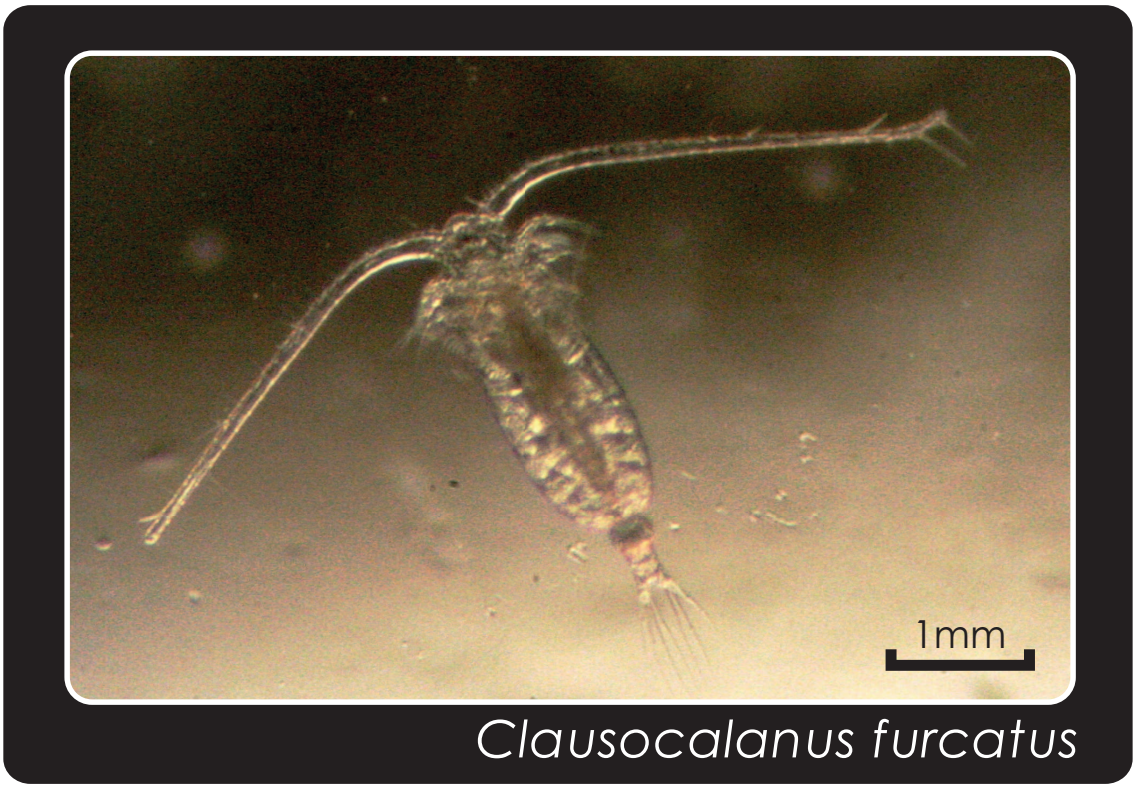

Figure 2.6: *Clausocalanus furcatus* collected in the Gulf of Aqaba, Red Sea, near Eilat, Israel (photo by Ellen True)

The environment is in fact patchy at finescales ($< 1m$), and plankton use cue hierarchies in locating isolated resource patches. For calanoid copepods, foraging and feeding behavior are driven by mechano- and chemoreception in an effort to locate resource patches. Field studies by Mullin and Brooks (Mullin and Brooks 1976) found that the copepod *Calanus pacificus* would not be able to survive in the water column except at a preferential depth with concentrated food resources. Similarly, Daro (Daro 1988) found that a dominant copepod species was food limited at most depths and that minimum concentrations necessary for survival (200 $mg\ Cm^{-3}$) were only found in one narrow depth range between 20 and 30 m. Furthermore, massive *in situ* evidence for microscale patchiness (Derenbach et al. 1979, Cowles et al. 1993, Jaffe et al. 1998) shows that often limited food resources inhibit copepod growth and thus copepods must be able to actively locate and exploit isolated resource patches in order to survive. Indeed, the idea of area-restricted search behavior (Tinbergen et al. 1967) in individuals through decreased swimming speed and increased turn frequency can often produce population-scale aggregations. Many species of copepod including *Pseudocalanus minutus* (Buskey 1984), *Temora longicornis* and *Pseudocalanus elongans* (Tiselius and Jonsson 1990), and *Acartia tonsa* (Tiselius 1992), are observed to decrease swimming speed (or hop frequency) when encountering food patches. Leising et al. (Leising et al. 2005) also note predation risks for a foraging copepod exploiting different portions of the water column, and modeling studies by Leising and Franks (Leising and Franks 2000, Leising and Franks 2002) examined the effect of food concentrations and patchiness on copepod swimming behavior and found behavior consistent with area-restricted foraging.

In addition to habitat partitioning, prey capture and predator detection and avoidance behaviors also are stimulated by a variety of chemical and fluid mechanical cues. Whereas there are many types of feeding behavior (Kiørboe 2011), one option is for copepods to set up a complex three-dimensional feeding current to entrain remote

phytoplankton cells (Malkiel et al. 2003) and sense hydrodynamic (Kiørboe and Visser 1999) and chemical (Paffenhöfer 1998) signals to accept or reject incoming particles. Fields and Yen (Fields and Yen 1997, Fields and Yen 1997) quantified threshold shear strain rate values that triggered escape responses in various calanoid copepods (Table 2.1). Viitasalo et al. (Viitasalo et al. 1998) examined the effect of predator foraging technique and copepod sensitivity in the hydrodynamic signal perception of an ensuing strike, whereas Holzman and Wainwright (Holzman and Wainwright 2009) performed a quantitative PIV analysis of suction forces and signal perception in fish feeding on copepods.

Another important behavior mediated by the generation and perception of chemical and fluid mechanical signals is reproductive and mating behaviors. Yen et al. (Yen et al. 1998) observed male calanoids tracking pheremone trails left by females. They discuss the importance of chemical and fluid mechanical signal persistence by quantifying diffusivities for the chemical cue. In fact, the low Re and low Pe regime was found to be significantly important in the success of the male in locating the female. Similarly, Bagøien and Kiørboe (Bagøien and Kiørboe 2005, Bagøien and Kiørboe 2005) observed mating behavior in two calanoid copepods. In *Acartia tonsa*, a hop-sink swimmer, mating appeared to be controlled by fluid mechanical signals as a series of 7 - 8 synchronized hops often ended in mating (Bagøien and Kiørboe 2005). On the other hand, for *Centropages typicus*, a cruiser, mating appeared to be chemically-mediated, as males were observed to accelerate and zig-zag across the females pheromone trail (Bagøien and Kiørboe 2005). Thus, individual species of copepods with different morphologies can best exploit their own sensing abilities to optimize the mating process.

Finally, habitat partitioning through diel vertical migration (DVM) and behavioral responses to fluid mechanical, chemical, and phototactic cues can have significant trophic consequences. Many calanoid copepods, like many other zooplankters,

are diel vertical migrators, i.e. they exhibit large changes in depth on a diel cycle driven by photactic cues (Enright and Hamner 1967). When vertical migratory behavior is superimposed on the physical structure of the water column and coupled with individual behavioral responses to patchy cues, population-scale, high-density aggregations can results. Early experiments by Harder (Harder 1968) on a variety of zooplankton showed that almost every species tested aggregated at salinity and/or temperature interfaces (i.e., the pycnocline). Field work by Mackas et al. (Mackas et al. 1993) showed multiple species of copepods aggregating in the layer just above the permanent halocline. Interestingly, depth-distribution was species-segregated. Bollens et al. (Bollens et al. 1994) tested the effects of a variety of mechanical, chemical, and visual cues in producing patchy aggregations of the copepod *Acartia hudsonica*. Genin et al. (Genin et al. 2005) acoustically tracked over 375,000 zooplankters over a coral reef in the Red Sea and observed active behavioral choices to swim against vertical flows and thus maintain depth that on a population scale could lead to dense aggregations. Finally, Pierson et al. (Pierson et al. 2009) documented that copepods make periodic forays into deeper waters throughout the night, suggesting a higher frequency component to classical conceptualization of DVM.

In summary, many aspects of a calanoid copepod's life are dominated by behavioral responses to hydrodynamic (Jiang et al. 2002), chemical (Poulet and Ouellet 1982), and phototactic (Bollens et al. 1994) cues. The way in which behavioral responses change when multiple cues are combined leads to the idea of a cue hierarchy and provides a basic tool for quantifying the ecological implications of individual behavior.

2.2.2.3 Mysids: Life History and Morphology

Crustaceans of the order Mysidacea are shrimp-like organisms that occur in vast numbers and diversity in the world's coastal oceans. There are 780 known species of

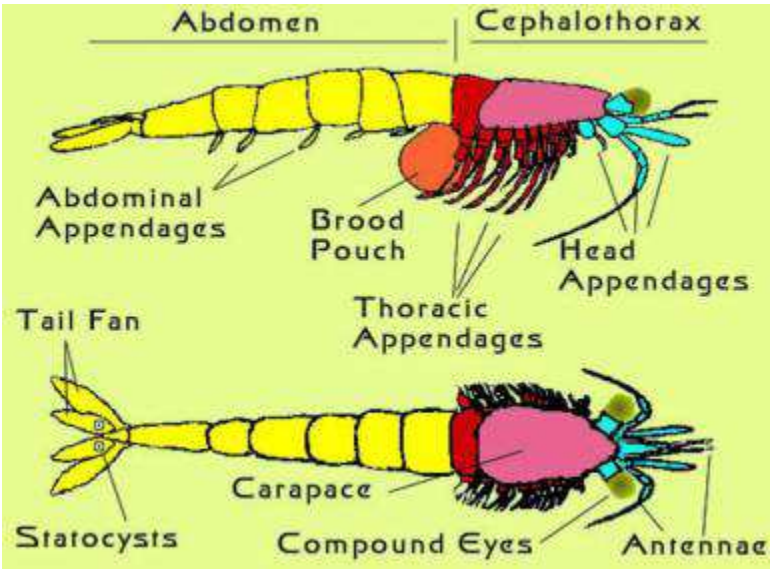

Figure 2.7: Body Morphology of a Typical Mysid Species from McLaughlin (McLaughlin 1980)

mysids, distributed among 120 genera. Individual species can be identified by differences in external morphology, such as the structure of thoracic legs, antennal scales, and other appendages, all of which are shrimp-like in morphology (Figure 2.7). They have fan-shaped tails emanating from a multi-segmented abdomen that terminates in the carapace, upon which are set two compound eyes. Thoracic appendages emanate from the abdomen, and by beating the exopodites on these appendages mysids generate both propulsion and circulation for respiration. Emanating from the head are antennules and antennae covered in mechanosensitive setae allowing mysids to skillfully navigate the dynamic estuarine environment (Clutter 1969, Mauchline 1980, McLaughlin 1980).

Statocysts on thoracic appendages can detect acceleration and joint receptors are sensitive to vibrations (Clutter 1969). Position and movement sensing setae can be divided into three classes, all of which are responsive to both tacticle and hydrodynamic stimuli: setulate sensilla, simple setae, and bifid setae and/or rake-ended setae. Deformation of setae due to qualitatively described strengths of tactile and hydrodynamic stimuli are identical, although the deformations are all characteristic of the

setal type, being manifest by increased curvature of the shaft (Crouau 1986). Lastly, the bridge between neural and behavioral responses occurs as the initial reception of a mechanical stimulus is transmitted, amplified, and transduced into an electrical signal (Crouau 1982).

The vast diversity of mysid behavior and morphology can be attributed to the wide spectrum of habitats in which various species dwell, from meso-, bathy- and epipelagic marine environments to coastal/neritic, littoral, and even freshwater/brackish environments (McLaughlin 1980).

2.2.2.4 Mysid Sensory Ecology

Neomysis americana is the most abundant mysid in the estuaries of the western Atlantic from Nova Scotia to Argentina, and serves a crucial role in estuarine and coastal trophic transfer as an emerger (Schiariti et al. 2006, Sato and Jumars 2008). Field observations by Whiteley (Whiteley 1948) show that *N. americana* lives in close proximity to the surface of the sediment (the hyperbenthos) during the day, but emerges and migrates vertically towards the water surface at night. However, a significant portion of the population is seen to remain at depth, suggesting that *N. americana* is not a true diel vertical migrator (Herman 1963). Sato and Jumars (Sato and Jumars 2008) suggest that there is a higher frequency behavioral component of its vertical migration most likely due to behavioral responses to changes in hydrographic variables (salinity, temperature, tidal flow, turbidity, etc.), which have diel, tidal and lunar rhythms that shift seasonally, resulting in a continuous vertical interchange of the population throughout the night, or a vertical spreading of the population.

It has been suggested by Abello et al. (Abello et al. 2005), and supported by Rudstam et al. (Rudstam et al. 1989), that emergence and vertical migration provide mysids with increased fitness through an opportunity to feed on metabolically-rich foods higher in the water column. Low-nutrient, organic matter-covered sediment and

Figure 2.8: *Neomysis americana* Collected in the Damariscotta River Estuary, Maine, USA (Photo by Rachel Lasley)

detritus are insufficient to sustain energy-intensive activities such as egg-production, particularly when benthic diatoms become scare in midsummer. Sato and Jumars (Sato and Jumars 2008) describe the unique and crucial role that *N. americana* plays as an emerger and vertical migrator in the estuarine environment: "Repeated, diel emergence is a vector connecting benthic and pelagic communities through bidirectional transfer of organic matter and excreted inorganic nutrients." Furthermore, as an omnivore feeding on detritus, phytoplankton, and zooplankton (Allen 1975, Pezzack and Corey 1979, Zagursky and Feller 1985) and as a crucial prey item of juvenile fishes in many estuarine spawning grounds (Williams et al. 1973), *N. americana* is a cornerstone of the estuarine trophic system.

The ability of mysids to make active behavioral responses to the physical and chemical cues around them (shear strain rate, turbidity, salinity and temperature gradients, dissolved organics and inorganics) gives them a distinct competitive advantage. In particular, sensory cues play a crucial role in position maintenance, breeding, predator avoidance, and foraging in the highly dynamic estuarine environment (Clutter 1969). Recent field studies have shown that *N. americana* aggregates around the Estuarine Transition Zone (ETZ), a region characterized by sharp gradients of salinity, temperature, and dissolved nutrients (Schiariti et al. 2006). Furthermore, horizontal pressure gradients driven by buoyancy forces associated with temperature and salinity (i.e. density) gradients set up strong recirculation zones that act as retention cells for everything from dissolved nutrients to planktivores (Winkler et al. 2007, Winkler et al. 2003). Thus, it is clear that *N. americana* actively incorporates sensory cues on the individual level, which on the population level can produce dense aggregations, swarms, schools, and shoals (Clutter 1969, Ritz 1994, Buskey 2000). Social behavior (swarming, schooling, shoaling, etc.) acting in concert with individual behavioral responses to discontinuities in the estuarine environment can produce considerable patchiness in the estuarine environment (Mauchline 1980, Ritz

1994). What is unclear, however, is the interaction among these cues and the relative importance of each in driving individual behavioral processes that manifest on the population scale.

Nonetheless, some physical and chemical cues important in regulating the spatial distribution of *N. americana* have recently begun to be documented and undoubtedly include light intensity, flood and ebb tides, temperature and salinity gradients, dissolved oxygen concentration, hydrodynamic flow fields, and hydrostatic pressure (Mauchline 1980). Light intensity appears to be an important physical parameter regulating depth, with *N. americana* showing negatively phototactic behavior towards high intensity (normal diurnal) light levels and positively phototactic behavior towards low intensity light levels (Herman 1962). Rice (Rice 1964) showed that mysids are sensitive to small changes in hydrostatic pressure. Furthermore, many species of mysid are rheotactic, that is, they orient themselves in the direction of incoming flow, with various species able to maintain position in flow velocities ranging from 12 - 40 cm/s, with avoidance behaviors shown for currents greater than these thresholds (Turner and Heubach 1966, Clutter 1969, Boroditch and Havlena 1973, Roast et al. 1998, Sato and Jumars 2008). Undoubtedly, the ability of mysids to sense gradients of velocity helps in position maintenance and avoidance of tidal displacement (Roast et al. 1998), population organization in swarms and schools (Clutter 1969), nighttime aggregations (Buskey 2000), and foraging success (Schiariti et al. 2006, Winkler et al. 2007).

2.2.2.5 Brachyuran Crab Larvae: Life History and Morphology

Decapod crustaceans of the infraorder Brachyura are common crabs that inhabit a variety of aquatic ecosystems. There are 93 families of Brachyuran crabs and at least 6,793 individual species. Different species are distinguished by variations in external morphology, sexual dimorphism, and larval developmental stages. Brachyuran

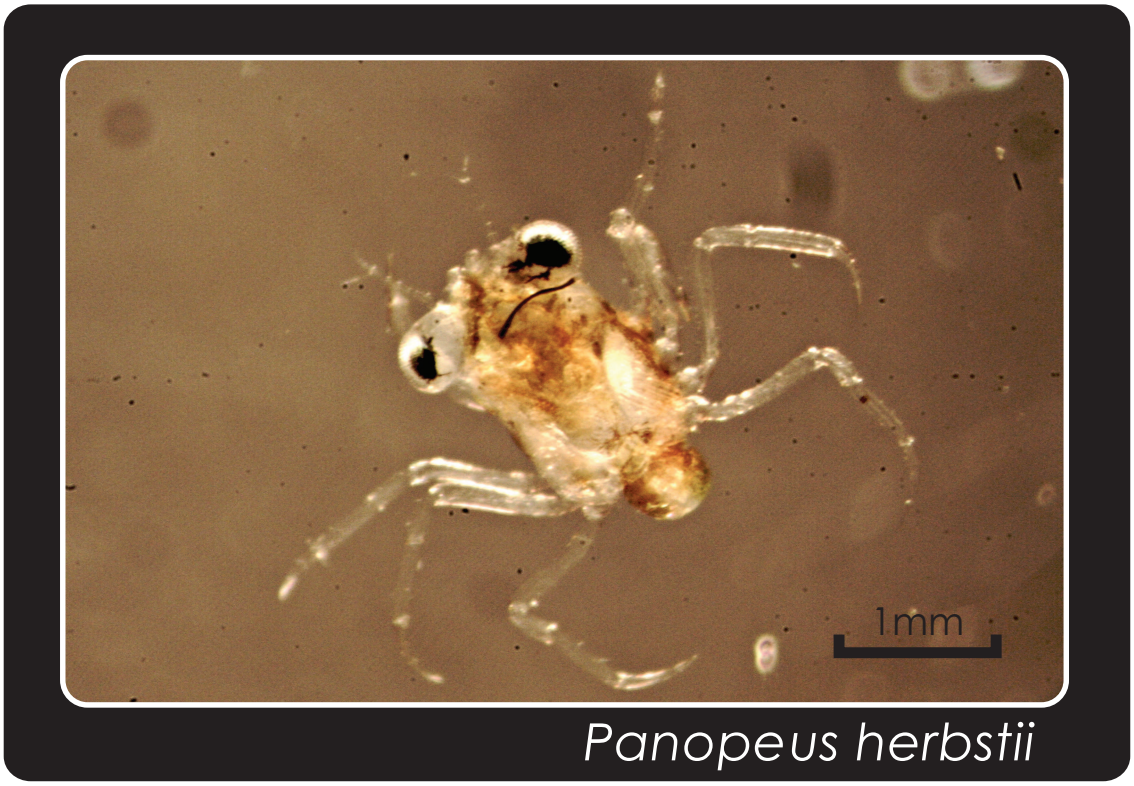

Figure 2.9: *Panopeus herbstii* Collected in Wassaw Sound, Skidaway Island, GA, USA (Photo by Ellen True)

crabs reproduce sexually, after which larvae are dispersed to feed in surface waters as a planktonic stage during which they progress through a number of zoeal stages. Following the final zoeal stage, larvae molt into the megalopa stage after which they settle out to the benthic stage and molt again into the first crab (juvenile) stage (Forward et al. 2001). Thus, these crabs are mandatory ontogenetic migrators, that is the vertical distribution of the population is life-stage dependent. Ontogenetic, diel, and tidal vertical migration, along with higher frequency behavioral responses to physical and chemical cues, superimposed on the ambient hydrodynamic environment lead to complex larval dispersal trajectories and have important implications for structuring coastal marine ecosystems (Queiroga and Blanton 2005).

There is vast literature on the ways in which individual behavioral responses to various physical and chemical cues combine with physical forcing mechanisms to

regulate dispersal and metamorphosis in planktonic larval stages (Ott and forward Jr. 1976, Queiroga and Blanton 2005, Lecchini et al. 2010). The species employed in this study is the estuarine Atlantic mud crab, *Panopeus herbstii*, and thus the focus here will be on understanding the interactions of estuarine hydrodynamic forcing and individual behavioral processes in regulating dispersal and settling in the planktonic larval stages of this, and similar, Brachyuran crab.

2.2.2.6 Brachyuran Crab Larvae Sensory Ecology

The manner in which crab larvae interact with their estuarine environments is a complex subject owing to behavioral variability among and within larval stages (Shanks 1986, Jamieson and Phillips 1988, Hobbs and Botsford), a wide variety of physical forcings (Officer 1976), and relevant length and time scales spanning many orders of magnitude (Queiroga and Blanton 2005). The literature is vast, and there are two major recurring biophysical themes. The first is the ability of crab larvae to exploit vertical gradients of horizontal velocity during various vertical migrations (ontogenetic, tidally-synchronized, diel, etc.) to control the extent of horizontal dispersion (e.g. Cronin and R. B. Forward 1986, Eggleston et al. 1998, Forward et al. 2004). The second is the role of physical and chemical cues in delaying or inducing larval metamorphosis and settling (e.g. Forward et al. 2001, Houser and Epifanio 2009).

Brachyuran crab larvae are some of the strongest swimmers in the zooplankton and are capable of sustaining swimming velocities from 0.2 - 8.3 cm/s, though most measurements fall in the range from 0.5 - 2 cm/s (Mileikovsky 1973, Sulkin et al. 1979, Forward 1989, Forward 1989). Larvae can effectively navigate vertically throughout the water column during ontogenetic, tidal, and diel migrations, but their swimming capabilities are generally insufficient to counteract displacement by horizontal currents for an extended amount of time (Chia et al. 1984, Young 1995). Furthermore, competent larval stages have mechanosensing setae distributed along the appendages

capable of sensing spatial gradients of flow (Santana et al. 2004, Kornienko et al. 2008). Thus, larvae can sense vertical gradients of horizontal velocity to effectively maintain position or induce shoreward or shelfward transport depending on the goals of that particular larval stage. Hill (Hill 1991, Hill 1991) noted that vertical migration must extend into the bottom boundary layer for larvae to escape high tidal velocities and thus displacements. Olmi (Olmi 1994) and Queiroga (Queiroga 1998) document how high vertical shear during tidal exchange in shallow estuaries can be exploited by larvae to influence their own transport. By swimming vertically down during ebb tide and up during flood tide, larvae gain net transport shoreward. This effect is aptly named Selective Tidal Stream Transport (STST) and describes the means by which larvae can exploit vertical gradients of horizontal velocity to control the extent of horizontal dispersion (Forward et al. 2001, Forward et al. 2003). It should be noted that the term *Selective Tidal Stream Transport* refers specifically to tidal cyclic migrations that exploit vertical shear for optimal horizontal transport, but the idea of larval behavioral responses to fluid mechanical shear strain rate can be considered a generalization of this behavior (Queiroga and Blanton 2005) and is an ecologically-important adaptation in practically all species.

Whereas shear strain rate sensing and vertical migrations are dominant behaviors in Brachyuran larvae, other environmental variables can also act to regulate and modify larval behavior. Sulkin (Sulkin 1984) modeled the negative feedback effects of pressure and gravity on larval behavior and found depth-keeping behavior, although there is considerable variability in the effects of barokinesis and geotaxis in different larval stages. Various studies have found positive phototaxis to directional light, again with changes in effects with larval stage and the presence of other sensory cues (Forward 1974, Sulkin 1975, Sulkin et al. 1980). Depth-keeping seems to be regulated by negative geotaxis in darkness and changes in phototaxis combined with a sinking response above a threshold light level (Queiroga and Blanton 2005).

Another interesting interaction among cues occurs when larvae exposed to increasing pressure respond by swimming vertically up. However, this effect is dampened in the presence of high light levels (Tankersley et al. 1995). Increasing salinity levels were observed to trigger vertical migrations upwards and the process was noted to be rate dependent (Forward 1989), whereas high temperatures have been observed to reverse geotactic behavior from negative to positive in zoeae of *Rhithropanopeus harrisii* (Ott and forward Jr. 1976). Changes in turbulent kinetic energy levels up to a saturation level of 1.1 $cm^2 s^{-2}$ triggered exited swimming behavior in *Callinectes sapidus* (Welch et al. 1999). Finally, chemical cues play an important role in inducing or delaying metamorphoses between larval stages and in site selection for settlement. In general, positive cues that accelerate metamorphosis and/or benthic settling behavior include adult habitat substrate, aquatic vegetation, conspecific odors, estuarine water, odor of a related crab species, and prey odor. Negative cues that delay metamorphosis and/or settling include ammonium and ammonia, hypoxia, predator odor, and extreme temperatures and salinities. Cues found to have no effect are clean seawater, clean structural material, and odor of other non-related species (Forward et al. 2001 and the references therein).

The effects of various interacting physical and chemical cues on larval behavior are certainly complicated and case dependent. Nevertheless, it is clear that behavioral responses to changing physical variables (light, temperature, salinity, current velocity) associated with tidal fluctuations have the potential to significantly modify vertical migratory behavior and ultimately larval dispersal trajectories. Additionally, chemical cues play an important role in dictating larval behavior, and most importantly it is the superposition of these interacting effects (behavioral responses, vertical migrations, physical forcing) that dictates the dispersal trajectories of planktonic Brachyuran crab larvae.

2.3 Experimental Methods in Fluid Mechanics

In this study we aim to reproduce ecologically-relevant gradients of vertical velocity for zooplankton behavioral assays. Importantly, we need to fully quantify the flow structure to ensure that conditions replicated in the lab are indeed what a zooplankter would experience *in situ*. This section reviews several methods employed in this study. Specifically, the Bickley jet is used to produce repeatable and continuous shear strain rate fields and particle image velocimetry (PIV) is used to fully resolve the two-dimensional velocity and shear strain rate fields.

2.3.1 Particle Image Velocimetry (PIV)

Particle Image Velocimetry (PIV) is a well-known, noninvasive flow measurement technique employed widely in the fluid mechanics research community. In PIV, the flow of interest is seeded with small, neutrally-buoyant particles that are passively advected with the flow. The flow is then illuminated with laser light and the light scattered from the seeding particles is filmed digitally. The images are post-processed to compute particle displacements between successive frames. With a known temporal resolution, the velocity and shear strain fields can be fully resolved in space and time (Raffel et al. 1998). Some experimental considerations relevant to PIV concerning optics, lasers, cameras, and image postprocessing algorithms are reviewed here.

2.3.1.1 The Hardware: Cameras, Lasers,and Optics

The flow in a typical planar PIV setup is illuminated with a sheet of laser light. Continuous wave (CW) Argon-ion lasers (488 nm, 514.5 nm) and pulsed Nd:YAG lasers (532 nm) are by far the most commonly used in the literature. Ion lasers typically have superior beam quality than Nd:YAG lasers (i.e. Gaussian beam cross-sections) but are also much less powerful. For this reason, scanning mirrors have been used to generate laser sheets from a ion laser beam as a means of maximizing sheet intensity with the lower characteristic laser power. Alternatively, a cylindrical

lens could be used to generate the laser sheet at the cost of sheet intensity, which is typically not a problem with Nd:YAG lasers. The flow is then seeded with neutrally-buoyant particles (e.g. 5 μm titanium dioxide particles) and filmed digitally, typically using an external trigger to synchronize laser pulses (Nd:YAG) and image capture. Matching camera specifications to experimental needs usually involves a balance of three main parameters: pixel count, bit-depth, and frame rate. The bit-depth, n, determines the maximum intensity resolution as the total number of resolved intensity levels (2^n). The pixel count and frame rate obviously set the spatial and temporal resolutions of the system.

2.3.1.2 The Software: Post-processing Algorithms and Error Control

During post-processing, each image is typically divided into interrogation subwindows and a two-dimensional spatial cross-correlation is performed in wavenumber space between successive images for each interrogation subwindow. Particle displacement between successive frames is estimated by the location of the cross-correlation peak. A peak fit analysis is employed to determine the displacement vector in all interrogation windows to subpixel accuracy. The displacement vectors are then divided by the time delay between laser pulses to produce the instantaneous two-dimensional velocity field (Cowen and Monismith 1997, Wereley and Meinhart 2001, Gui and Wereley 2002, Dasi 2004).

Typical sources of error in PIV algorithms include loss of particles due to particles entering or exiting the laser sheet, inaccurate or false correlation peaks, and too few particles per interrogation subwindow. The result of these errors is typically to produce false or unrealistic velocity vectors. These errors can be partially mitigated by matching experimental parameters (flow regime, laser pulse delay, camera resolution, particle density, etc.) and PIV algorithm parameters (interrogation subwindow size) to most accurately capture the hydrodynamics (Raffel et al. 1998, Dasi 2004).

2.3.2 Free Shear Flows and the Bickley Jet

By definition, free shear flows are characterized by unrestricted spatial gradients of fluid velocity and commonly include jets, wakes, and shear layers (Kundu and Cohen 2004). Shear flows are a ubiquitous feature in the marine environment and most often take one of two forms as an artifact of the prevalent density stratification in many coastal marine environments: a plane jet (fluid intrusion) and/or a shear layer. A plane jet is characterized by a maximum velocity on the centerline of the jet with gradual decrease towards the stagnant layers above and below, whereas shear layers are characterized by a gradually changing velocity profile linking two layers of differing horizontal velocity (Figure 2.10). Field observations of thin layers (e.g. McManus et al. 2003, Velo-Suarez et al. 2010) document the co-occurrence of thin layers with physical structure in the water column, specifically the pycnocline and/or thermocline that essentially demarks an interface between two fluid layers. Thus, an appropriate model for a laboratory thin layer could be based on a free shear flow design. The Bickley jet is a laminar planar free jet (with known analytical solutions) that can be fine-tuned to produce ecologically-relevant gradients of velocity (shear strain rate). We will consider more closely the governing equations and analytical solutions for the Bickley jet as well as some considerations concerning hydrodynamic instabilities and implications for nozzle design.

2.3.2.1 The Bickley Jet: Governing Equations and Analytical Solution

Following the analysis of Bickley (Bickley 1937), we consider a steady, incompressible, two-dimensional flow generated by a viscous jet issuing from a long narrow orifice into a fluid body at rest. Assuming the Prandtl boundary layer equations provide a good approximation to the free jet and noting that pressure is invariant in the streamwise, x, and transverse, y, directions, the flow is governed by the continuity equation,

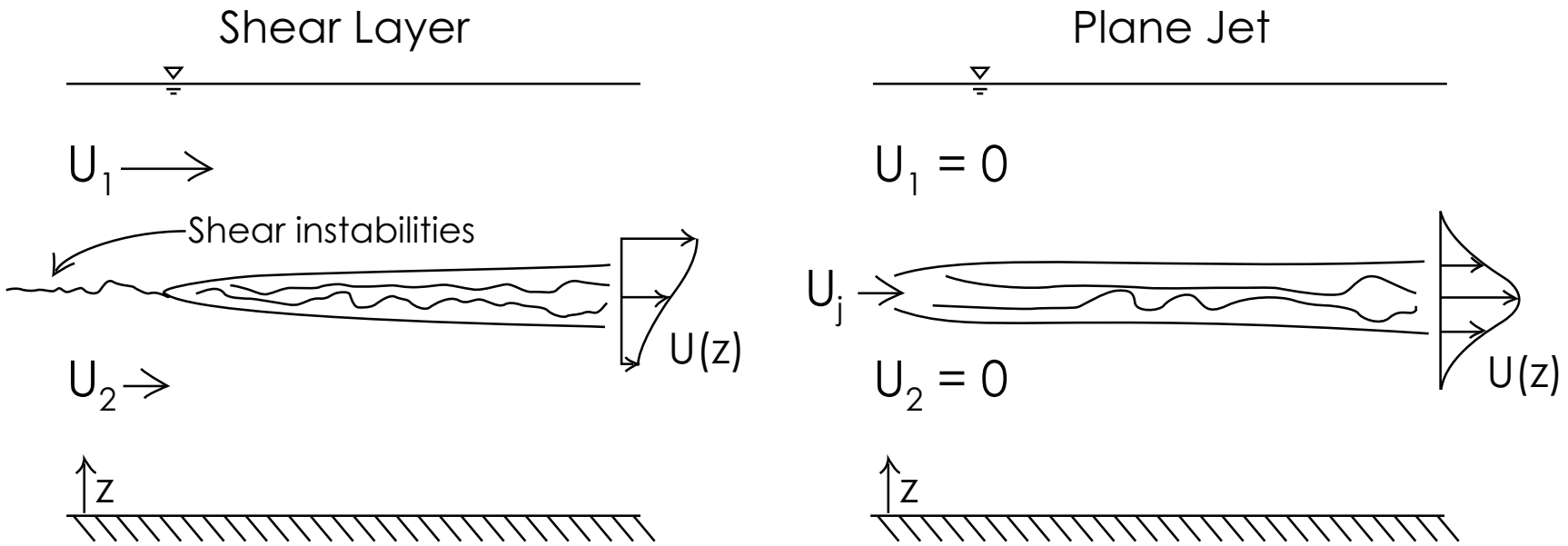

Figure 2.10: Typical Free Shear Flows in the Marine Environment (Adapted from Woodson 2005)

$$\frac{\partial u}{\partial x} + \frac{\partial v}{\partial y} = 0 \tag{2.6}$$

and the x momentum equation,

$$u\frac{\partial u}{\partial x} + v\frac{\partial u}{\partial y} = \nu\frac{\partial^2 u}{\partial y^2} \tag{2.7}$$

where u and v are the x and y components of velocity, respectively, and ν is the kinematic viscosity. The flow is subject to the following three boundary conditions concerning symmetry about the jet centerline, purely parallel flow, and boundedness in the transverse direction:

$$\frac{\partial u}{\partial y} = 0 \tag{2.8}$$

$$v = 0 \; at \; y = 0 \tag{2.9}$$

$$u \to 0 \; as \; y \to \infty \tag{2.10}$$

Finally, the total x momentum, M, is conserved such that

$$M = \rho \int_{-\infty}^{\infty} u^2 dy = Initial \; Jet \; Momentum \; Flux \tag{2.11}$$

Following the solution method of Schlichting (Schlichting 1933) and presenting the results per Sato and Sakao (Sato and Sakao 1964), the non-dimensional analytical velocity field results as

$$\frac{u}{u_o} = \operatorname{sech}^2\left(\frac{ay}{\delta}\right) \tag{2.12}$$

where $a = 0.88136$. The maximum, or centerline velocity, u_o, deceases with distance downstream due to entrainment of low momentum fluid as

$$u_o = \left(\frac{3M^2}{32\nu x}\right)^{1/3} \tag{2.13}$$

and the jet half-width δ (based on the velocity field) is given as

$$\delta = a\left(\frac{48\nu^2 x^2}{M}\right)^{1/3} \tag{2.14}$$

It is clear that the analytical solution for the centerline velocity is singular at $x = 0$ and this has given rise to the idea of a virtual origin to account for a non-zero nozzle width as the x location of a point source of momentum from which the jet can be considered to emanate (da C 1939, Revuelta et al. 2002, Peacock et al. 2004).

Andrade (da C 1939) noted that the "plane jet is difficult to realize experimentally", but was able to reproduce the Bickley solution in the neighborhood of an orifice if the flow was considered to emanate from a virtual origin a small distance upstream of the orifice. Sato (Sato 1960), however, was unable to reproduce the self-similar profiles of Bickley precisely because the plane jet is difficult to experimentally

operate. The reasons for these difficulties are considered below as well as some design precautions.

2.3.2.2 Hydrodynamic Instabilities and Design Considerations

It is useful to consider the linear stability analysis to gain a better understanding of the stability characteristics of the Bickley jet and the critical parameters. As for all parallel shear flows, the hydrodynamic stability of the viscous Bickley jet is governed by the Orr-Sommerfeld Equation via normal modes analysis as

$$(i\alpha Re)^{-1}\left(\frac{\partial^2}{\partial y^2}-\alpha^2\right)^2\Phi=(U-c)\left(\frac{\partial^2}{\partial y^2}-\alpha^2\right)\Phi-\frac{\partial^2 U}{\partial y^2}\Phi \tag{2.15}$$

where α is the perturbation wavenumber, c is the perturbation wave celerity, U is the base flow velocity distribution in the y direction, and Φ is the eigenfunction of the perturbation streamfunction. This equation is essentially a linearized equation of motion (conservation of mass and momentum) for small perturbations superposed on the base flow. With a known base flow and set boundary conditions, α can be varied and the behavior of c observed. Various numerical and expansion solution techniques have been proposed (Tatsumi and Kakutani 1958, Sato 1960, Drazin and Reid 1981) that yield the marginal stability curves. Experimental results by Sato (Sato 1960) observed two sinusoidal instability modes that manifest as velocity fluctuations symmetric and antisymmetric about the jet centerline.

The marginal stability curves in Figure 2.11 were derived by Peacock et al. (Peacock et al. 2004) using a Newton-Raphson relaxation scheme to numerically solve the Orr-Sommerfeld Equation for the Bickley jet base flow. The symmetric and antisymmetric modes are unstable at different Reynolds numbers for a given ω. The critical Re for the antisymmetric mode is small for virtually all frequencies of perturbation, $Re \approx 4$, whereas the symmetric mode is stable to most perturbation frequencies until

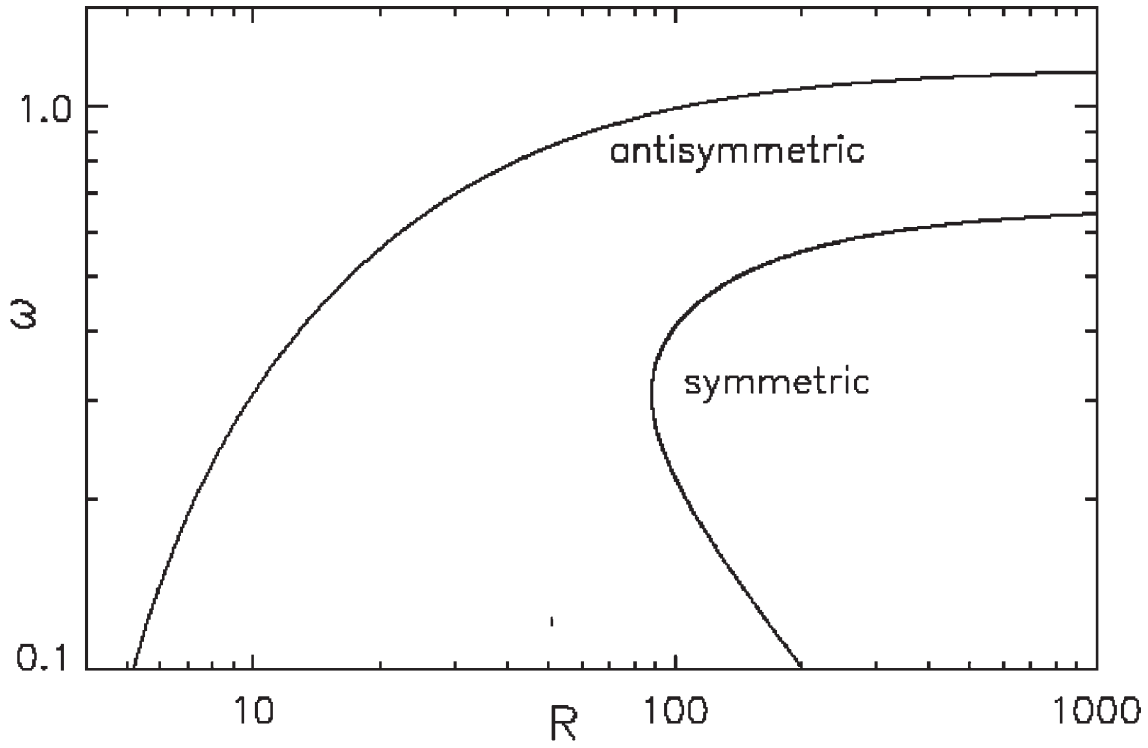

Figure 2.11: The Bickley Jet Marginal Stability Curve. ω is the non-dimensional perturbation frequency and R is the local Reynolds number based on the centerline velocity and the velocity half-width. Source: Peacock et al. 2004

Table 2.2: Jet Stability Characteristics as a Function of Re_j from Sato and Sakao 1964

Re_j	Jet Behavior
$12 < Re_j < 20 \sim 30$	The jet is entirely laminar with possible periodic instabilities in limited regions
$20 \sim 30 < Re_j < 40 \sim 60$	Pseudo-steady periodic instabilities, found in a wide region of the jet, are dampened before transitioning to highly irregular instabilities
$40 \sim 60 < Re_j$	Periodic fluctuations transition to highly irregular instabilities downstream

$Re \approx 80$. Thus, the critical experimental parameter governing jet stability is revealed as the jet Reynolds number:

$$Re_j = \frac{u_j d}{\nu} \tag{2.16}$$

that describes the ratio of the destabilizing momentum forces to the stabilizing effect of shear. Sato and Sakao (Sato and Sakao 1964) experimentally investigated instabilities in the Bickley jet based on Re_j and found good agreement with linear stability theory for $Re_j \geq 10$ (Table 2.2). For smaller Re_j, the theory does not account for the streamwise variation of the base flow through entrainment and spreading of the momentum distribution, i.e. the *local* Reynolds number, Re_o, which is a function of the downstream distance x.

Considering the inherent instabilities in free shear flows and the particularly fickle behavior of the Bickley jet, a few main design considerations for reducing instabilities and producing the desired flow field have arisen from experimental studies of both laminar and turbulent planar jets. Many modern experimental studies suggest honeycomb and wire mesh baffles and a fifth-order polynomial contraction upstream of the nozzle exit to prevent flow separation and ensure a top-hat exit velocity profile

(Mehta and Bradshaw 1979, Hussein 1994). Deo et al. (Deo et al. 2007) suggested a criteria for ensuring a top-hat profile as the ratio of the nozzle radius of curvature just upstream of the jet entrance, r, to the nozzle width, d, as $r/d \rightarrow 3.6$. Similarly, Deo et al. (Deo et al. 2007) suggested that a statistically two-dimensional mean velocity field is only achievable in turbulent jets aspect ratios greater than or equal to 20. Finally, Alnahhal and Panidis (Alnahhal and Panidis 2009) discuss the effect of sidewalls downstream of the jet exit and found statistically different flow fields with and without sidewalls. Specifically, there is a trade-off between boundary layer growth downstream of the jet, which acts as a lateral momentum sink (sidewalls), and lateral entrainment that causes departure from two-dimensional mean flow. Each of these design considerations have been incorporated in the final design of the Bickley jet nozzle used here.

CHAPTER III

METHODS

A laminar, planar, free jet (Bickley jet) apparatus in a recirculating flume was used to recreate ecologically-relevant gradients of vertical flow that commonly occur in coastal marine ecosystems. Particle image velocimetry (PIV) was used to fully resolve the steady, laminar flow fields. The controlled flow environments were used to conduct behavioral assays on various species of zooplankton including:

- A temperate mysid, *Neomysis americanus*, from the Damariscotta River, Walpole, Maine, USA
- Two tropical copepods, *Acartia negligens* and *Clausocalanus furcatus*, from the Gulf of Aqaba, Red Sea, Elat, Israel
- An estuarine mud crab larvae (megalop), *Panopeus herbstii*, from Priest Landing, Wassaw Sound, Savannah, Georgia, USA

Free-swimming animal trajectories were filmed and digitized (LabTrack software, BioRAS Inc.) under control (stagnant), upwelling, and downwelling flow configurations separately. Behavioral data were processed in two consecutive analyses. The first examines individual zooplankton paths (as well as the population as a whole) to determine threshold shear strain rate values that trigger changes in animal behavior (relative swimming speed, turn frequency, and directional heading). The second uses the determined shear strain rate threshold to quantify statistically significant changes in behavioral parameters. Path kinematics were computed for overall paths, portions inside and outside the velocity gradient layer (defined by a species-specific threshold shear strain or vertical velocity), and portions pre/post-contact with the

velocity gradient layer. Finally, statistical tests of path kinematic data were used to evaluate the significance of observed behavioral changes due to exposure to finescale horizontal gradients of vertical velocity.

3.1 Recirculating Flow System and Experimental Parameters

The recirculating flow system and laminar, planar free jet apparatus used in this study follow on a previous study of horizontal thin layers (Woodson et al. 2005). The current apparatus was modified to create horizontal gradients of vertical velocity consistent with a range of oceanic conditions.

The recirculating flow system consists of an elevated constant head tank (28L, US Plastics) with a free surface overflow to ensure a time-invariant supply of potential energy to the system. The sealed main flume (1 m x 30 cm x 30 cm) is constructed of clear acrylic for optical access and is aligned with the gravity vector (Figures 3.1 and 3.2). The flow passes through a specially designed slot jet nozzle (316 SS, jet opening 1 cm x 25 cm) to create a laminar planar jet in the vertical direction (Figures 3.1 and 3.2). The design features of the newly-fabricated stainless steel nozzle were consistent with the Woodson et al. (Woodson et al. 2005) study, following the recommendations of Hussein (Hussein 1994) and Mehta and Bradshaw (Mehta and Bradshaw 1979). Specifically, a 12:1 area ratio contraction was employed with a 5th-order polynomial defining the shape of the contraction in order to prevent flow separation. Three stainless steel mesh screens (50 % open area) and a layer of high porosity polypropylene sponge inside the main body of the nozzle served to induce head loss and dampen any large flow inhomogeneities in the contraction. The nozzle features ensuring a uniform (top-hat) velocity profile at the nozzle exit and the desired laminar flow field immediately downstream in the observation section.

The flow in the main flume section is channeled through an acrylic flow conditioner designed to prevent recirculation, flow instability, and exit geometry effects. The

channeled flow then continues through a rotameter into an intermediate reservoir (14 L, US Plastics) designed to apply back-pressure to the main tank and prevent air intrusion, unsteady (pulsating) effects, etc. Note that the intermediate reservoir was not employed in the downwelling configuration (Figure 3.2). Finally, the flow continues via a free surface overflow to the bottom receiving reservoir (28 L, US Plastics) where it is pumped through a 4 diaphragm, positive displacement pump (JABSCO Model 31801-1305) to the constant head tank.

During all behavioral assays a volumetric flowrate of 0.06 m^3/hr was selected to produce a well-defined and ecologically-relevant laminar flowfield. A flowrate of 0.06 m^3/hr for the given nozzle geometry results in a maximum jet exit velocity, U_j, of 6.7 mm/s. Therefore, the jet Reynolds number, $Re_j = U_j d/\nu$, is 52, which is in the transitionally stable and laminar regime. The maximum shear strain rate varies from 0.35 s^{-1} to 0.12 s^{-1} with distance downstream from the jet exit in the observation region (i.e. between $z = 5$ cm to $z = 15$ cm). The velocity and strain rate profiles vary in the transverse directions producing continuously-varying velocity and shear strain fields throughout the observation window.

3.2 Hydrodynamic Measurement Technique, Particle Image Velocimetry

Particle Image Velocimetry (PIV) is a well-known, non-invasive flow measurement technique employed widely in the fluid mechanics research community. The flow of interest is seeded with small, neutrally-buoyant particles that are passively advected with the flow. The flow is illuminated with laser light and the light scattered from the seeding particles is filmed digitally. The images are post-processed to compute particle displacements between successive frames. With a known temporal resolution, the velocity and shear strain fields can be fully resolved in space and time.

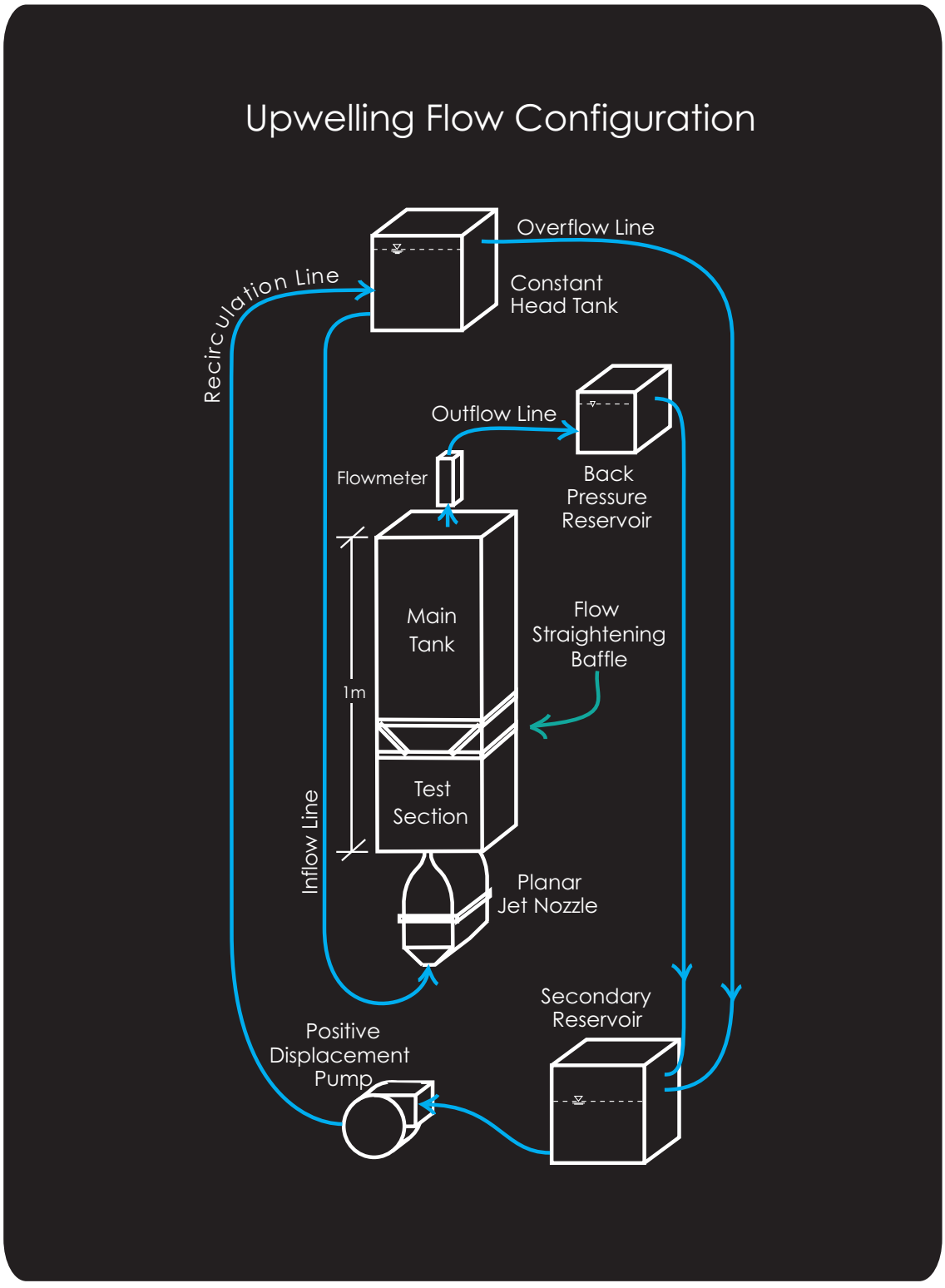

Figure 3.1: Schematic of the Apparatus in the Upwelling Flow Configuration.

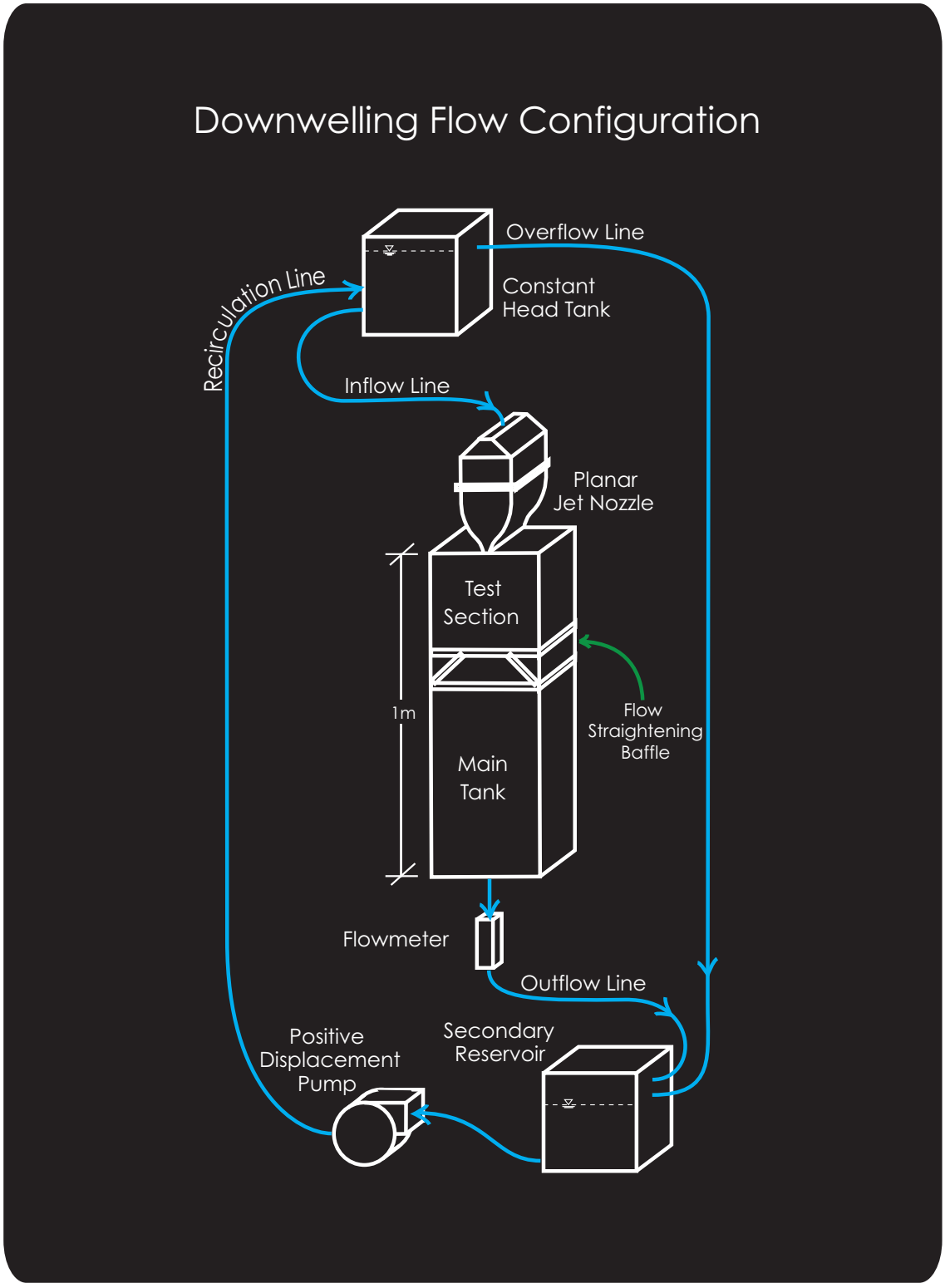

Figure 3.2: Schematic of the Apparatus in the Downwelling Flow Configuration.

3.2.1 System Components and Data Capture

The flow is illuminated with a planar sheet of laser light provided by a pair of Nd:YAG lasers (New Wave Research Gemini, 532 nm, 125 $mJ/pulse$)(Figure 3.3). The laser beam was first focused with a 1 m focal length spherical lens and then expanded with a -12.6 mm cylindrical lens resulting in a thin sheet of laser light in the observation region. In this study the flow was seeded with titanium dioxide particles of diameter less than or equal to 5 μm.

Data capture was controlled using an eight-channel pulse generator (Berkeley Nucleonics Model 500D), which triggered coordinated firing of the laser heads with the shutter of a CCD camera. The camera was a Kodak Megaplus ES 1.0 with 8 bit monochrome and 1 Megapixel image output. The camera was equipped with a 105 mm lens (Nikon AF Micro Nikkor) and interfaced with a PC running Windows XP via a Coreco Image Capture board. Hardware communication and image sequence capturing were achieved using Video Savant 3.0 software (IO Industries). Raw image sequences of the light scattered from the seeding particles was captured at 15 Hz for approximately 30 seconds, resulting in a 450 image sequence.

3.2.2 Data Processing

The image sequences were processed using software developed by Dasi (Dasi 2004). The algorithm developed by Dasi (Dasi 2004) was based on previous algorithms developed by Cowen and Monismith (Cowen and Monismith 1997), Wereley and Meinhart (Wereley and Meinhart 2001) and Gui and Wereley (Gui and Wereley 2002). The algorithm first computes a background image for the image sequence, which is defined as the minimum intensity achieved by any pixel for the duration of the sequence. The image sequence is then rescaled; essentially the background intensity is removed to enhance the contrast and signal strength of the light scattered by the seeding particles. Next each image is divided into 16 x 16 pixel interrogation subwindows and

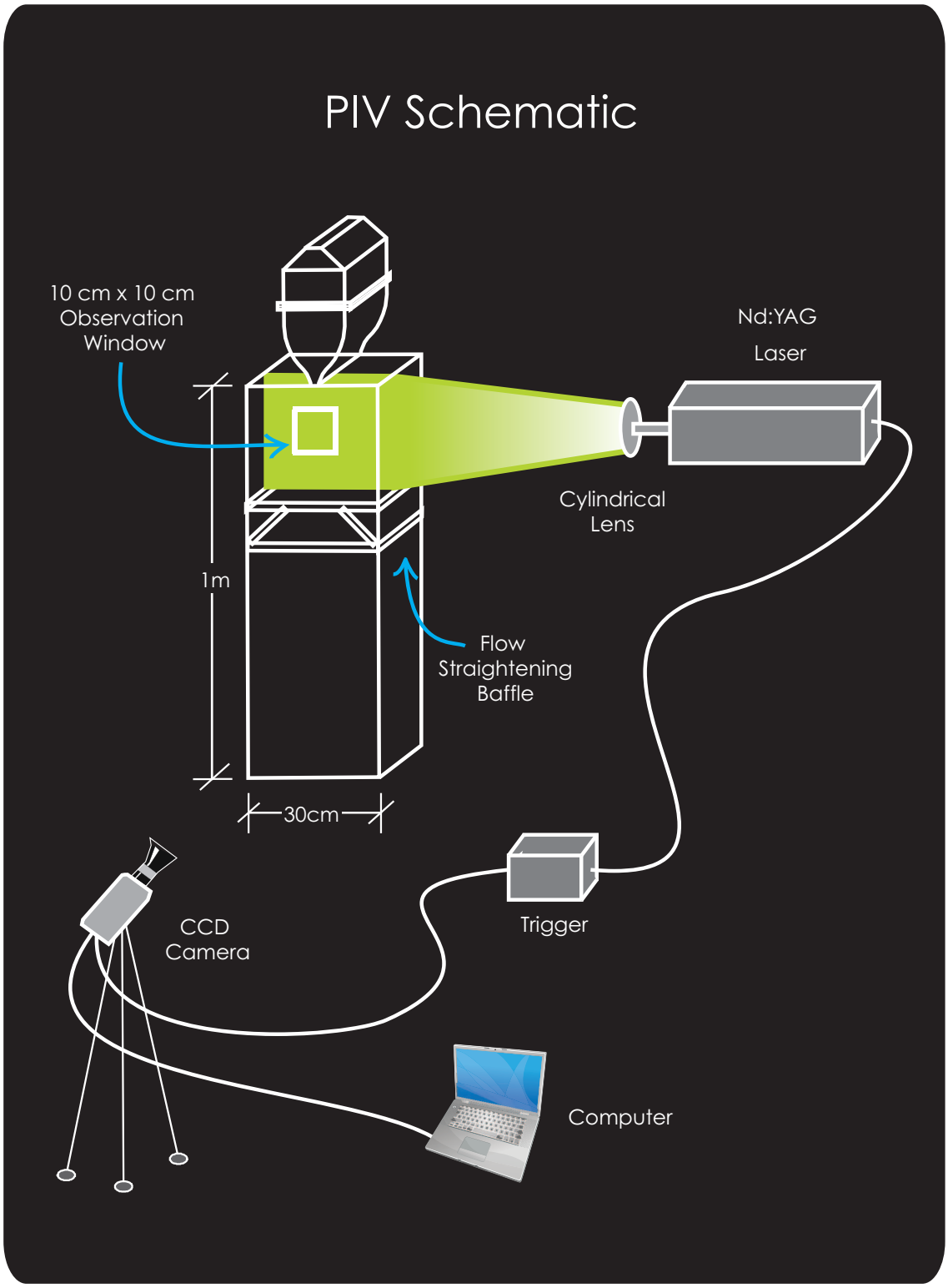

Figure 3.3: Schematic of Equipment Configuration for PIV Measurements.

a 2D spatial cross-correlation is performed in wavenumber space between successive images for each interrogation subwindow. Particle displacement between successive frames is estimated by the location of the cross-correlation peak. A Gaussian peak fit analysis is employed to determine the displacement vector in all interrogation windows to subpixel accuracy. The displacement vectors are then divided by the time delay between laser pulses (0.05 s) to produce the instantaneous 2D velocity field, from which the shear strain field is easily computed.

The analysis algorithm filtered erroneous vectors iteratively using a threshold of 3 to 4 standard deviations from the mean. These errors can be alleviated preemptively by matching experimental parameters (flow regime, laser pulse delay, camera resolution, etc.) and PIV algorithm parameters (interrogation subwindow size) to most accurately capture the hydrodynamics. The interrogation subwindow size and time delay between laser pulses were selected to achieve resolution of the velocity field at the scale of individual copepods (<100 μm), (Woodson et al. 2005).

3.3 Behavioral Assays and Measurement Techniques

3.3.1 Animal Collection

Panopeus herbstii larvae were collected in June of 2010 at Priest Landing on Skidaway Island near Savannah, GA, USA and brought back to Georgia Tech to conduct behavioral assays. A light trap was constructed and deployed from the dock at Priest Landing between 10 pm and midnight for 2 consecutive nights. The light trap consisted of a large plastic jar (approximately 5 L Nalgene) with an inverted funnel at the wide mouth, designed to increase plankton retention in the trap. A dive light was secured to the bottom of the jar in an effort to attract phototactic zooplankton into the trap. The jar was suspended horizontally between a weighted mooring device on the bed and a float on the water surface. The trap was retrieved after a two hour deployment, and the animals were taken to the laboratory to be processed. The crab

larvae were immediately sorted out and kept in recirculating seawater, while being fed copepod nauplii (*Acartia tonsa*), before being transported to Atlanta in coolers. In Atlanta, the crabs were kept in well-oxygenated artificial seawater (Instant Ocean) at estuarine conditions ($\sim 30\ ppt$, $28\ ^{\circ}C$). The crabs were fed copepod nauplii and brine shrimp nauplii (*Artemia spp.*) over the 2 week duration in which all behavioral assays were conducted. Larvae were not feed in the 24 hours prior to each behavioral assay.

Acartia negligens and *Clausocalanus furcatus* were collected from the Gulf of Aqaba (Red Sea) off the dock of the InterUniversity Institute in Elat, Israel for on-site behavioral assays during the summer of 2009. Two primary methods were used to collect animals for behavioral assays: hand net tows and boat net tows. Hand net tows were conducted between the hours of 9 pm and 11 pm when the abundance of zooplankton in the near surface water column was high. A 0.5 m diameter plankton net with a 250 μm mesh cod end was towed by hand parallel to the shore at approximately 1 - 2 m depth for about 20 minutes. For boat tows, the same plankton net and cod end were towed parallel to shore (at 0.5 $knots$) at a depth of approximately $3-5m$ between the hours of 8 pm and 9 pm. For each collection method, the cod end was taken ashore and the plankton were processed immediately. The copepods were sorted by species into groups of approximately 50 - 60 mixed-sex individuals and kept in filtered seawater (50 μm) in 1 L jar, where they were starved for 24 hours before being used for behavioral assays.

Neomysis americanus specimens were collected off the dock of the Darling Marine Center in Walpole, Maine, USA. The mysids were collected at night via vertical tows from the dock. A plankton net with a 250 μm mesh cod end was released into the water column and kept just above the bottom bed for several minutes and then pulled to the surface. Mysids were immediately processed, sorted, and kept in aerated 20 L buckets and fed mixed zooplankton and *Rhodomonas spp.* and *Tetraselmis spp.*

phytoplankton. Mysids were measured under a microscope, and individuals in the range 7 - 10 *mm* were sorted for shipment to Atlanta. Mysids were shipped to Atlanta where they were kept in well-oxygenated artificial seawater (Instant Ocean) and fed brine shrimp nauplii (*Artemia spp.*) and *Tetraselmis spp.* phytoplankton over the 2 week duration in which all behavioral assays were run. Again, the animals were starved for the 24 hours before behavioral assays were run.

3.3.2 Behavioral Assays

All behavioral assays were conducted in the same apparatus and under identical flow conditions as for the PIV characterization. All experiments used either filtered seawater (FSW) or artificial seawater (Instant Ocean) in the recirculating flow system at conditions (temperature and salinity) nearly identical to *in situ* conditions. For all experiments, the animals were collected between the hours of 8 pm and 12 pm in the upper layer of the water column (<5 *m* depth), sorted and acclimated in the lab, and starved for the 24 hours immediately preceding the experiments. All behavioral assays were run in mixed-sex, species specific trials.

Two hour behavioral assays under both upwelling and downwelling flow configurations (separately) were run in which animals were introduced to the tank and allowed to acclimate for one hour prior to the experiment. During this period the thin velocity layer flow was started and allowed to reach steady state. Two replicates of each combination of species and treatment were performed. One hour control experiments were run for all species tested. The control experiments consisted of animals swimming freely in a stagnant tank. In all cases, animals were filmed in the 10 *cm* x 10 *cm* observation window.

The experimental setup was identical for all behavioral assays except for the number of animals present (variations in size and overcrowding possibilities). Optical

elements mounted behind the tank allowed for visualization of animal swimming trajectories via shadowgraph observation (Figure 3.4). An infrared (IR) fiber-coupled diode (CVI Melles Griot, 57PNL054/P4/S, 660 nm, 22 mW) was collimated via a 15.24 cm spherical mirror (Edmunds Optics, NT32-845, effective focal length 1524 mm) and reflected at 45° via a planar mirror perpendicularly into the rear of the tank (Figure 3.4). This method provides uniform illumination through the depth of the tank. The back illumination projects a silhouette of the swimming animals onto the front surface of the tank, on which is placed a sheet of film paper (Sam Flax), resulting in a crisp, high contrast shadow. The shadowgraph trajectories produced over the course of each two hour behavioral assay were recorded via a CCD video camera (Pulnix, 745i, 768 x 494 pixels) linked to a digital video recorder (mini dv tapes). All experiments were recorded at 30 frames per second (fps), the maximum temporal resolution of the camera, which fully resolves all swimming behaviors of all the species tested.

3.3.3 Data Processing

The mini dv tapes containing the raw trajectory data were converted to avi (Audio-Video Interleave) movie files using iMovie HD (Apple Inc.). Each one hour tape was broken into approximately 15 four-minute video clips. This was done carefully so as not to chop up tracks in an effort to save memory and computational intensity while running the tracking software. The avi files were exported with the following settings: no compression, 15 fps, 256 color intensity scale. The reduction in temporal resolution was warranted to reduce memory requirements (order of 1 TB for all assays), and this frame rate is sufficient to resolve all swimming behaviors of the species tested. For example, *Neomysis americana*, by far the swiftest swimmer, exhibited bouts of behavior with maximum swimming speeds around 5 cm/s. So at a typical magnification of 500 $pixels/10cm$, or 0.2 $mm/pixel$, a swimming speed of 5 cm/s results in

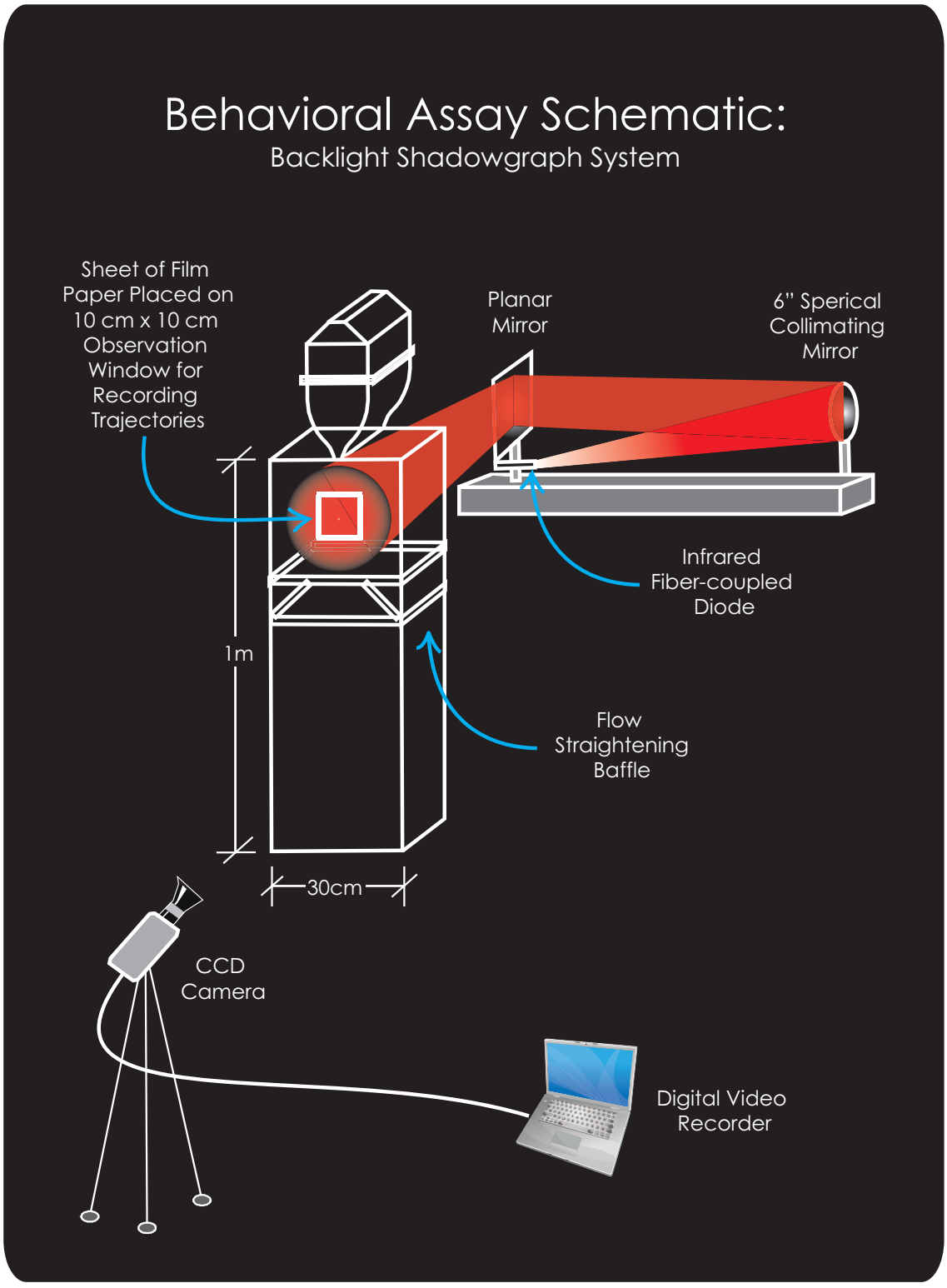

Figure 3.4: Equipment Configuration for the Behavioral Assays.

a displacement of 250 $pixels/s$. When considering a typical mysid body length of 8.5 mm (42.5 $pixels$), the displacement is only about five body lengths per second, or 1/3 body length per frame. Thus, 15 Hz is a sufficient temporal resolution to accurately resolve displacement of the body centroid for all animals tested.

The animal swimming trajectories were digitized using LabTrack Software (Bio-RAS) from the raw avi files. The resulting data sets, which include time and spatial (i.e., x and z) coordinate information, are post-processed in two phases using a suite of custom MATLAB codes. The first phase involved determining threshold shear strain or vertical velocity values for each species that elicit the maximum behavioral responses. The second phase involved computing path kinematic parameters for portions of each trajectory inside and outside the vertical layer (boundaries defined by the threshold level), as well as pre- and post-contact with the threshold level. The path kinematics computed in this study are relative swimming speed (the swimming speed of the animal minus the local fluid velocity from the PIV results), turning frequency (where a turn is defined as a change of direction of 15° or more), and the vertical net-to-gross displacement ratio ($VNGDR$ = net vertical displacement/gross vertical displacement). The proportional residence time (PRT = time in velocity gradient layer/total time in the observation window) was also computed for all paths.

3.3.4 Statistical Analyses

Statistical analyses of path kinematic data were conducted using one-way (single-factor) analysis of variance (ANOVA). ANOVA is a widely-used hypothesis testing tool that tests for the equality of the mean values of two (or more) datasets by evaluating sources of variance both within individual treatments and across groups. ANOVA is particularly useful in the present study to evaluate the behavioral responses of a population of zooplankton to gradients of vertical velocity as compared to a population (all else equal) swimming in a stagnant tank. The fact that ANOVA does

not require equal sample sizes across treatments makes it particularly useful in the present study in which animal availability and mortality are ever-present concerns. Assumptions inherent to the statistical validity of ANOVA include the following: random sampling and normal distributions of independent samples as well as treatment groups with the same variance. Randomly selecting individuals from the same species and size class ensures these assumptions are valid for this study and thus that application of ANOVA is warranted to detect statistically significant changes in zooplankton behavior.

Zar (Zar 1999) summarizes the computations necessary for a one-way ANOVA. These computations result in a value that corresponds to the F-distribution; this computed value is then compared to the critical tabulated value for the F-distribution as dictated by the group and error degrees of freedom at a given confidence level (usually 95%). If the computed F value is equal to or greater than the critical tabulated value, then the null hypothesis, Ho, is rejected. In the present study, H_o is given as follows: Exposure to horizontal gradients of vertical velocity does not induce a change of swimming speed (proportional residence time, turning frequency, etc.). The most commonly reported statistic for ANOVA is the p value, which is obtained from the critical F value. The p value is the probability that the means of some measured quantity of two experimental groups are equal, and for most ecological experiments a p value less than 0.05 is recognized as a statistically significant result.

CHAPTER IV

RESULTS AND DISCUSSION

4.1 Physical Layer Characterization

4.1.1 Upwelling Jet

Figure 4.1 shows the experimental PIV results for an upwelling, laminar planar free jet located at the origin with jet Reynolds number equal to 52. Examination of the two dimensional velocity vector and shear strain rate fields shows a close match to the analytical solution by Bickley (Bickley 1937) throughout the observation section (Figure 4.2).

The maximum shear strain rate varies from approximately 0.35 s^{-1} to 0.12 s^{-1} with distance downstream from the jet exit (i.e., between $z = 5$ cm and $z = 15$ cm) due to the entrainment of low velocity fluid and the gradual broadening of the velocity profile due to the transverse diffusion of momentum. The maximum velocity along the jet centerline likewise varies from approximately 6 mm/s to 4.7 mm/s and decreases in the transverse direction. Closer observation of the analytical (Figure 4.2) and experimental (Figure 4.1) shear strain rate fields shows a slight divergence from theory in the experimental results. Namely, the jet velocity profile is narrower through the entire observation section and the shear strain rate values are slightly higher at a given z position, as illustrated by the closeness of the shear strain rate contours as compared to the Bickley shear strain rate field. To examine this effect further, individual profiles of vertical velocity (Figure 4.3) and shear strain rate (Figure 4.4) were plotted versus the corresponding Bickley profiles 100 mm downstream of the jet origin ($z = 100$ mm).

The PIV velocity profile is narrower and more peaked near the jet centerline, with

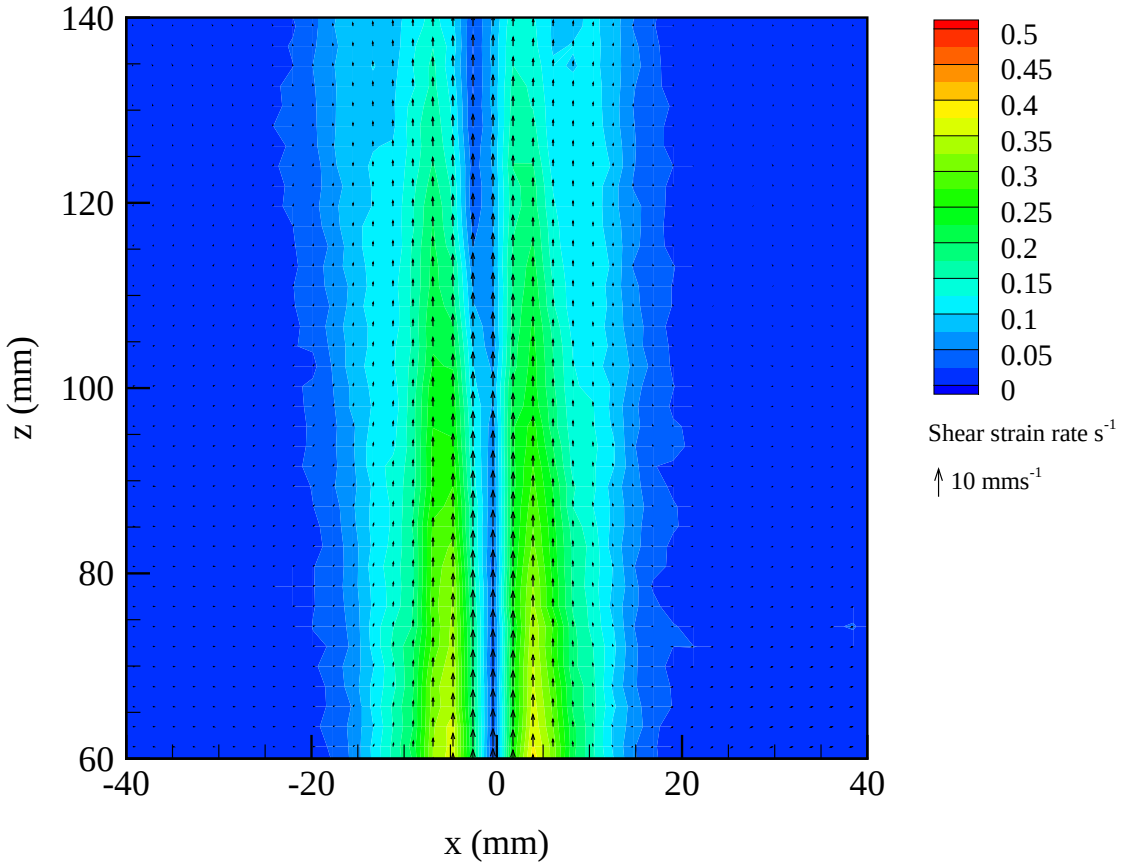

Figure 4.1: Velocity (vectors) and Shear Strain Rate (contours) Fields for the Upwelling Experimental Configuration

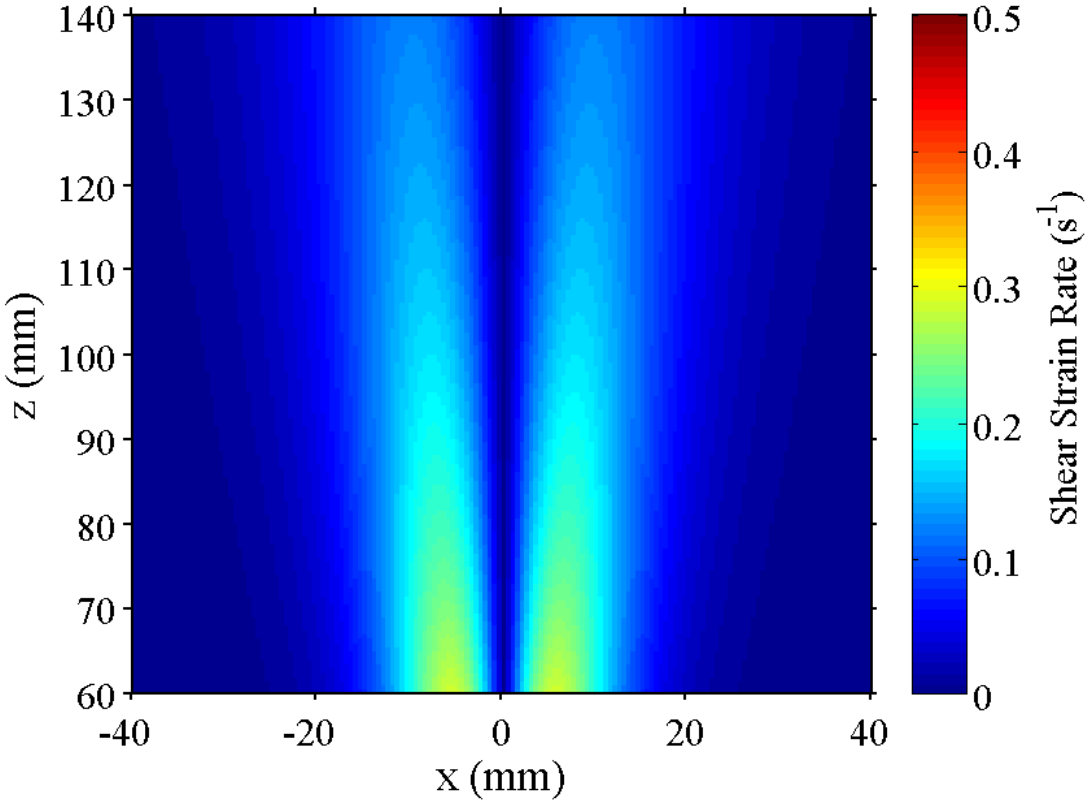

Figure 4.2: Analytical Shear Strain Rate Field from Bickley (Bickley 1937) for an Upwelling Free Jet

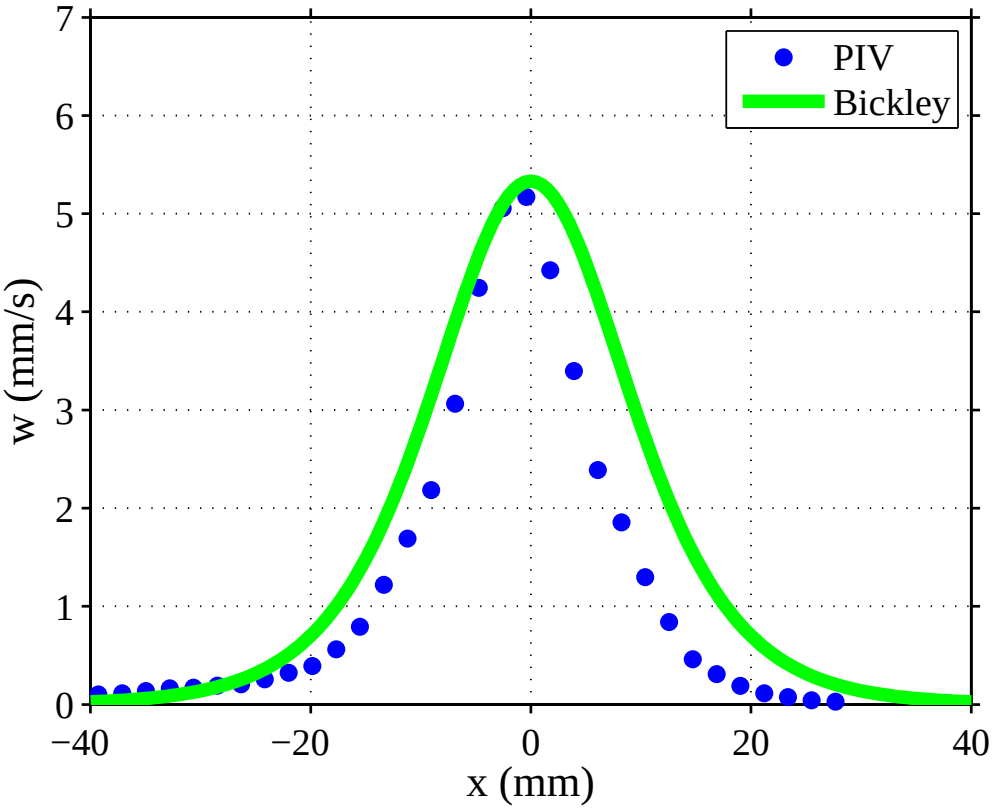

Figure 4.3: Analytical versus Experimental Velocity Profiles in an Upwelling Free Jet at $z = 100\ mm$

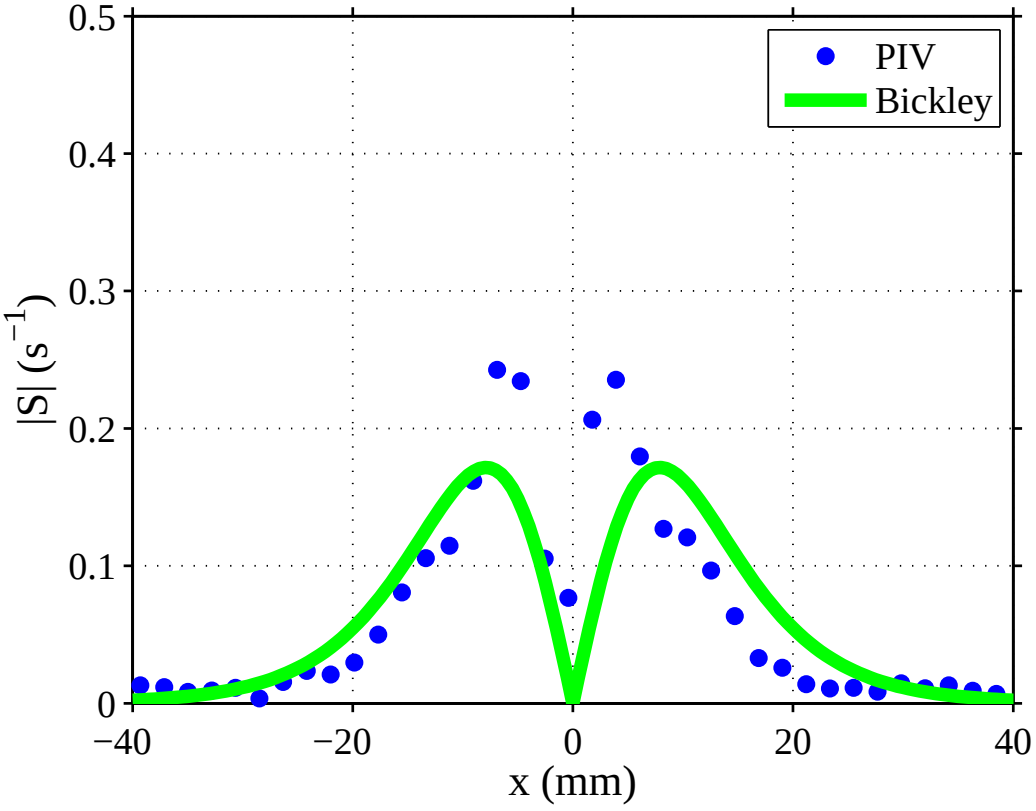

Figure 4.4: Analytical versus Experimental Shear Strain Rate Profiles in an Upwelling Free Jet at $z = 100\ mm$

slightly lower velocities further from the centerline when compared to the Bickley profile (Figure 4.3). Similarly, the PIV shear strain rate profile shows higher values near the centerline and lower values further out when compared to the Bickley profile (Figure 4.4). These divergences from the analytical solution were traced to a slight positive buoyancy of the jet due to a temperature difference between the jet and the receiving fluid body of approximately $0.1°C$. This thermal difference was caused by slight heating of the recirculating fluid by the centrifugal pump over time. Thus, the buoyancy acted very slightly to accelerate the jet vertically upward (in the case of upwelling) and delay the diffusion of momentum in the transverse direction (through the gradual broadening of the velocity profile). The slight buoyancy effect was observed to be constant over the course of an experiment and did not destabilize the jet. Furthermore, all analyses of animal behavior used experimental PIV shear strain rate values, not analytical values, and thus results are true to what the zooplankters experienced throughout the course of an assay.

4.1.2 Downwelling Jet

Figure 4.5 shows the experimental PIV results for a downwelling, laminar planar free jet located at the origin with jet Reynolds number equal to 52. Again, examination of the two dimensional velocity vector and shear strain rate fields shows a close match to the analytical solution by Bickley (Bickley 1937) throughout the observation section (Figures 4.5 and 4.6), similar to the upwelling results.

The range of maximum shear strain rate values and vertical velocities throughout the observation window is identical to the upwelling case, as expected for two dynamically similar jets (Figure 4.5). Closer observation of the analytical (Figure 4.6) and experimental (Figure 4.5) shear strain rate fields again shows a slight divergence from theory in the experimental results. In contrast to the upwelling case, the jet velocity profile is broader through the entire observation section and the shear strain

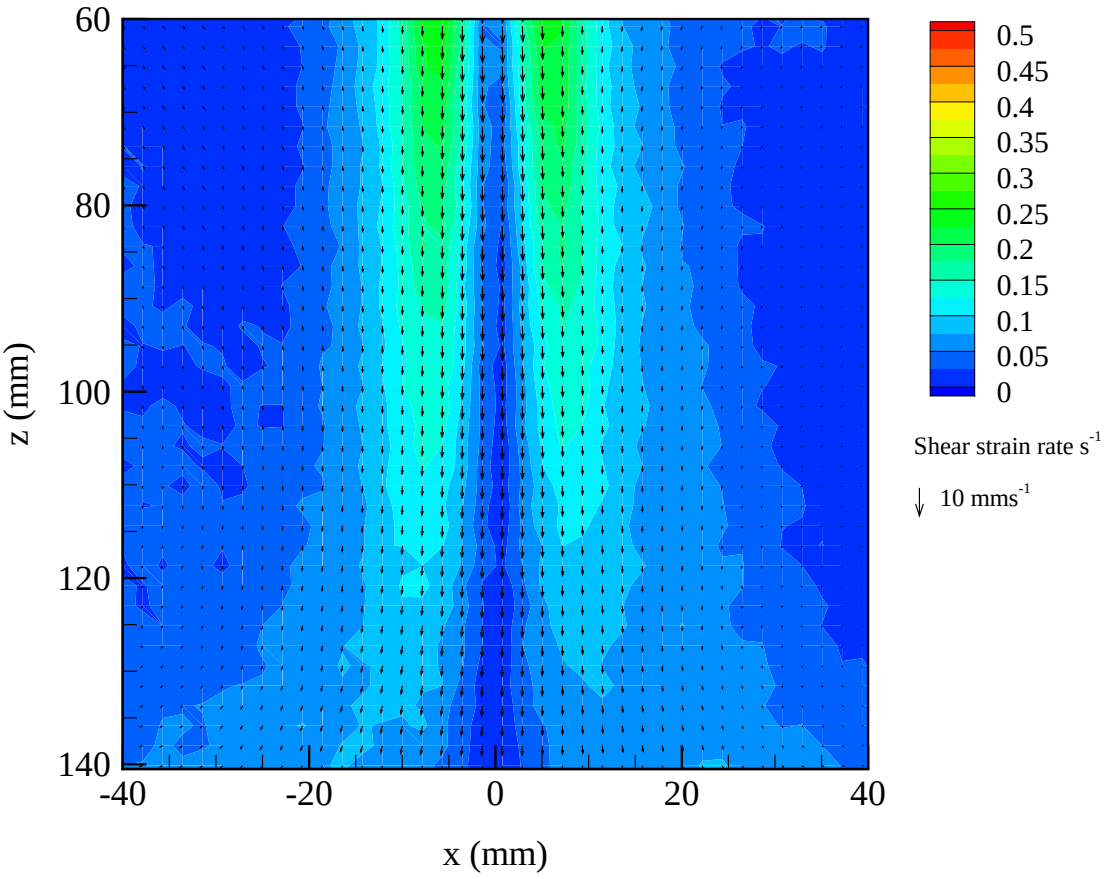

Figure 4.5: Velocity (vectors) and Shear Strain Rate (contours) Fields for the Downwelling Experimental Configuration

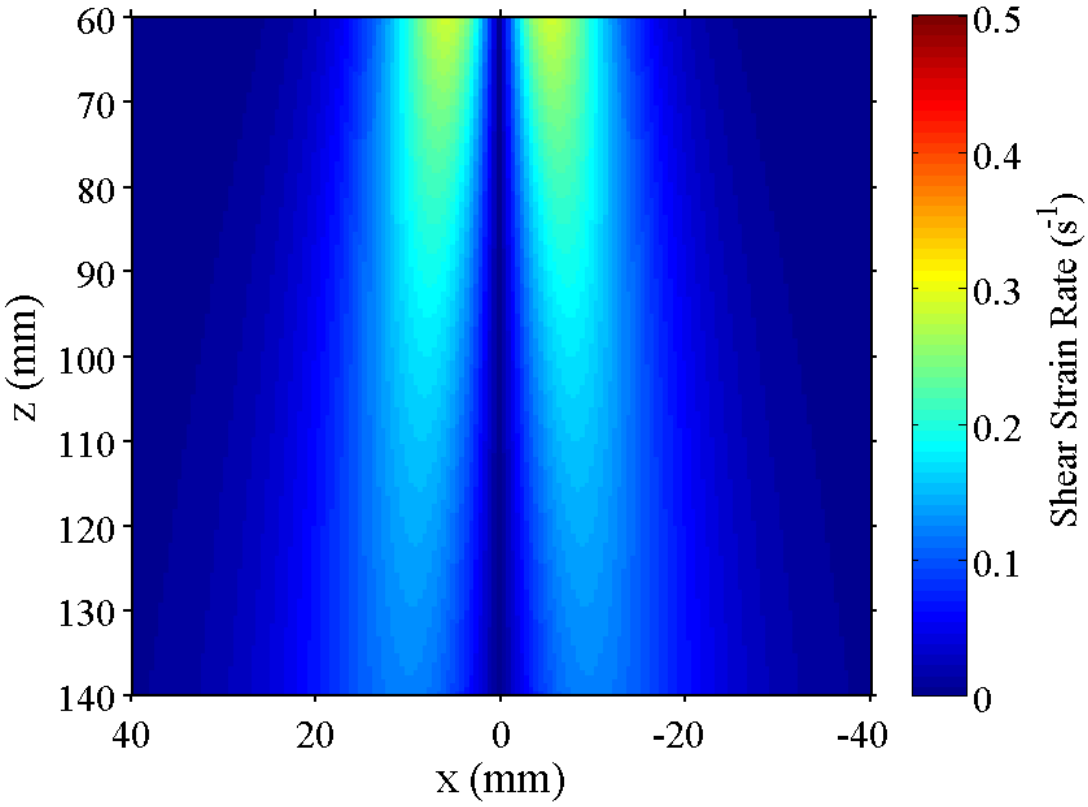

Figure 4.6: Analytical Shear Strain Rate Field from Bickley (Bickley 1937) for a Downwelling Free Jet

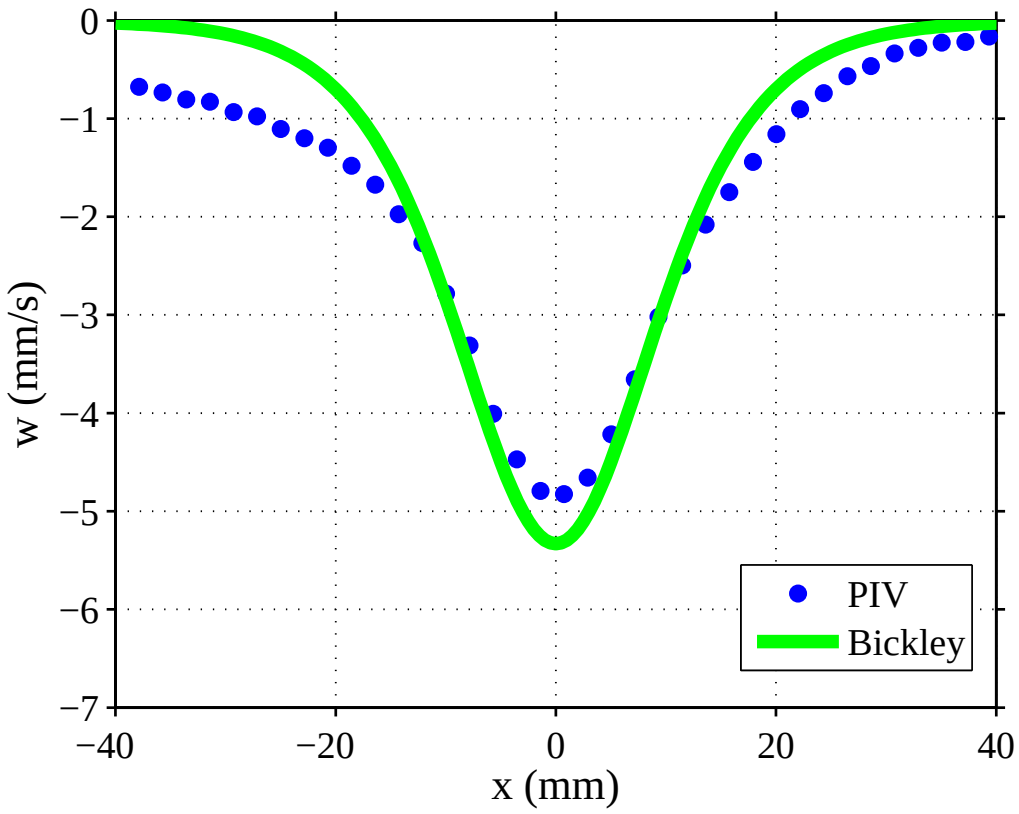

Figure 4.7: Analytical versus Experimental Velocity Profiles in a Downwelling Free Jet at $z = 100\ mm$

rate values are slightly lower at a given z position, as illustrated by the spreading of the shear strain rate contours as compared to the Bickley shear strain rate field.

Once again, individual profiles of vertical velocity (Figure 4.7) and shear strain rate (Figure 4.8) were plotted versus the corresponding Bickley profiles 100 mm downstream of the jet origin ($z = 100\ mm$). As expected, the PIV velocity profile is broader and more rounded near the jet centerline when compared to the Bickley profile with slightly higher velocities further from the centerline. Similarly, the PIV shear strain rate profile shows lower values near the centerline and higher values further out when compared to the Bickley profile. These results are consistent with the slight effects of buoyancy discussed in the upwelling case above, with the exception that the buoyancy force is now in the opposite direction of the jet momentum. Thus, the buoyancy force

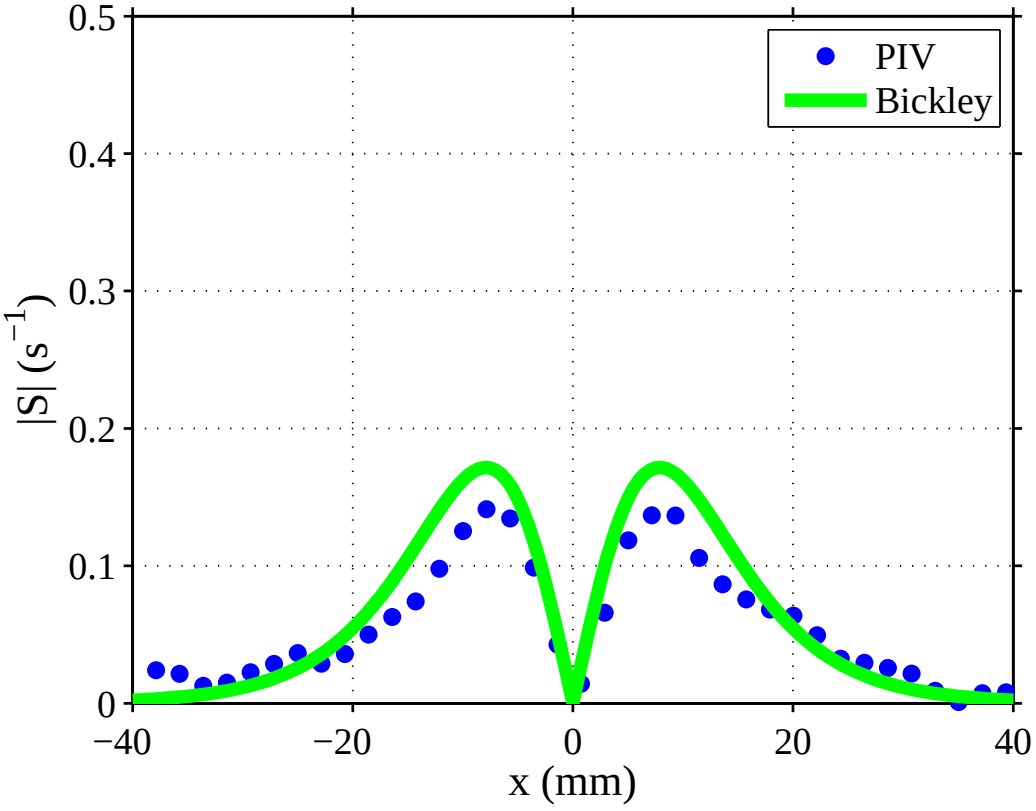

Figure 4.8: Analytical versus Experimental Shear Strain Rate Profiles in a Downwelling Free Jet at $z = 100\ mm$

of the slightly warmer ($\Delta T \sim 0.1°C$) jet entering the fluid body acts very slightly to decelerate the jet vertically upward and expedite the diffusion of momentum in the transverse direction (through the relatively rapid broadening of the velocity profile). Again, this slight buoyancy effect was observed to be constant over the course of an experiment and did not destabilize the jet. The important fact again remains that all analyses of animal behavior used experimental PIV shear strain rate values, not analytical values, and thus results are true to what the zooplankters experienced throughout the course of an assay.

4.2 Behavioral Assays

Behavioral data, which consists of digitized zooplankton trajectories (e.g. Figure 4.9), are processed in two consecutive analyses. The first examines individual zooplankton paths (as well as the population as a whole) to determine threshold shear strain rate values that trigger changes in animal behavior (relative swimming speed, turn frequency, and directional heading). The second uses the determined shear strain rate threshold to quantify statistically significant changes in animal behavioral parameters. The results are considered in the ecological context of plankton patchiness.

4.2.1 Behavioral Shear Strain Rate Thresholds

In order to determine threshold shear strain rates that trigger species-specific behavioral responses in zooplankton, the behavior of individual zooplankters is examined as the animal is exposed to varying shear strain rates as it progresses along its trajectory. Three specific behavioral parameters are chosen and examined as a function of various threshold shear strain rates: relative swimming speed, turn frequency, and direction of heading. Relative swimming speed is defined as the animals total swimming speed minus the fluid velocity obtained from PIV results. Turn frequency is defined as the number of turns per individual per second, where a turn event is a change of direction of 15° or more. Finally, directional heading is the angular direction of the

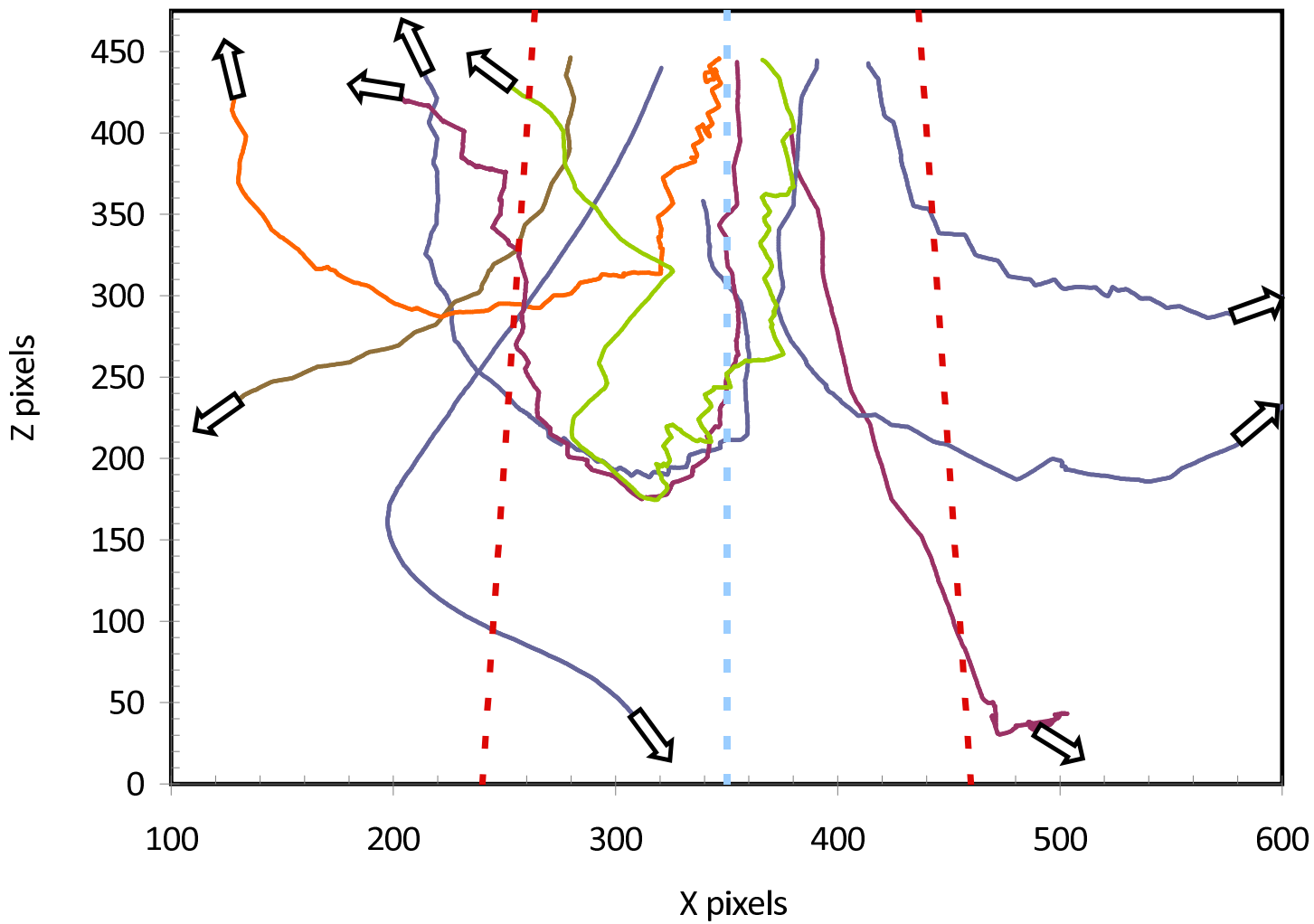

Figure 4.9: Examples of Digitized Trajectories of *Acartia negligens* in a Downwelling Jet, Arrows Indicate Direction of Swimming Trajectory. The Straight Vertical Blue Line Indicates Jet Centerline, and the Straight Red Lines Indicates the Approximate Edge of Jet Layer Based on a Behaviorally-Determined Threshold Shear Strain Rate.

displacement vector with respect to the jet centerline.

For each zooplankter trajectory, the mean and standard deviation of each of these behavioral parameters are computed for portions of the trajectory above and below a given threshold shear strain rate value based on the physical location of the animal with respect to the jet structure, and the absolute value of the difference between these values is plotted as a function of the particular threshold shear strain rate value. This process is repeated for each shear strain rate value a zooplankter encounters along its trajectory. This entire analysis is completed for each zooplankter in a given experimental replicate. Figures 4.10, 4.11, and 4.12 show the combined upwelling and downwelling results of these analyses for turn frequency, relative swimming speed, and heading, respectively, for *Acartia negligens*.

Once this analysis has been completed for each trajectory within a given experimental group, the results are ensemble averaged at each threshold shear strain rate value. The benefit of completing analyses on individual paths and then ensemble averaging over the entire population is that it retains the variability of individual behavior while also revealing the population scale phenomena. Often, examining individual paths gives a general idea of a threshold strain rate but fails to reveal a single, well-defined threshold value. Ensemble averaging the data at each shear strain rate value in Figures 4.10, 4.11, and 4.12 produces the data in Figures 4.13, 4.14, and 4.15, respectively, and most often reveals well-defined threshold strain rate values.

Because Figures 4.13, 4.14, and 4.15 show the magnitude of differences in behavior above and below a given shear strain rate threshold, sudden increases (sharp gradients) in the differences of mean (top panels) behavioral parameters and the standard deviation (bottom panels) indicate a transition. A transition is indicative of direct behavioral responses that manifest as changes in both the magnitude (mean) and the variability (standard deviation) of behavior above and below a given shear strain rate value. The vertical cyan line in both panels of Figures 4.13 – 4.15, as well as

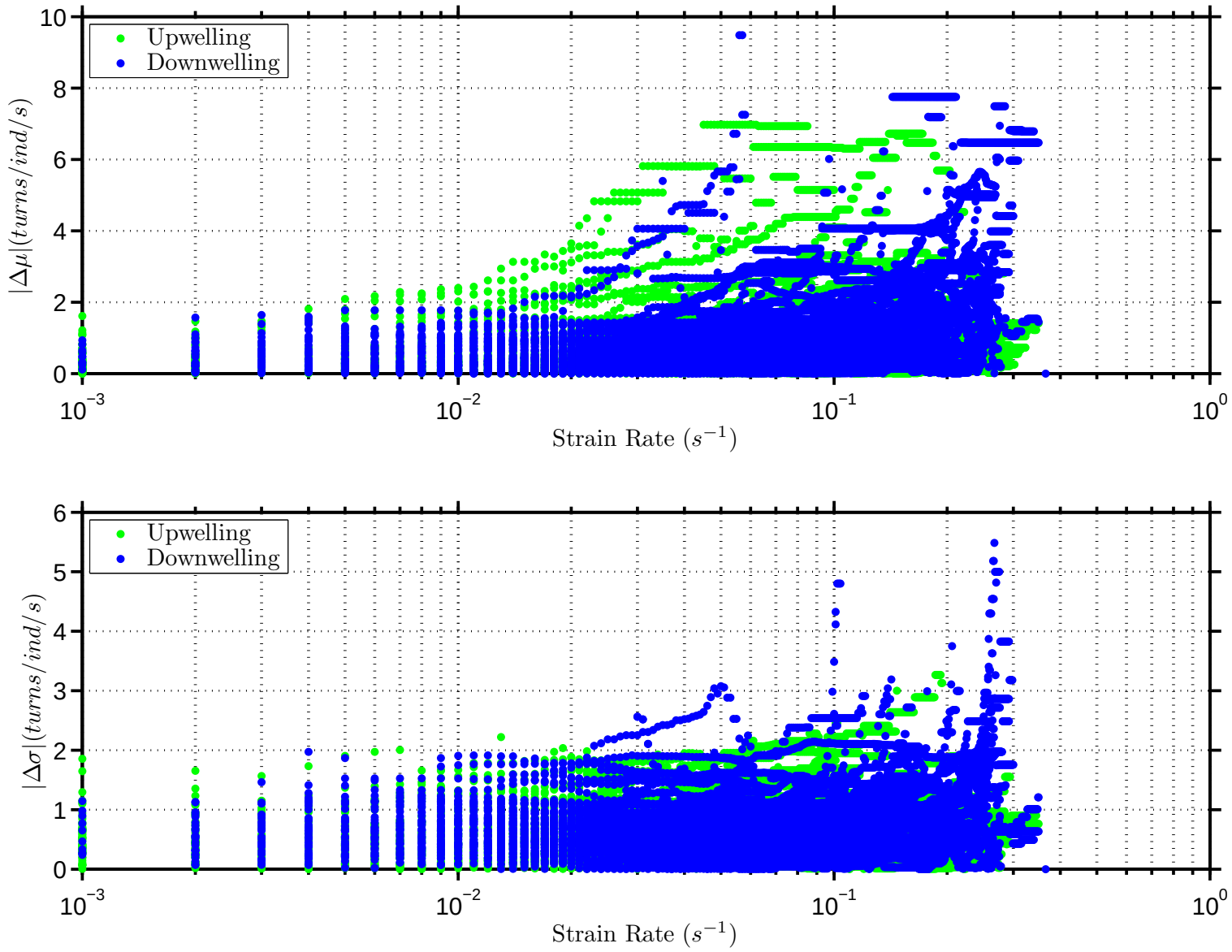

Figure 4.10: Cumulative Plot of Threshold Shear Strain Rate Analyses based on Turn Frequency for All Individual Trajectories of *Acartia negligens*. The top panel show differences in mean behavior above and below various strain rate values, and the bottom panel shows differences in behavioral variability (standard deviation) above and below various strain rate values, both as a function of threshold strain rate. See text for more information.

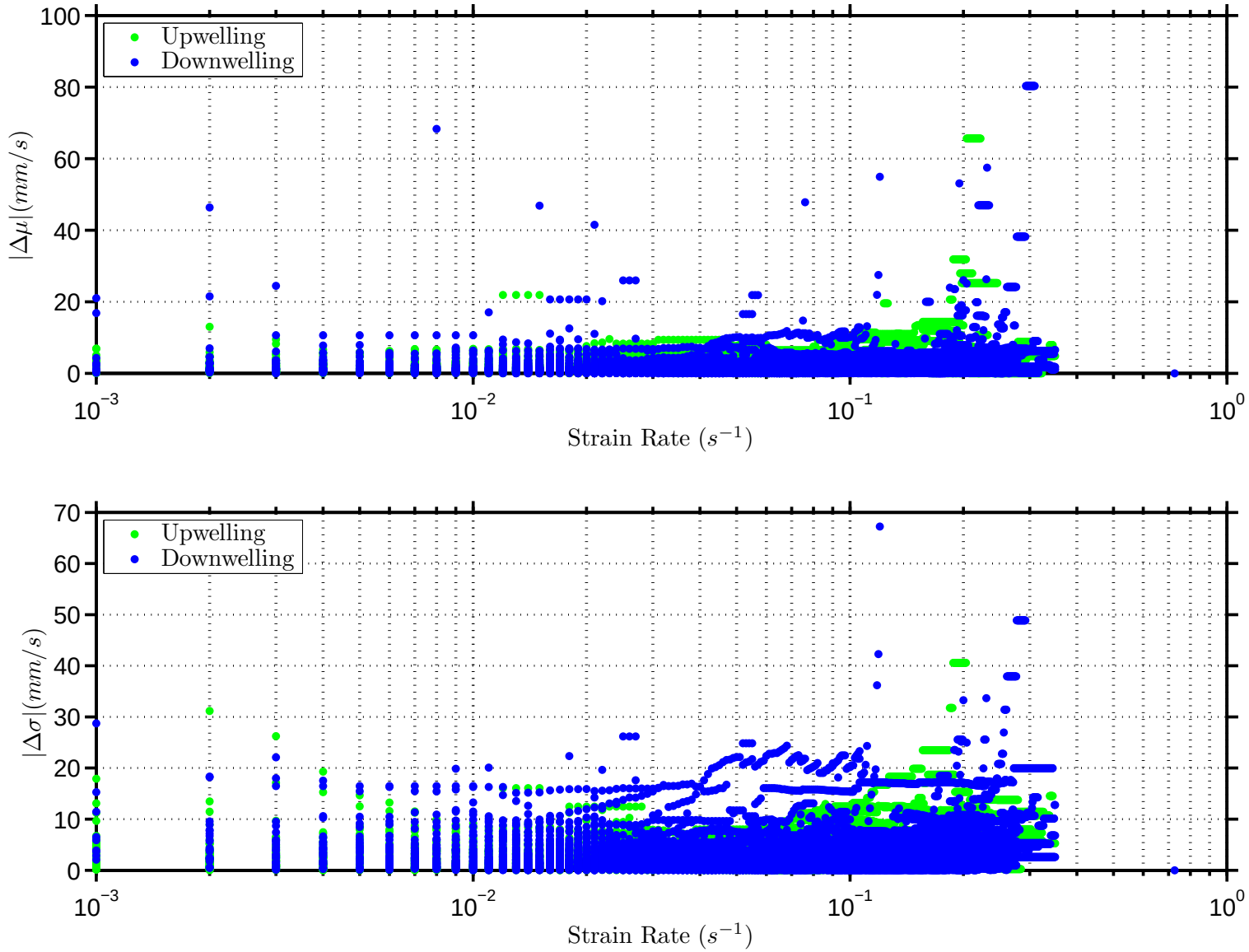

Figure 4.11: Cumulative Plot of Threshold Shear Strain Rate Analyses based on Relative Swimming Speed for All Individual Trajectories of *Acartia negligens*. The top panel show differences in mean behavior above and below various strain rate values, and the bottom panel shows differences in behavioral variability (standard deviation) above and below various strain rate values, both as a function of threshold strain rate. See text for more information.

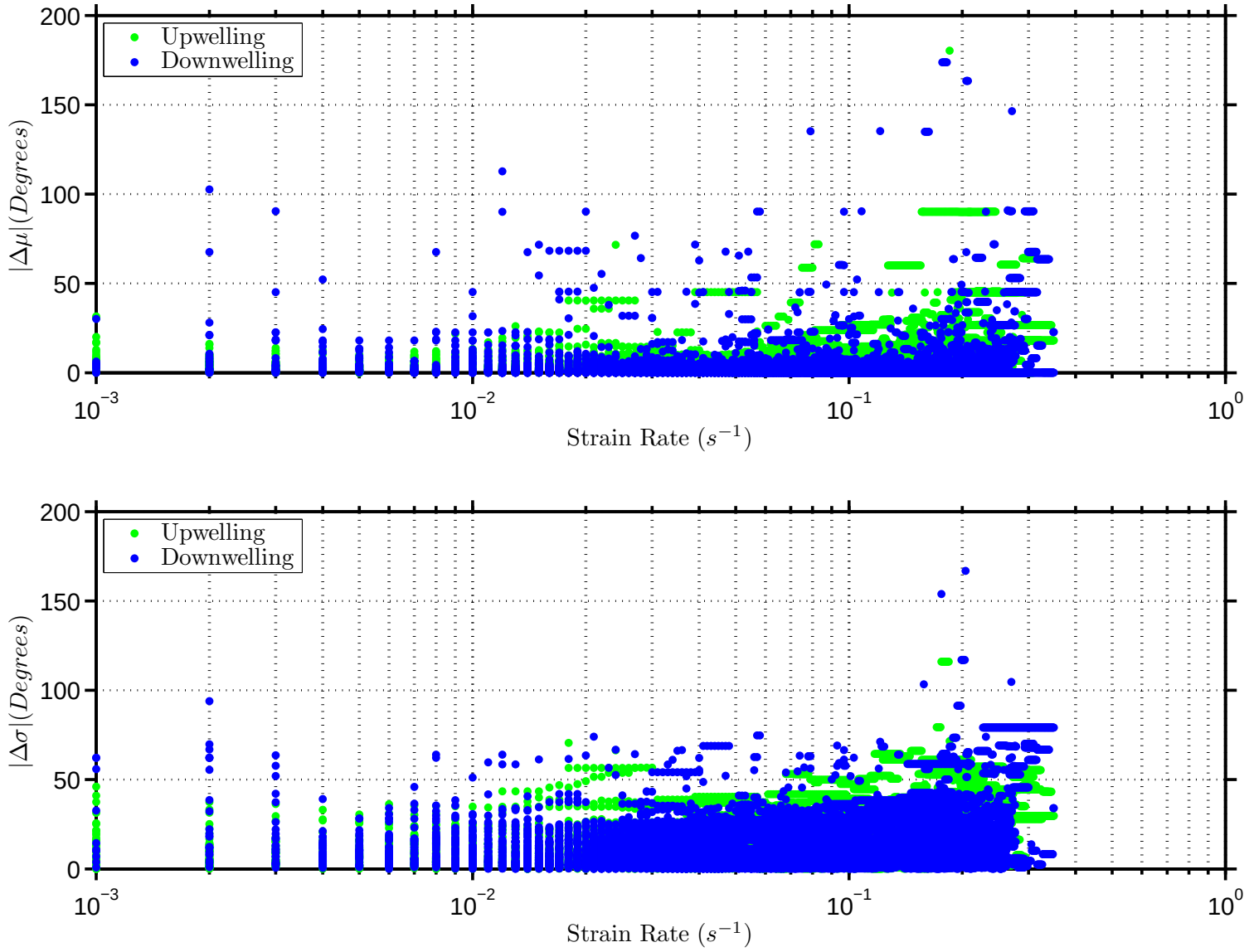

Figure 4.12: Cumulative Plot of Threshold Shear Strain Rate Analyses based on Directional Heading for All Individual Trajectories of *Acartia negligens*. The top panel show differences in mean behavior above and below various strain rate values, and the bottom panel shows differences in behavioral variability (standard deviation) above and below various strain rate values, both as a function of threshold strain rate. See text for more information.

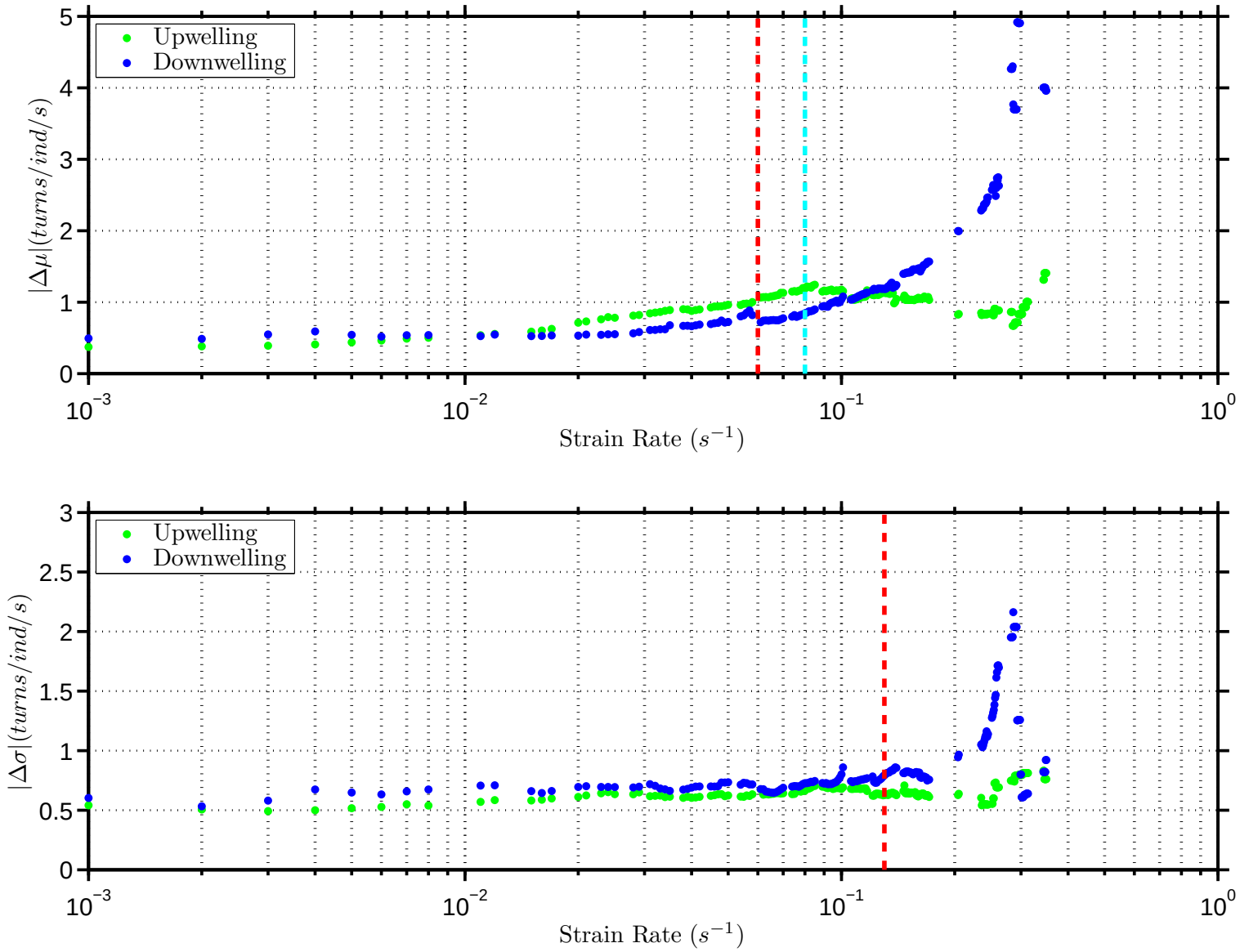

Figure 4.13: Population Ensemble of Turn Frequency versus Threshold Shear Strain Rate Values for *Acartia negligens*. Vertical Cyan Line Indicates Chosen Threshold Strain Rate Cutoff for Upwelling, Red Line for Downwelling. The Absence of a Threshold Line for Upwelling, Standard Deviation Plot Indicates that no Clear Threshold was Defined.

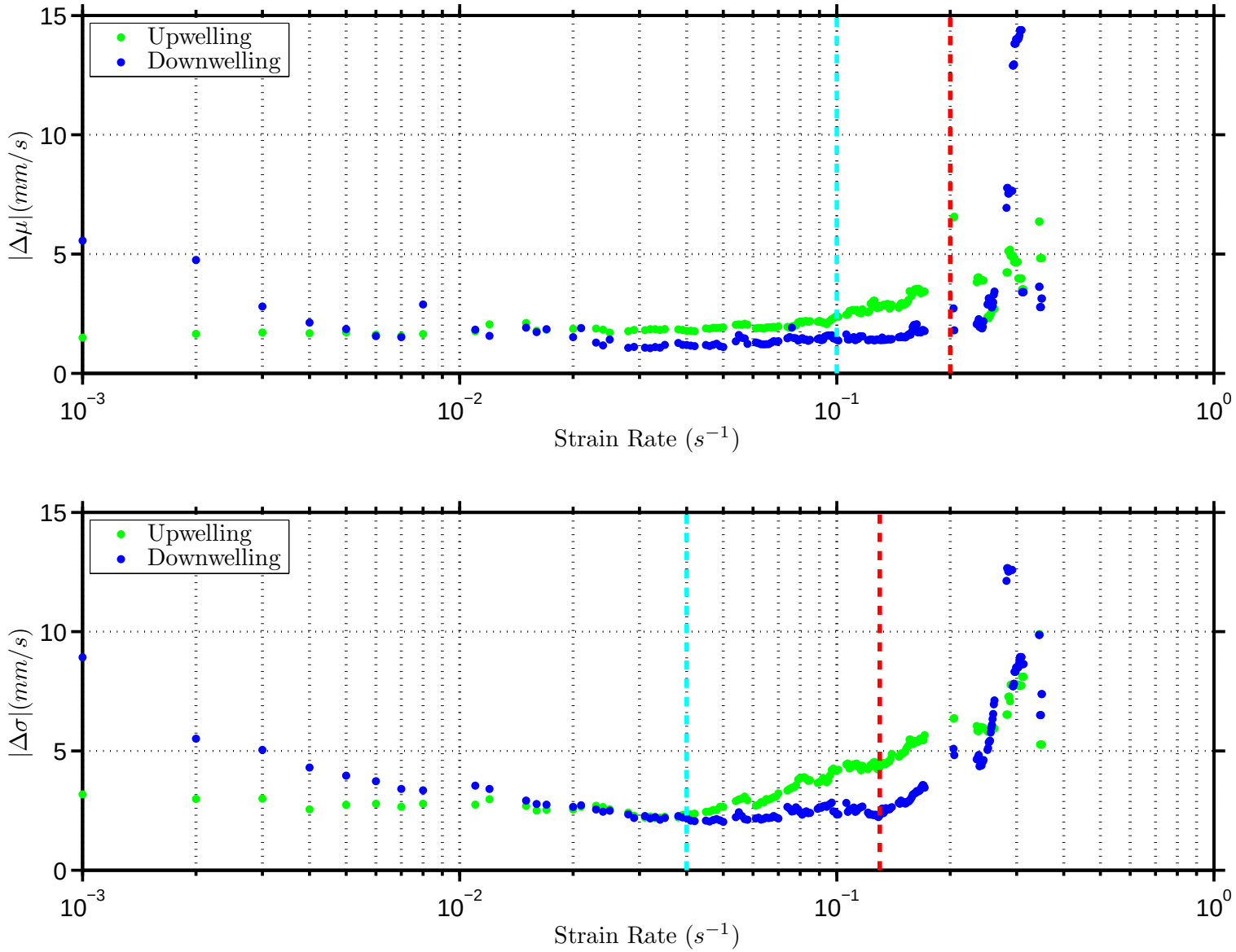

Figure 4.14: Population Ensemble of Swimming Speed versus Threshold Shear Strain Rate Values for *Acartia negligens*. Vertical Cyan Line Indicates Chosen Threshold Strain Rate Cutoff for Upwelling, Red Line for Downwelling.

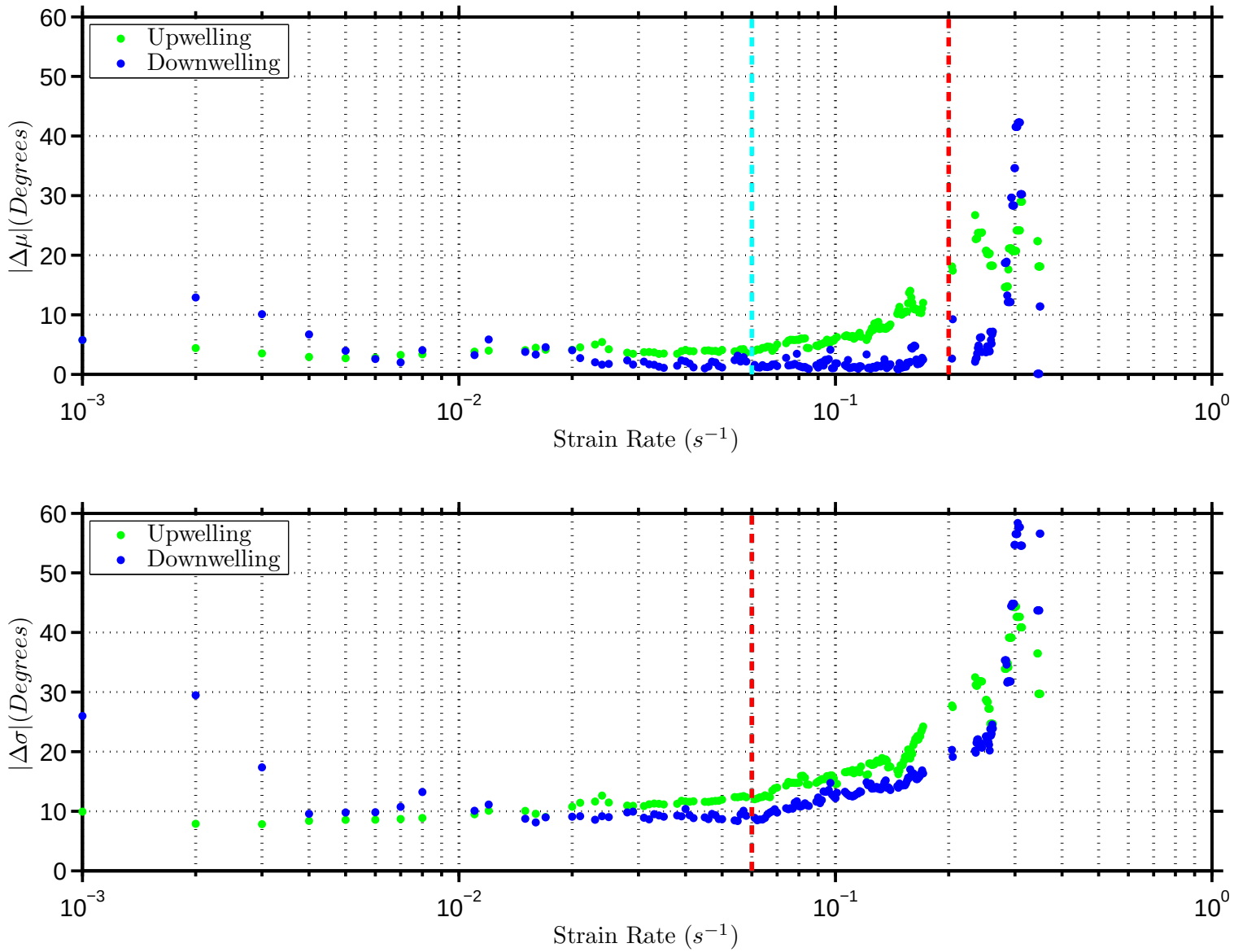

Figure 4.15: Population Ensemble of Change in Heading versus Threshold Shear Strain Rate Values for *Acartia negligens*. Vertical Cyan Line Indicates Chosen Threshold Strain Rate Cutoff for Upwelling, Red Line for Downwelling. Threshold Lines are Coincident on Standard Deviation Plot.

the analogous figures for all other species given in Figures 4.16 – 4.24, indicates the chosen threshold strain rate for upwelling conditions for a given behavioral parameter after close examination of the data. Similarly, the vertical red line in each of these figures indicates the chosen threshold strain rate for downwelling conditions for a given behavioral parameter. If a threshold is not clearly defined by the data, it is not considered in the final selection of a single threshold value. Once all threshold values have been selected for both mean (top panels) and standard deviation (bottom panel) data sets for all behavioral parameters (relative swimming speed, turn frequency, and directional heading) inder both upwelling and downwelling conditions for a single species, the arithmetic mean of all threshold values is taken as the single, species-specific behavioral threshold strain rate value. The same analyses were conducted for all species to determine threshold shear strain rate values that trigger changes in behavior. Figures 4.16 – 4.24 show the results of these analyses for the other three species tested, and Table 4.1 gives a summary of the final threshold shear strain rates for each species, as well as the range of thresholds observed.

It should be noted that there are inherent difficulties in defining a single threshold strain rate value due to the high levels of behavioral variability among individual zooplankters of a given species; however, it is absolutely necessary in order to continue the analysis and quantify the effects of vertical shear layers on zooplankton behavior. The methodology detailed above for defining species-specific threshold values is not perfectly objective, but it is the least subjective, most quantitative, and truest to the data possible given the experimental constraints and the available data sets. The final threshold strain rate values computed for each species accurately capture behavioral phenomena in both upwelling and downwelling conditions, as detailed in the discussions and statistical data below.

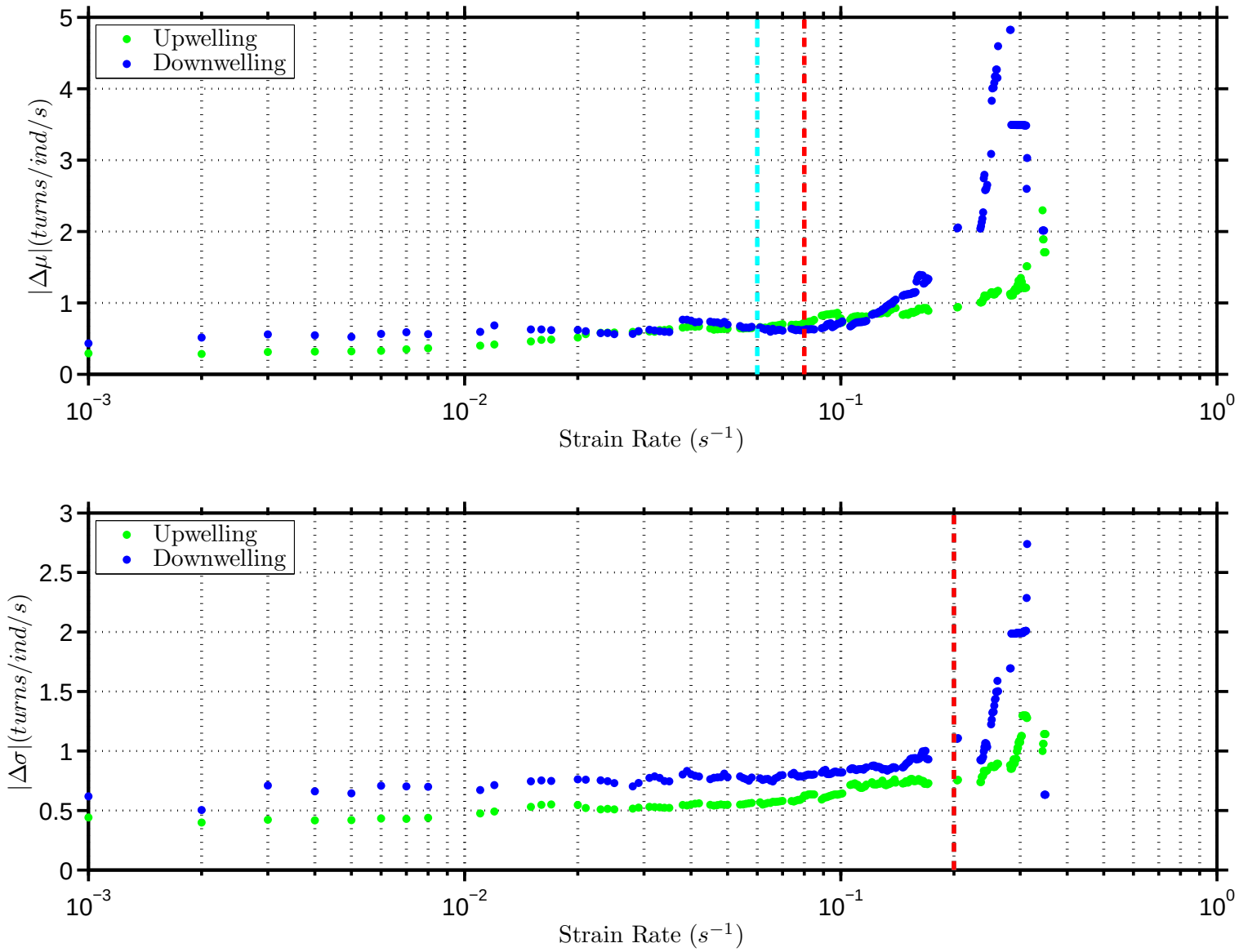

Figure 4.16: Population Ensemble of Turn Frequency versus Threshold Shear Strain Rate Values for *Clausocalanus furcatus*. Vertical Cyan Line Indicates Chosen Threshold Strain Rate Cutoff for Upwelling, Red Line for Downwelling. Threshold Lines are Coincident on Standard Deviation Plot.

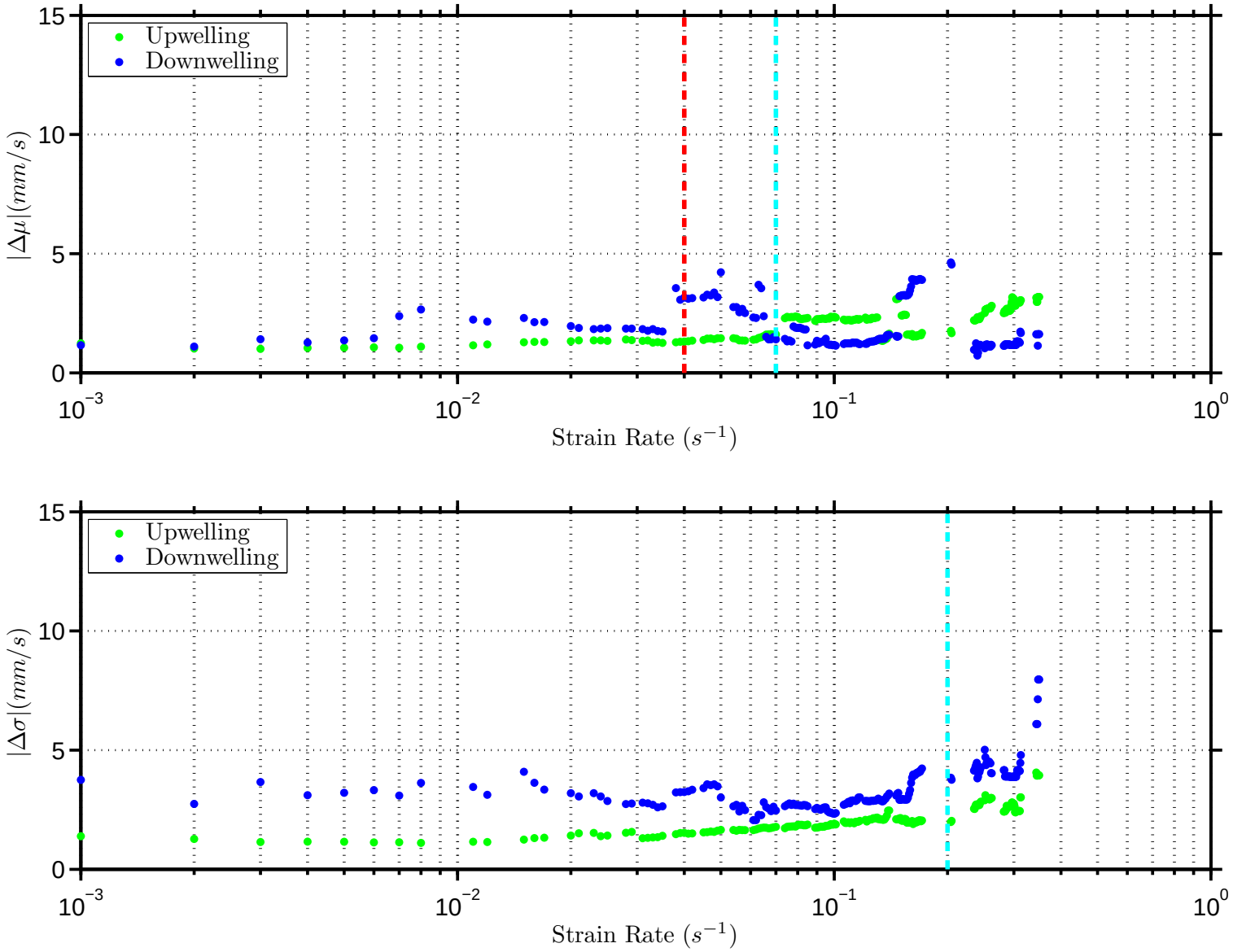

Figure 4.17: Population Ensemble of Swimming Speed versus Threshold Shear Strain Rate Values for *Clausocalanus furcatus*. Vertical Cyan Line Indicates Chosen Threshold Strain Rate Cutoff for Upwelling, Red Line for Downwelling. The Absence of a Threshold Line for Downwelling, Standard Deviation Plot Indicates that no Clear Threshold was Defined.

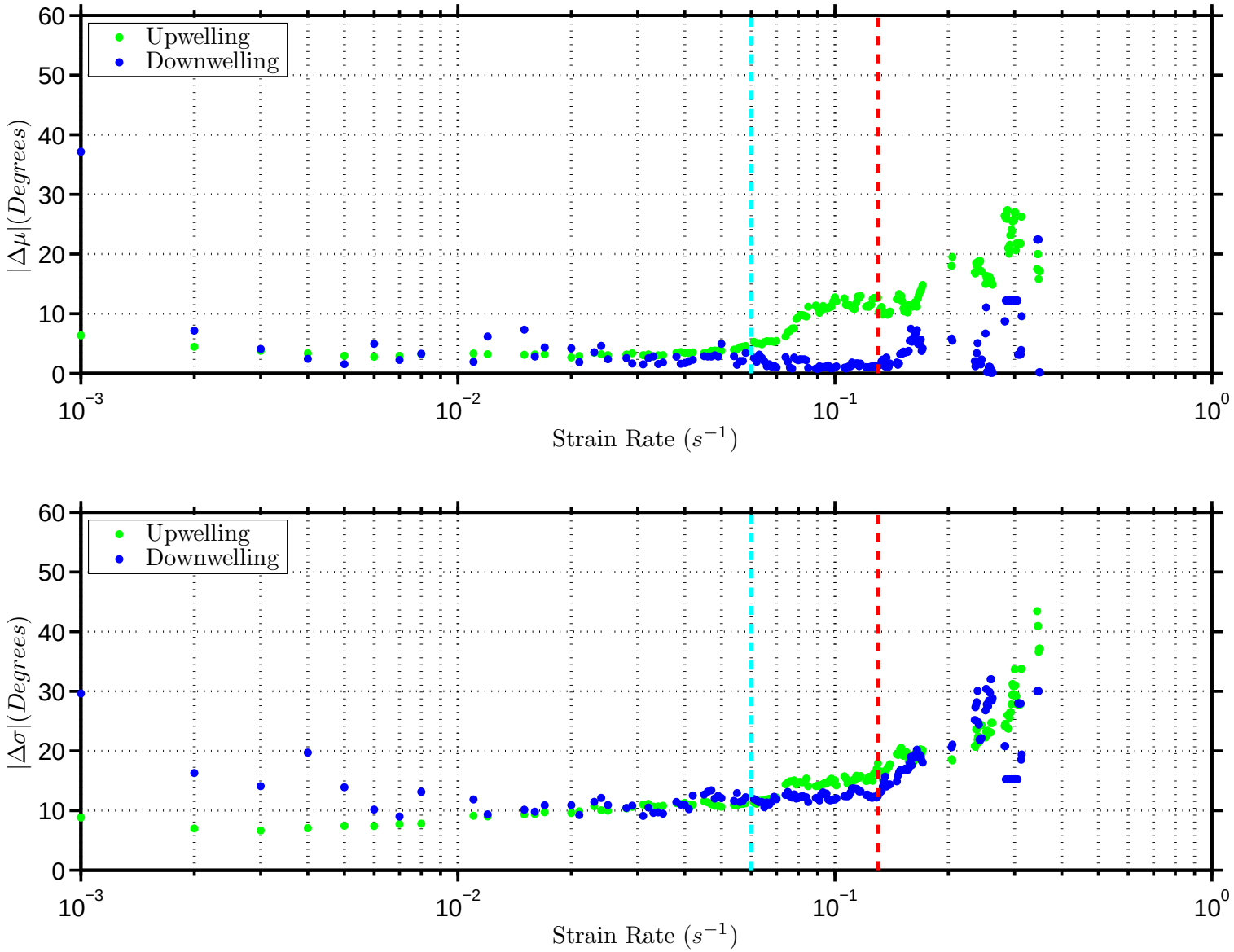

Figure 4.18: Population Ensemble of Change in Heading versus Threshold Shear Strain Rate Values for *Clausocalanus furcatus*. Vertical Cyan Line Indicates Chosen Threshold Strain Rate Cutoff for Upwelling, Red Line for Downwelling.

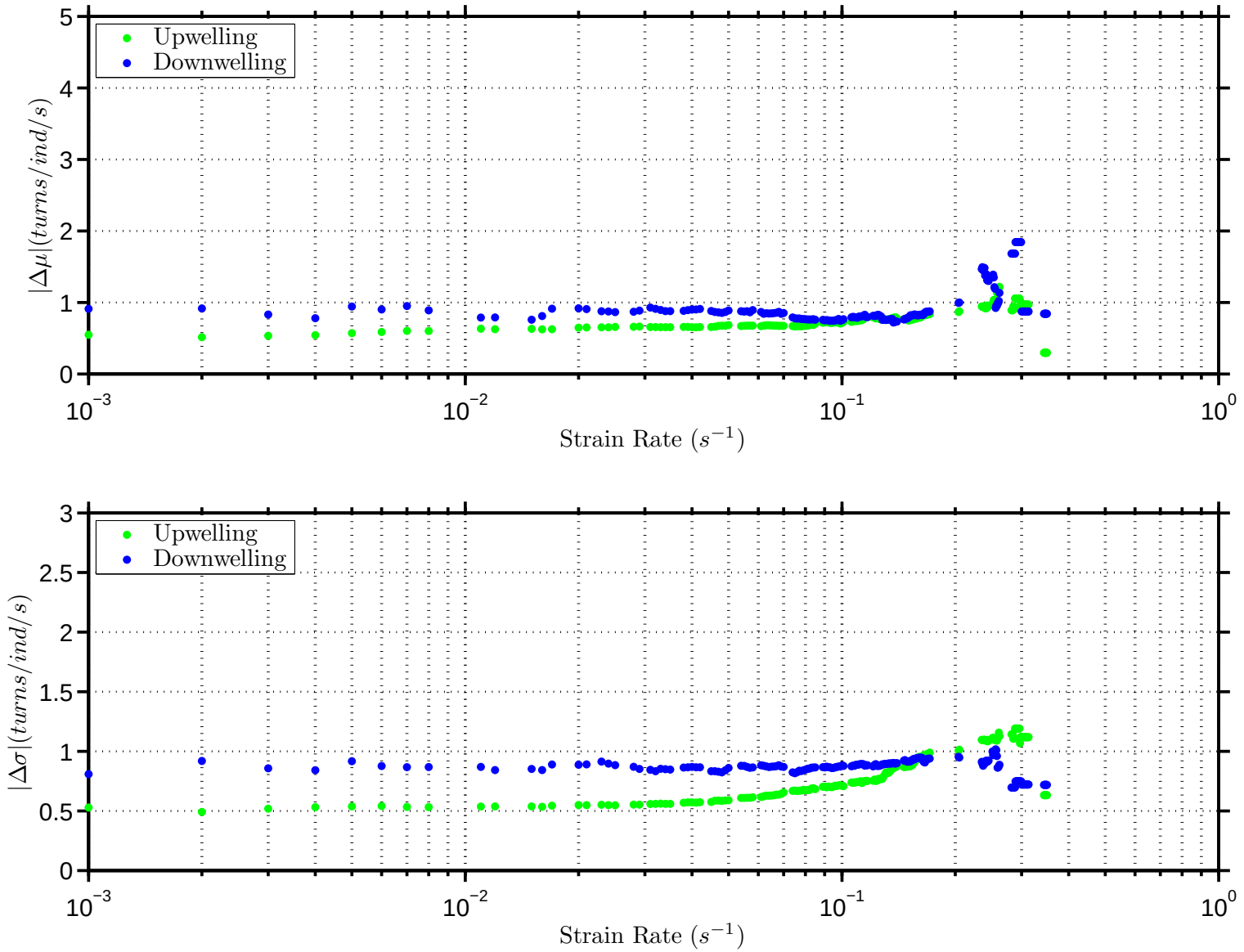

Figure 4.19: Population Ensemble of Turn Frequency versus Threshold Shear Strain Rate Values for *Panopeus herbstii*. Absence of Threshold Lines for both Plots Indicates that no Clear Thresholds were Defined.

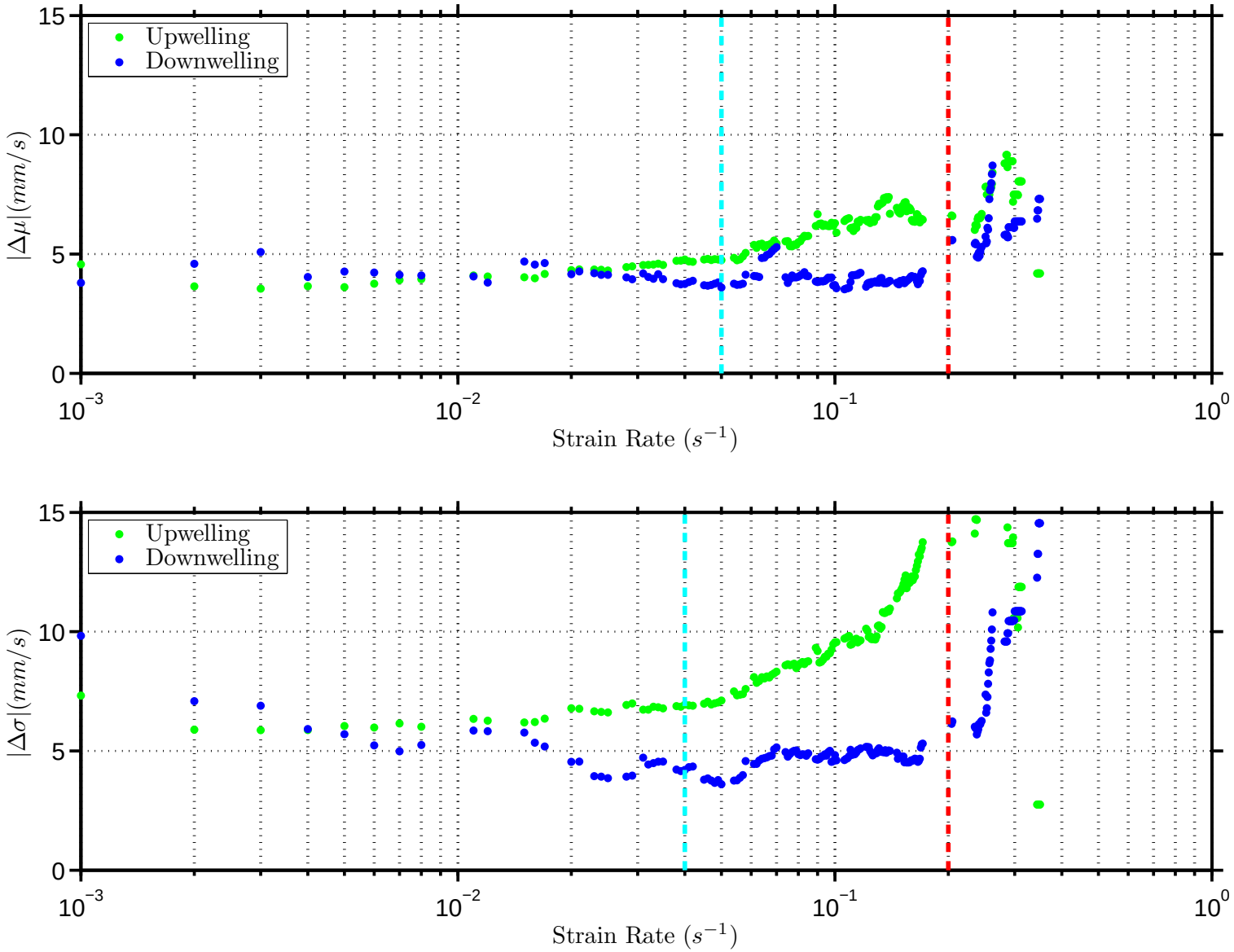

Figure 4.20: Population Ensemble of Swimming Speed versus Threshold Shear Strain Rate Values for *Panopeus herbstii*. Vertical Cyan Line Indicates Chosen Threshold Strain Rate Cutoff for Upwelling, Red Line for Downwelling.

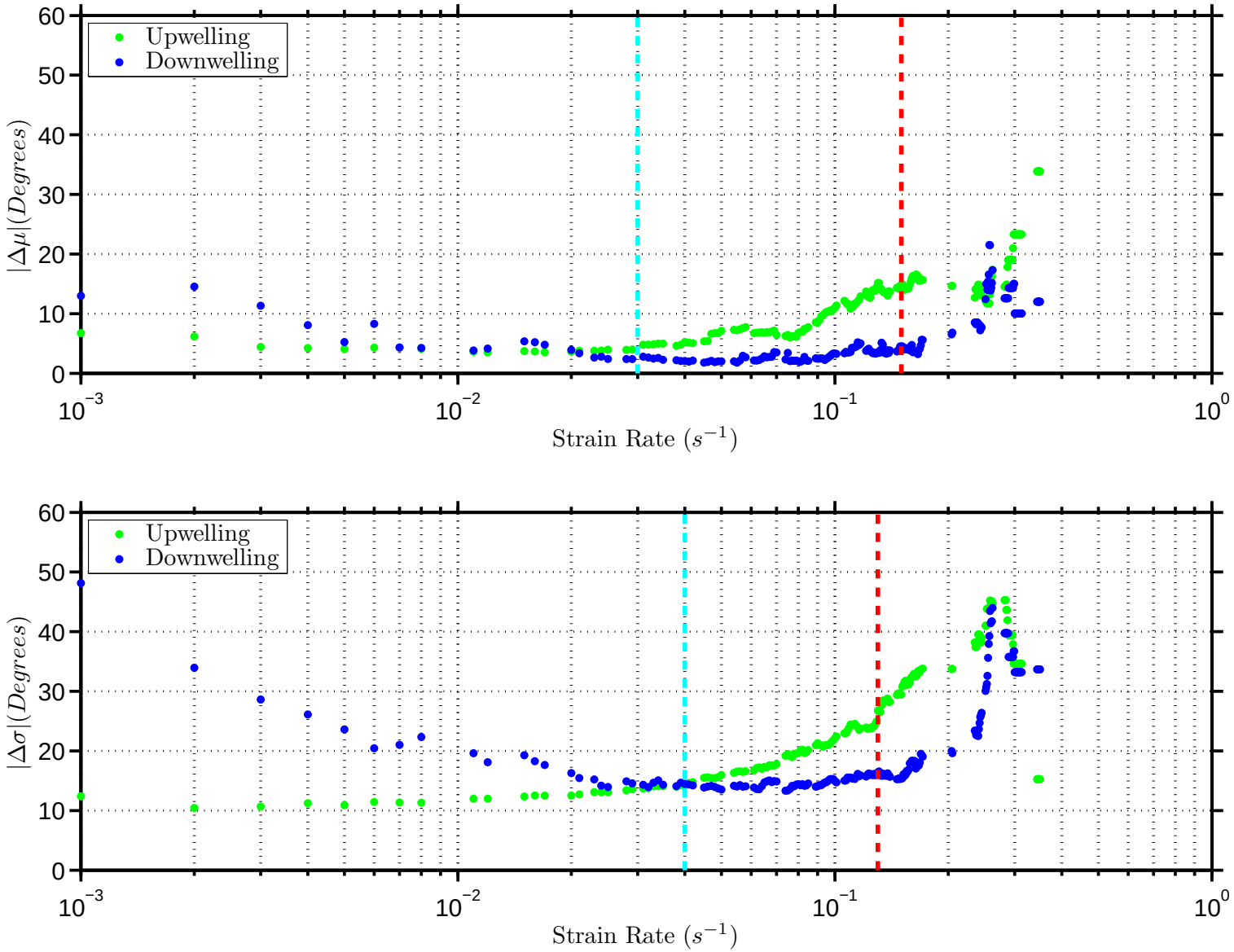

Figure 4.21: Population Ensemble of Change in Heading versus Threshold Shear Strain Rate Values for *Panopeus herbstii*. Vertical Cyan Line Indicates Chosen Threshold Strain Rate Cutoff for Upwelling, Red Line for Downwelling.

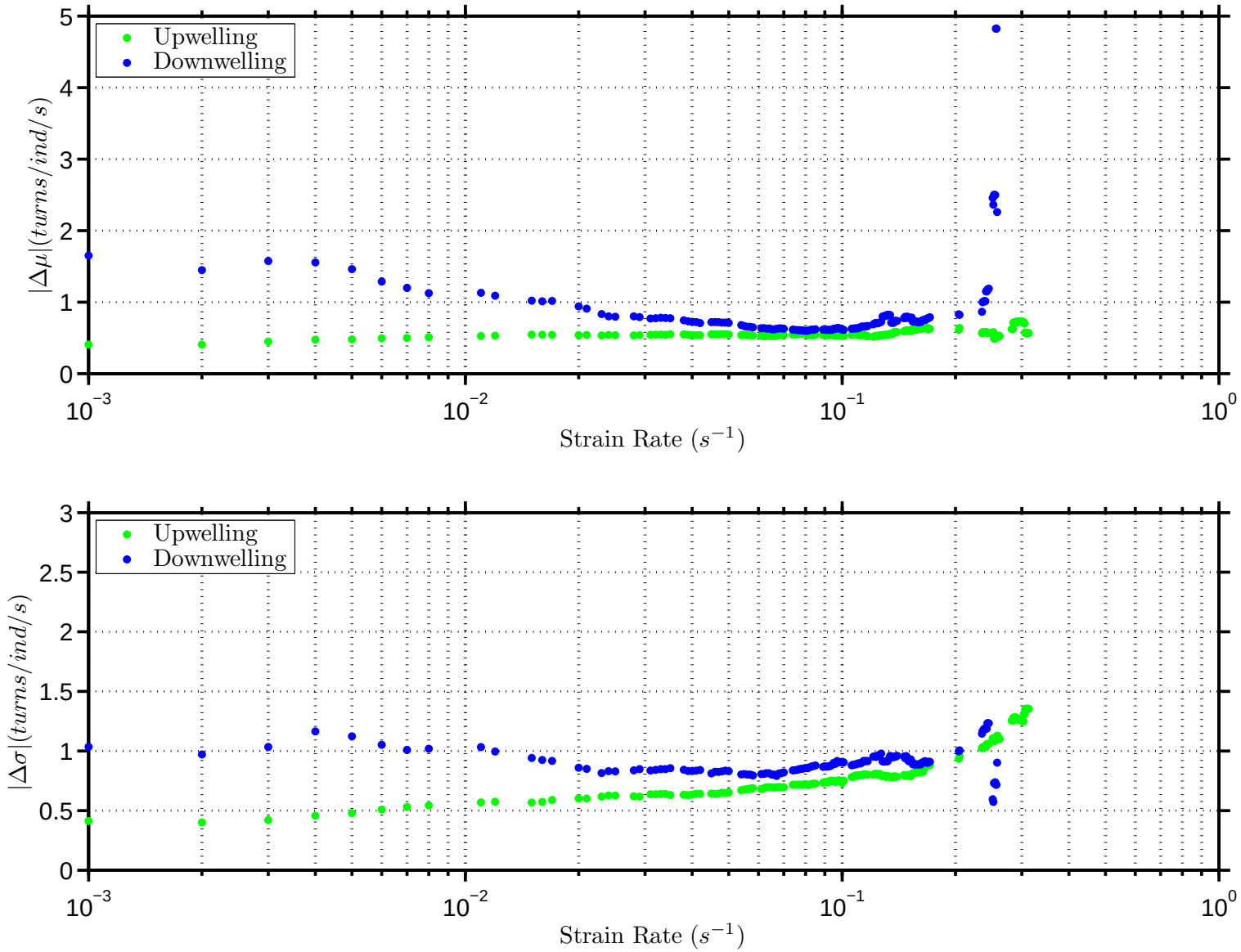

Figure 4.22: Population Ensemble of Turn Frequency versus Threshold Shear Strain Rate Values for *Neomysis americana*. Absence of Threshold Lines for both Plots Indicates that no Clear Thresholds were Defined.

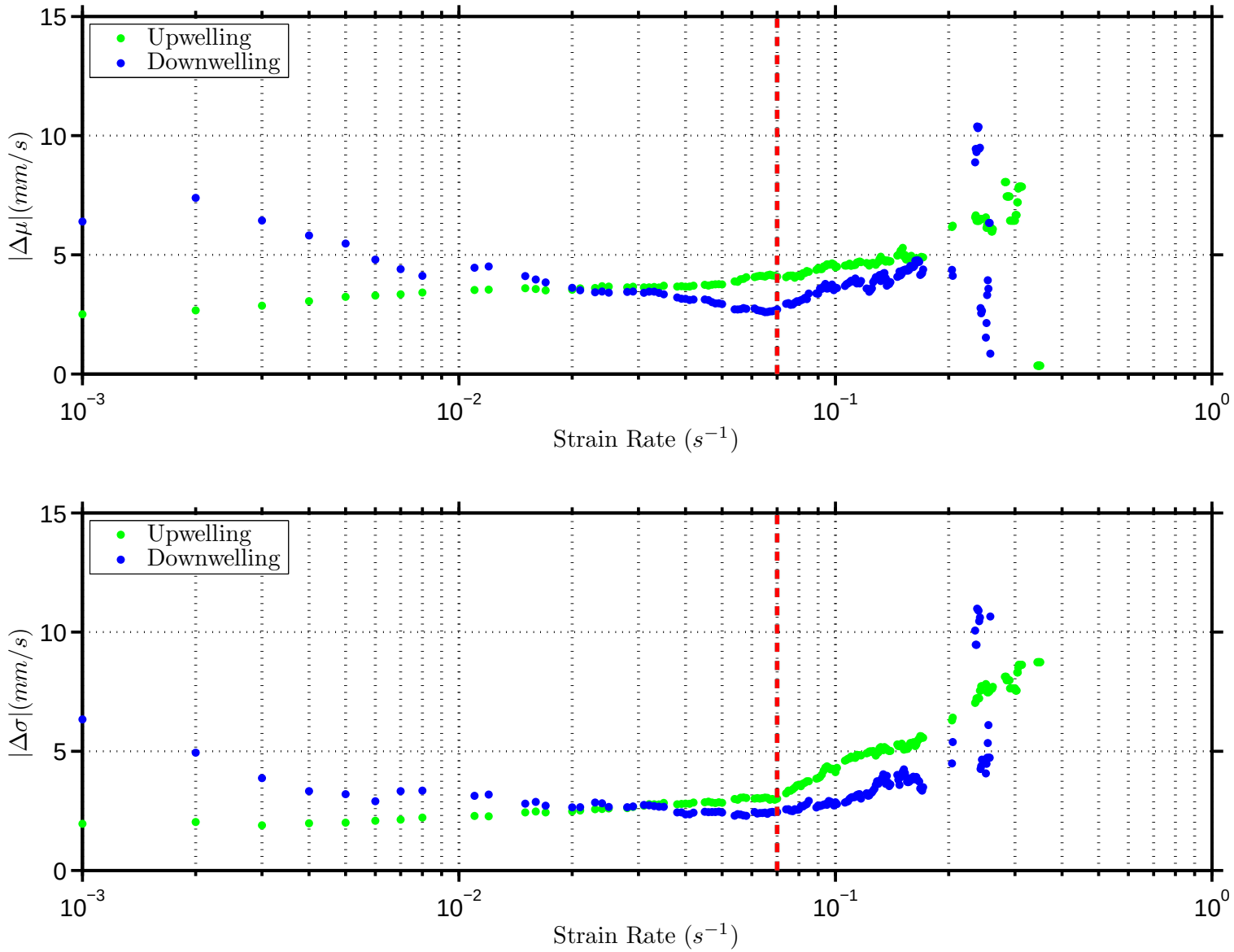

Figure 4.23: Population Ensemble of Swimming Speed versus Threshold Shear Strain Rate Values for *Neomysis americana*. Threshold Lines are Coincident for Both Plots.

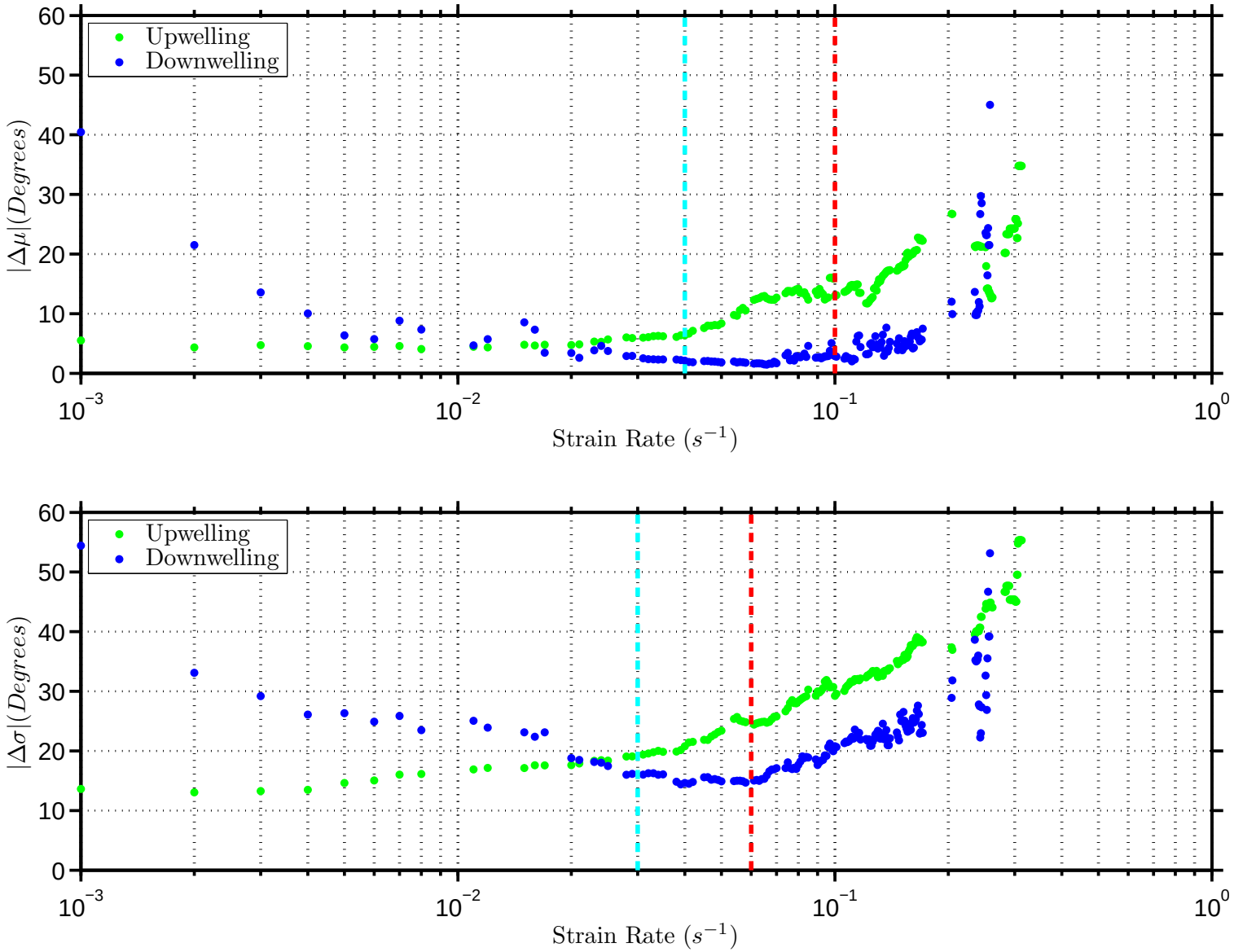

Figure 4.24: Population Ensemble of Change in Heading versus Threshold Shear Strain Rate Values for *Neomysis americana*. Vertical Cyan Line Indicates Chosen Threshold Strain Rate Cutoff for Upwelling, Red Line for Downwelling.

Table 4.1: Summary of Behavioral Threshold Shear Strain Rate Analyses for all Species

Species	Shear Strain Range (s^{-1})	Threshold Shear Strain (s^{-1})
Acartia negligens	0.04 - 0.2	0.08
Clausocalanus furcatus	0.04 - 0.2	0.08
Panopeus herbstii	0.03 - 0.2	0.1
Neomysis americana	0.03 - 0.1	0.065

4.2.2 Quantitative Behavioral Observations

The next stage of the analysis is to use the species-specific threshold shear strain rate values along with the PIV results for the shear strain rate field to divide the observation window into two geometric regions separated by the iso-contour of the threshold strain rate. Thus, the domain is divided into the "In-Layer" region (most shear strain rate values higher than threshold) and the "Out-of-Layer" region (all shear strain rate values lower than threshold). In this way, individual zooplankter trajectories can be analyzed by location (in-layer versus out-of-layer) as well as exposure to the threshold shear strain rate (pre-contact versus post-contact). Computing path kinematic parameters, such as relative swimming speed and turn frequency, in-layer versus out-of-layer as well as pre-contact versus post-contact allows us to investigate the statistical significance of change in animal behavior due to the presence of the shear layer. Additionally, gross trajectory parameters such as the vertical net-to-gross-displacement ratio ($VNGDR$ = net vertical displacement/gross vertical displacement) and the proportional residence time (PRT = time spent in-layer/total time in observation window) provide measures of the net effect of changes in behavior.

Statistical significance of changes in path kinematics (relative swimming speed, turn frequency) are investigated via a single factor, nested, repeated measures ANOVA between pre-contact and post-contact values and/or in-layer versus out-of-layer values. Similarly, statistical significance of changes in gross path parameters (PRT,

$NGDR$, $VNGDR$) are evaluated via a single factor, nested ANOVA between control and treatment (upwelling or downwelling) values. The single factor (or treatment) is the vertical shear layer itself, which has two treatments levels, upwelling and downwelling. The repeated measures aspect of the statistical analysis indicates that pre-contact versus post-contact or in-layer versus out-of-layer values are examined and compared for each individual zooplankter, not just the entire pre-contact (or in-layer) data set versus the entire post-contact (or out-of-layer) data set. This statistical design helps to account for individual variability in zooplankton behavior (e.g. male copepods typically swim faster than females Mauchline 1998, **?**). The general linear model is used because of the unbalanced design, whereas the nested aspect indicates that experimental replicate effects are tested for as a "factor" nested inside the treatment level. The data are pooled if replicate effects are insignificant and the pooled error variance is used. For some of the results presented below, experimental replicate effects are significant, but importantly the variance that this introduces in the analysis is accounted for in the nested design.

Examining the ANOVA results reported in Tables 4.2 – 4.6 sheds light on the effect of the finescale upwelling and downwelling shear layers in inducing behavioral responses in each zooplankter. The approach in interpretation will be to determine how shear-induced changes in path kinematics trickle up to larger scale phenomena, particularly in the context of foraging and high-density plankton aggregations. In Tables 4.2 and 4.3, three p-values are given from the ANOVA. The p-value reported in the first column (Layer Effect) indicates the significance of behavioral differences due to the effects of an upwelling versus downwelling jet on zooplankton. The p-value in the second column (Location Effect) indicates the significance of behavioral differences due to an individual zooplankters presence in the shear layer region versus outside of it, or pre-contact with the shear layer region versus post-contact. Finally, the p-value in the last column (Location by Layer Effect) indicates whether or not statistically

significant differences in in-layer versus out-of-layer or pre-contact versus post-contact are contingent upon layer type (i.e. upwelling versus downwelling). As shown in Tables 4.2 and 4.3, the repeated-measures portion of the ANOVA was conducted for "in-layer" versus "out-of-layer" for the copepods in contrast to "pre-contact" versus "post-contact" for the larger species. This was necessitated by the fact that an overwhelming proportion of the copepod trajectories entered the observation window "In-Layer" and thus there was no "Pre-contact" value for any behavioral parameter. Importantly, both analyses examine the same underlying question of the significance of the presence of the shear layer in inducing changes in behavior. Similarly, in Tables 4.4 and 4.6 the reported p-value (Treatment versus Control) evaluates the significance of either upwelling or downwelling shear layers in evoking changes in PRT, $NGDR$, or $VNGDR$ when compared to control values.

4.2.2.1 Acartia negligens

A. negligens showed an excited behavioral response through a statistically significant increase in relative swimming speed in-layer versus out-of-layer (Location Effect, p <0.0001, Table 4.2, Figure 4.25), indicating a direct behavioral response to the shear layer. The insignificant interaction effect (Location by Layer Effect, $p = 0.25$, Table 4.2) indicates that the behavioral response (i.e. increased relative swimming speed) was the same under upwelling and downwelling conditions, while the significant layer effect (Layer Effect, p <0.0001, Table 4.2) indicates that swimming speeds were higher on average under upwelling conditions.

A significant layer effect for turn frequency (Layer Effect, $p = 0.01$, Table 4.3, Figure 4.26) indicates that, as for relative swimming speed, turn frequency is higher on average under upwelling conditions. The significant interaction effect for turn frequency (Location by Layer Effect, $p = 0.04$, Table 4.3) indicates that changes in turn frequency in response to the shear layer show different trends under upwelling versus

Table 4.2: Single-factor, Repeated Measures ANOVA Results for Relative Swimming Speed. *Indicates Significant Difference for $p < 0.05$

Species and Flow Condition	n	In-Layer (mm/s)	Out-of-Layer (mm/s)	p (Layer Effect)	p (Location Effect)	p (Location by Layer Effect)
Acartia negligens						
Upwelling	39	9.0	7.6	< 0.0001*	< 0.0001*	0.25
Downwelling	72	6.8	6.0			
Clausocalanus furcatus						
Upwelling	56	6.6	5.2	0.15	0.01*	0.01*
Downwelling	40	6.5	6.6			
		Post-contact (mm/s)	Pre-contact (mm/s)	p (Layer Effect)	p (Exposure Effect)	p (Exposure by Layer Effect)
Panopeus herbstii						
Upwelling	80	19.7	18.0	0.68	0.96	0.02*
Downwelling	80	18.4	20.2			
Neomysis americana						
Upwelling	50	18.8	20.6	0.02*	0.03*	0.68
Downwelling	50	16.5	17.4			

Table 4.3: Single-factor, Repeated Measures ANOVA Results for Turn Frequency. * Indicates Significant Difference for p <0.05

Species and Flow Condition	n	In-Layer ($turn/ind/s$)	Out-of-Layer ($turn/ind/s$)	p (Layer Effect)	p (Location Effect)	p (Location by Layer Effect)
Acartia negligens						
Upwelling	39	6.7	7.0	0.01*	0.43	0.04*
Downwelling	72	6.5	5.9			
Clausocalanus furcatus						
Upwelling	56	6.1	5.8	0.29	0.04*	0.73
Downwelling	40	5.9	5.4			
		Post-contact ($turn/ind/s$)	Pre-contact ($turn/ind/s$)	p (Layer Effect)	p (Exposure Effect)	p (Exposure by Layer Effect)
Panopeus herbstii						
Upwelling	80	4.8	4.1	0.001*	0.002*	0.75
Downwelling	80	5.8	5.0			
Neomysis americana						
Upwelling	50	5.7	5.4	0.02*	0.17	0.78
Downwelling	50	6.6	6.1			

Table 4.4: Single-factor ANOVA Results for Proportional Residence Time. * Indicates Significant Difference for $p < 0.05$

Species and Flow Condition	n	PRT	p (Treatment to Control)
Acartia negligens			
Upwelling	39	0.43	0.44
Downwelling	72	0.39	0.76
Control	54	0.42	
Clausocalanus furcatus			
Upwelling	56	0.48	< 0.0001*
Downwelling	40	0.40	< 0.0001*
Control	24	0.22	
Panopeus herbstii			
Upwelling	80	0.31	0.95
Downwelling	80	0.31	0.98
Control	40	0.37	
Neomysis americana			
Upwelling	50	0.37	0.02*
Downwelling	50	0.45	< 0.0001*
Control	25	0.30	

Table 4.5: Single-factor ANOVA Results for Net-to-Gross-Displacement Ratio ($NGDR$). * Indicates significant difference for p <0.05.

Species and Flow Condition	n	$NGDR$	p (Treatment to Control)
Acartia negligens			
Upwelling	39	0.54	< 0.0001*
Downwelling	72	0.43	< 0.0001*
Control	54	0.18	
Clausocalanus furcatus			
Upwelling	56	0.51	< 0.0001*
Downwelling	40	0.51	< 0.0001*
Control	24	0.24	
Panopeus herbstii			
Upwelling	80	0.55	0.08
Downwelling	80	0.61	0.49
Control	40	0.65	
Neomysis americana			
Upwelling	50	0.60	0.84
Downwelling	50	0.51	0.14
Control	25	0.63	

Table 4.6: Single-factor ANOVA Results for Vertical-Net-to-Gross-Displacement Ratio ($VNGDR$). * Indicates significant difference for p <0.05.

Species and Flow Condition	n	$VNGDR$	p (Treatment to Control)
Acartia negligens			
Upwelling	39	0.61	< 0.0001*
Downwelling	72	0.47	0.003*
Control	54	0.25	
Clausocalanus furcatus			
Upwelling	56	0.56	< 0.0001*
Downwelling	40	0.62	< 0.0001*
Control	24	0.24	
Panopeus herbstii			
Upwelling	80	0.48	0.04*
Downwelling	80	0.50	0.08
Control	40	0.61	
Neomysis americana			
Upwelling	50	0.45	0.29
Downwelling	50	0.46	0.41
Control	25	0.55	

downwelling conditions. Namely, turn frequency remained statistically unchanged under upwelling conditions and increased under downwelling conditions (Table 4.3). Interestingly, a significant interaction term has the potential to mask the significance of individual levels of the main effect (i.e. location effects under upwelling versus downwelling conditions), as is the case for turn frequency here (Location Effect, $p = 0.43$, Table 4.3).

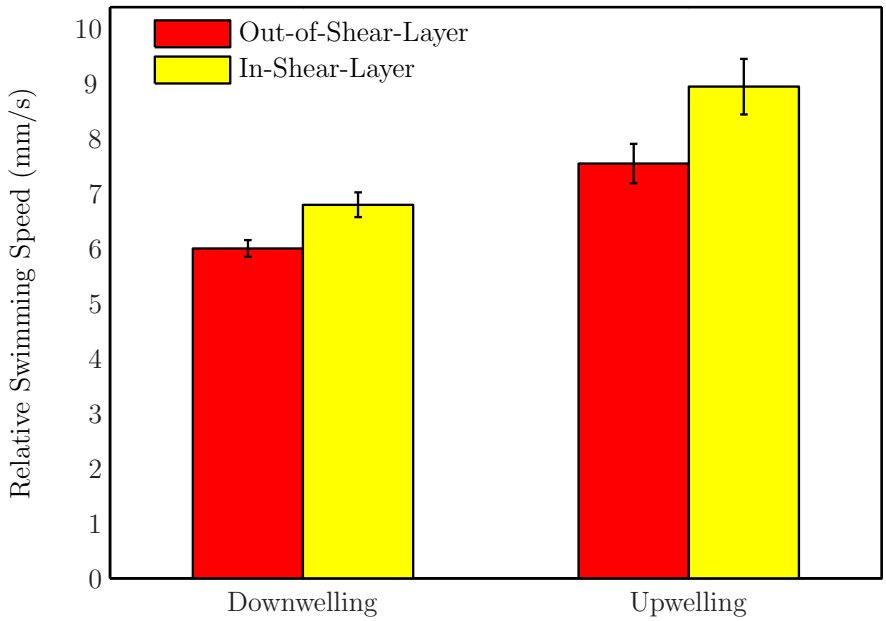

Figure 4.25: Relative Swimming Speed Responses in Upwelling and Downwelling Treatments for *Acartia negligens*. Error bars span a range of twice the standard error.

To more clearly assess the potential of finescale vertical shear layers to induce population scale aggregations of *A. negligens*, it is useful to examine changes in gross path parameters such as net-to-gross-displacement-ratio ($NGDR$) and proportional residence time (PRT) (Tables 4.4 and 4.5, Figure 4.27). Under upwelling conditions, this particular combination (i.e. the magnitude of the changes) of increased relative swimming speed and unchanged turn frequency in response to the shear layer resulted in no change in proportional residence time (Treatment to Control, $p = 0.44$, Table 4.4) as the animals simply cruised through the shear layer. Similarly under downwelling conditions, the combination of increased relative swimming speed

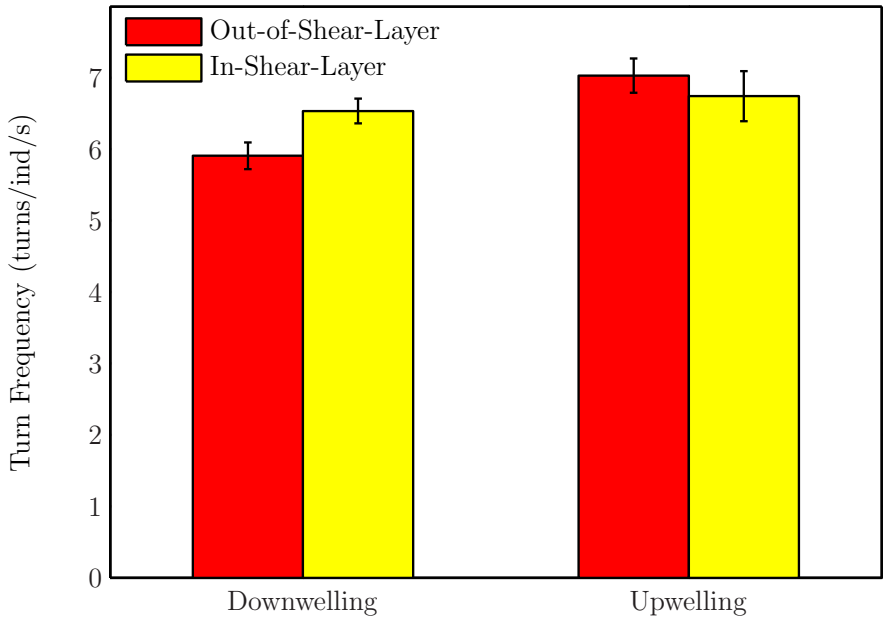

Figure 4.26: Turn Frequency Responses in Upwelling and Downwelling Treatments for *Acartia negligens*. Error bars span a range of twice the standard error.

and increased turn frequency in response to the shear layer resulted in no change in residence time (Treatment to Control, $p = 0.76$, Table 4.4, Figure 4.27).

It is important, however, to understand that observing a significant change in PRT is dependent on the spatial scale of behavioral observations. For example, if we observed animal behavior in a 50 cm by 50 cm window, rather than a 10 cm by 10 cm window, it is possible that larger scale aggregative phenomena would be revealed. For this reason, it is useful to further examine parameters which describe gross properties of zooplankton trajectories, such as the net-to-gross-displacement-ratio ($NGDR$). Significant increases in $NGDR$ were observed under both upwelling and downwelling conditions when compared to control values (p <0.0001 Upwelling; p <0.0001 Downwelling; Table 4.5, Figure 4.28). An increase in $NGDR$ indicates that copepod trajectories become more linear and less sinuous under both shear layer treatments.

To gain further insight into the potential for upwelling and downwelling shear layers to affect the vertical distribution of *A. negligens* populations, it is useful

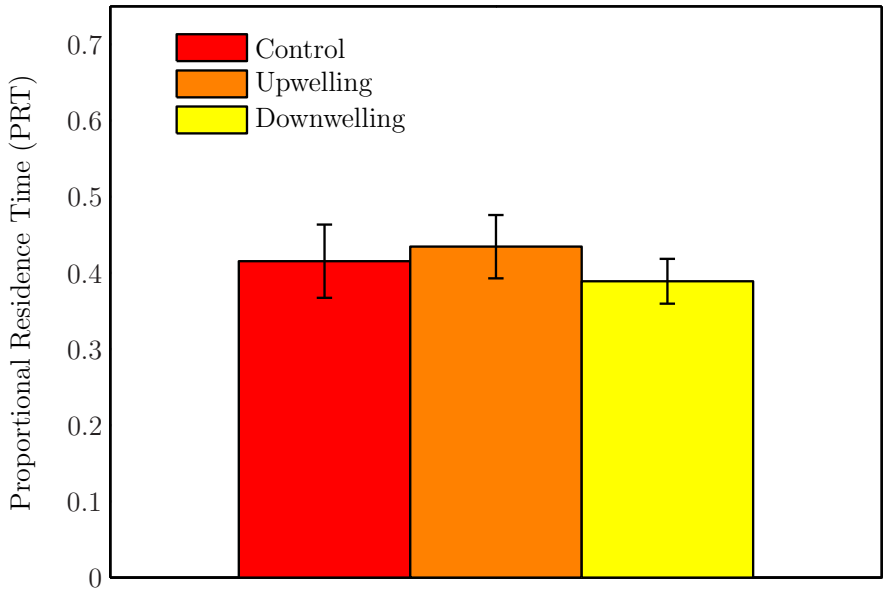

Figure 4.27: Proportional Residence Time (PRT) in Various Treatments for *Acartia negligens*. Error bars span a range of twice the standard error.

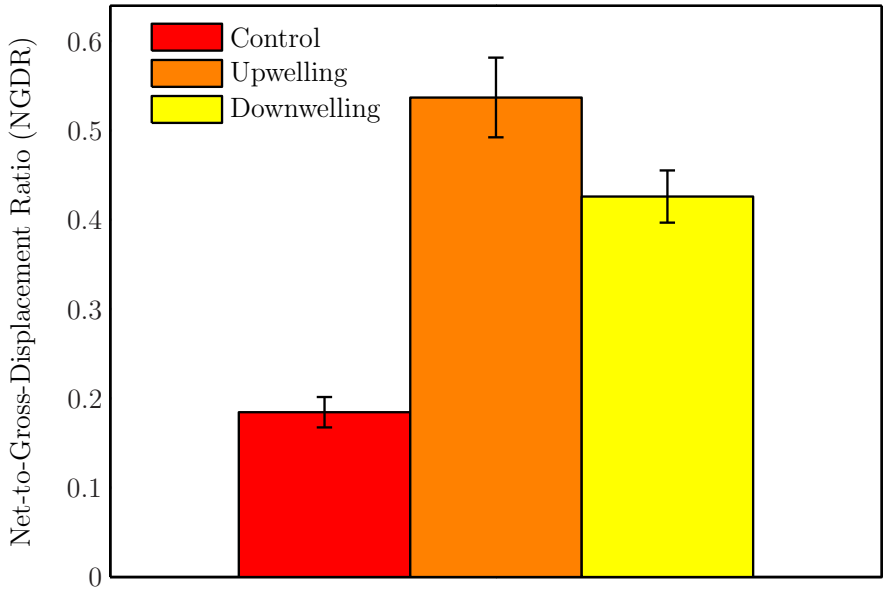

Figure 4.28: Net-to-Gross-Displacement Ratio ($NGDR$) in Various Treatments for *Acartia negligens*. Error bars span a range of twice the standard error.

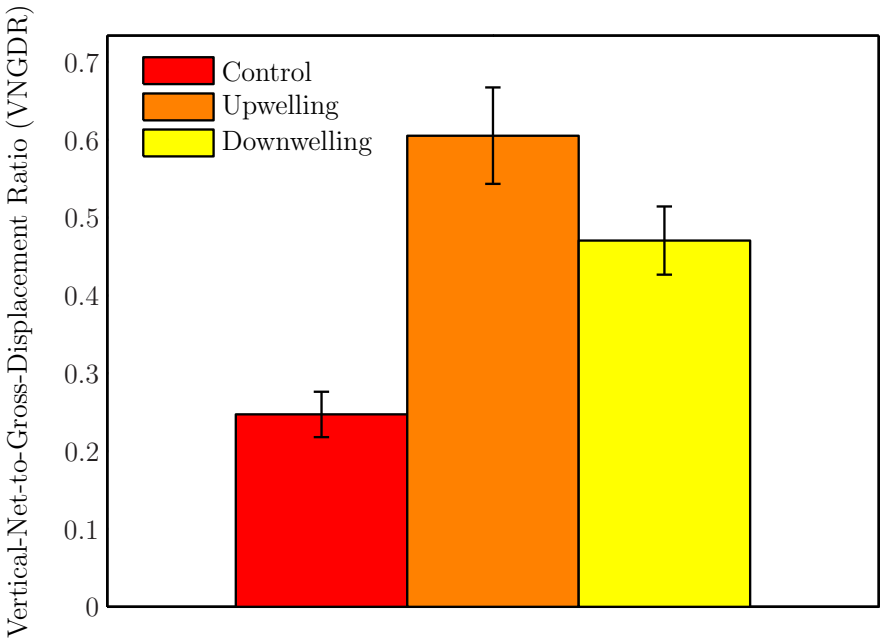

Figure 4.29: Vertical-Net-to-Gross-Displacement Ratio ($VNGDR$) in Various Treatments for *Acartia negligens*. Error bars span a range of twice the standard error.

to consider the *vertical*-net-to-gross-displacement-ratio ($VNGDR$). An increase in $VNGDR$ indicates that path trajectories become more linear vertically and that vertical displacement is not retraced throughout the course of the trajectory. Similarly, a decrease in $VNGDR$ indicates that all vertical displacement throughout the course of a trajectory was retraced, yielding low net vertical displacement. Significant increases in $VNGDR$ were observed under both upwelling and downwelling conditions when compared to control values (p <0.0001 Upwelling; $p = 0.003$ Downwelling; Table 4.6, Figure 4.29) indicating that the presence of the vertical shear layer causes a preferential alignment of the trajectory parallel to the shear strain rate isocontours (i.e. parallel to the gravity vector).

More information about population-level behavioral phenomena is gained by looking at histograms of $VNGDR$ under control and shear layer treatments (Figure 4.30). A $VNGDR$ histogram can be viewed as a spectra of depth-keeping behavior, where

low values ($\rightarrow 0$) indicate "U-shaped" or "C-shaped" trajectories with low net vertical transport and thus strong depth-keeping behavior. Similarly, high $VNGDR$ values ($\rightarrow 1$) indicate straight vertical trajectories with high net vertical transport and thus weak depth-keeping behavior, referred to here as active vertical advection. For *A. negligens*, it is clear that even though on average $VNGDR$ did increase, there was also a spread of population $VNGDR$ values towards both low and high values resulting in a somewhat bimodal distribution. This suggests that significant portions of the population were explicitly exhibiting both depth-keeping behavior (low $VNGDR$ values) and active vertical advection (high $VNGDR$ values). It is possible, but not *explicitly* shown in the data here, that straight vertical trajectories are simply portions of larger scale "U-shaped" or "C-shaped" trajectories, which would indicate that both are revealing similar behavioral phenomena on different spatial scales. Nonetheless, what is explicitly seen in the data for *A. negligens* is that not only do vertical shear layers cause a preferential trajectory alignment to the vertical along the shear isocontours (high $VNGDR$ values), but copepods are also resisting large scale vertical advection through depth-keeping behavior (low $VNGDR$ values), at least when gradients of vertical velocity are readily coherent and sensible and other sensory cues are absent.

4.2.2.2 Clausocalanus furcatus

The other calanoid copepod tested, *C. furcatus*, exhibited behavioral responses similar to *A. negligens*, but with some exceptional differences. As with *A. negligens*, *C. furcatus* showed excited behavior through a statistically significant increase in relative swimming speed in-layer versus out-of-layer (Location Effect, $p = 0.01$, Table 4.2), again indicating a direct behavioral response to the shear layer; however, responses to upwelling and downwelling were significantly different (Location by Layer Effect, $p = 0.01$, Table 4.2) such that relative swimming speeds increased under upwelling

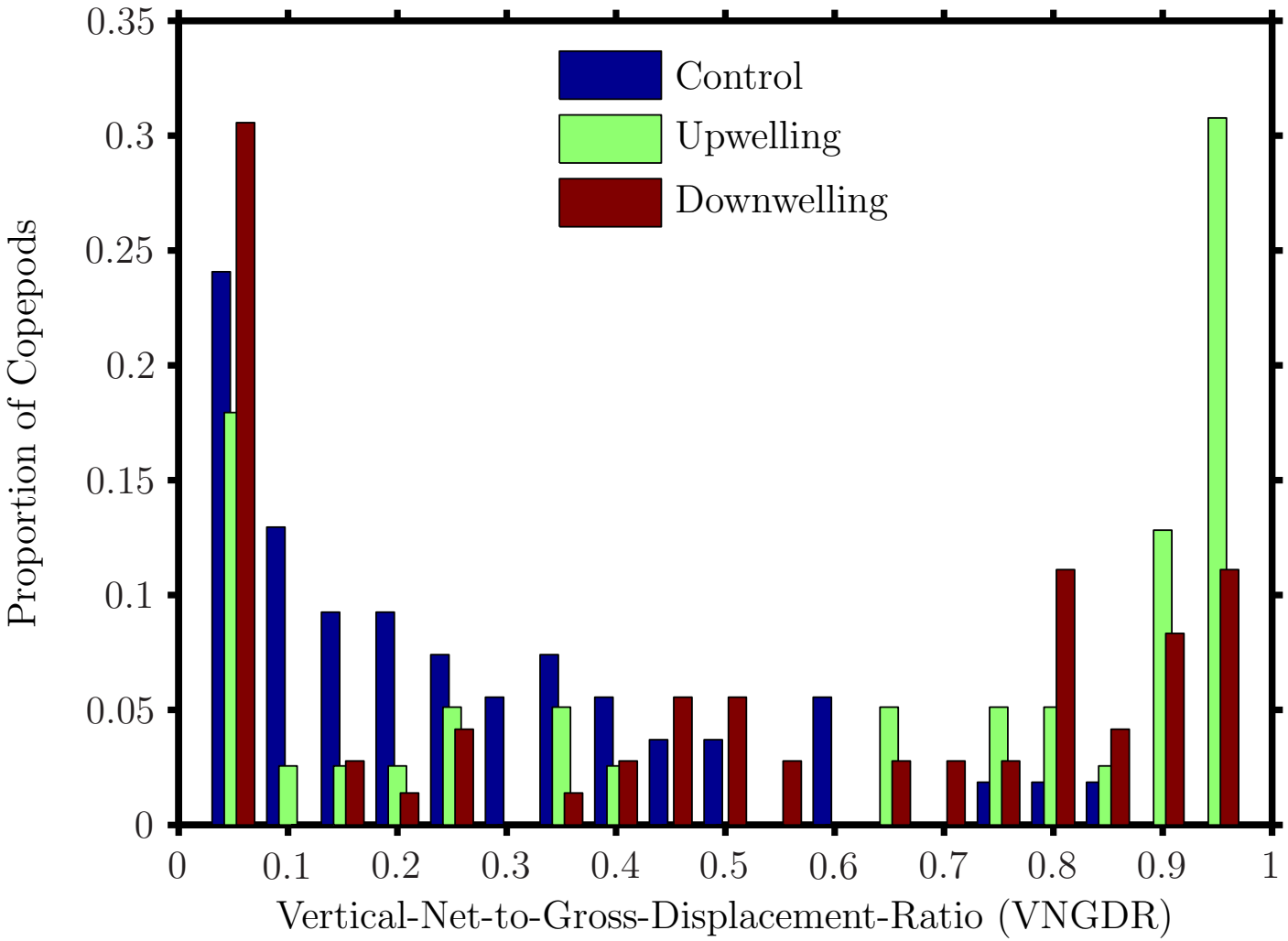

Figure 4.30: Histograms $VNGDR$ in Various Treatments for *Acartia negligens*

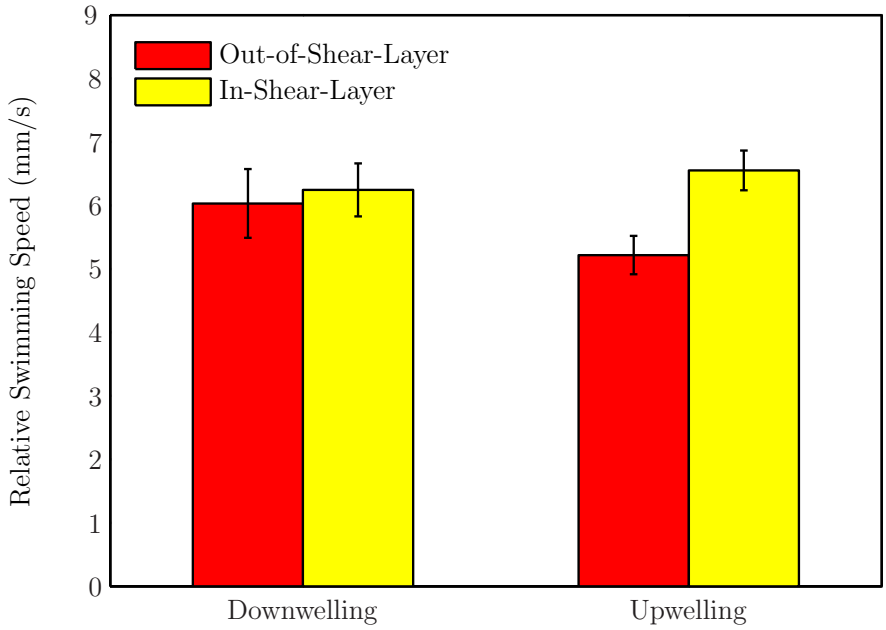

Figure 4.31: Relative Swimming Speeds in Upwelling and Downwelling Treatments for *Clausocalanus furcatus*. Error bars span a range of twice the standard error.

conditions and remained statistically unchanged under downwelling conditions (Table 4.2, Figure 4.31). Furthermore, in contrast to *A. negligens*, relative swimming speeds were, on average, equal under upwelling and downwelling conditions (Layer Effect, $p = 0.15$, Table 4.2).

C. furcatus showed significant increases in turn frequency in-layer versus out-of-layer for both upwelling and downwelling shear layers (Location Effect, $p = 0.04$, Location by Layer Effect, $p = 0.73$, Table 4.3). As with relative swimming speed, *C. furcatus* showed statistically identical turn frequencies, on average, under upwelling and downwelling conditions, indicating that it is the presence of the shear layer itself that is important in producing behavioral responses (Table 4.3, Figure 4.32).

Here, the combined effects of an increased (upwelling) or unchanged (downwelling) relative swimming speed in-layer plus an increased (upwelling and downwelling) turn frequency resulted in a significant increase in PRT for both upwelling and downwelling shear layer treatments when compared to control values (Layer to Control, $p < 0.0001$, Upwelling and Downwelling, Table 4.4, Figure 4.33). Thus, the presence of horizontal

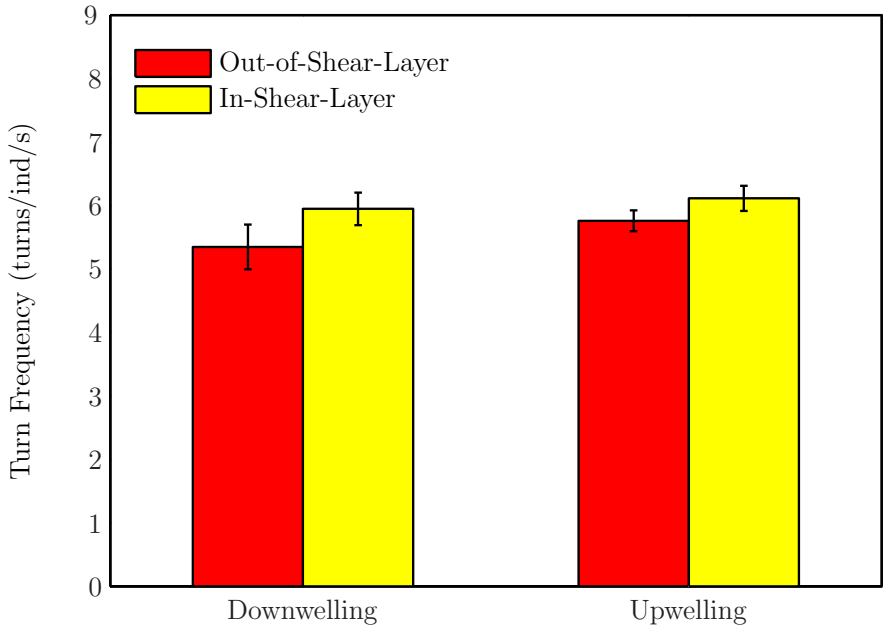

Figure 4.32: Turn Frequency in Upwelling and Downwelling Treatments for *Clausocalanus furcatus*. Error bars span a range of twice the standard error.

gradients of vertical velocity alone appears sufficient to cause finescale, population-level aggregations of *C. furcatus*.

Again, to evaluate the potential effects of the vertical shear layers in terms of larger scale aggregative phenomena, it is useful to examine changes in gross path parameters such as $NGDR$ and $VNGDR$. As for *A. negligens*, $NGDR$ increased significantly under both upwelling and downwelling conditions when compared to control values (p <0.0001 Upwelling; p <0.0001 Downwelling; Table 4.5, Figure 4.34), indicating that copepod trajectories became more linear and less sinuous.

As for *A. negligens*, it is useful to consider the *vertical*-net-to-gross-displacement-ratio ($VNGDR$) to evaluate shear layer effects on the vertical distribution of copepod populations. Recall that an increase in $VNGDR$ indicates that path trajectories become more linear vertically and that vertical displacement is not retraced throughout the course of the trajectory. Again, a decrease in $VNGDR$ indicates that all vertical displacement throughout the course of a trajectory was retraced, yielding low net vertical displacement. As with *A. negligens*, *C. furcatus* exhibited significant increases

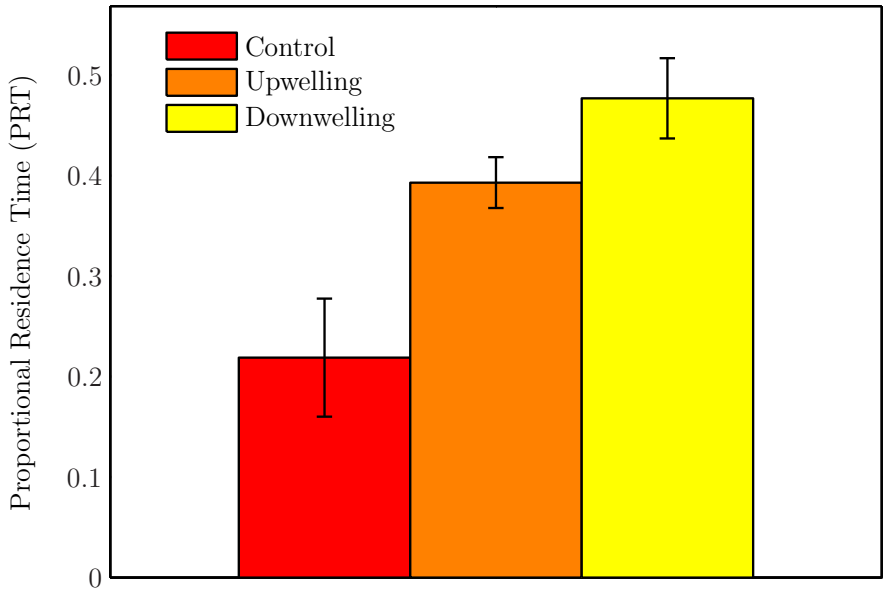

Figure 4.33: Proportional Residence Time (PRT) in Various Treatments for *Clausocalanus furcatus*. Error bars span a range of twice the standard error.

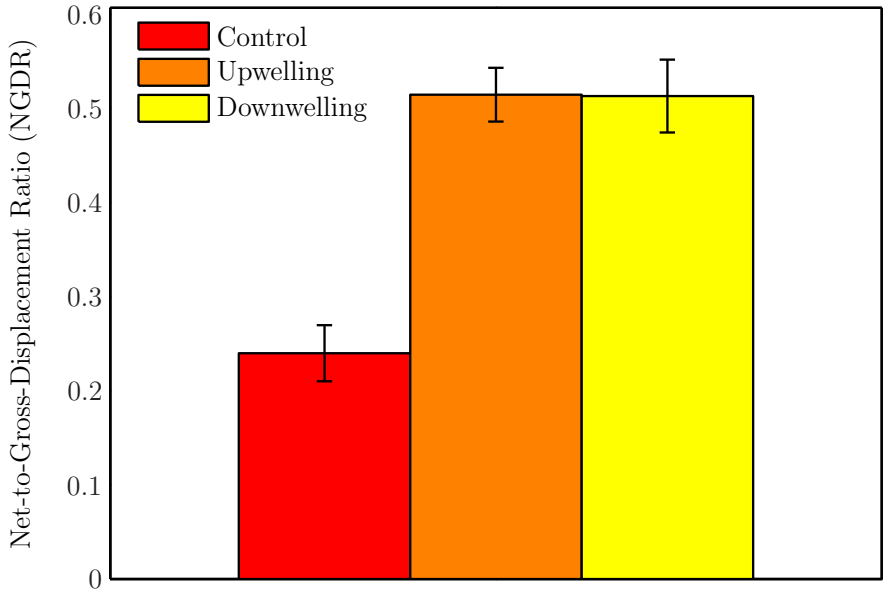

Figure 4.34: Net-to-Gross-Displacement Ratio ($NGDR$) in Various Treatments for *Clausocalanus furcatus*. Error bars span a range of twice the standard error.

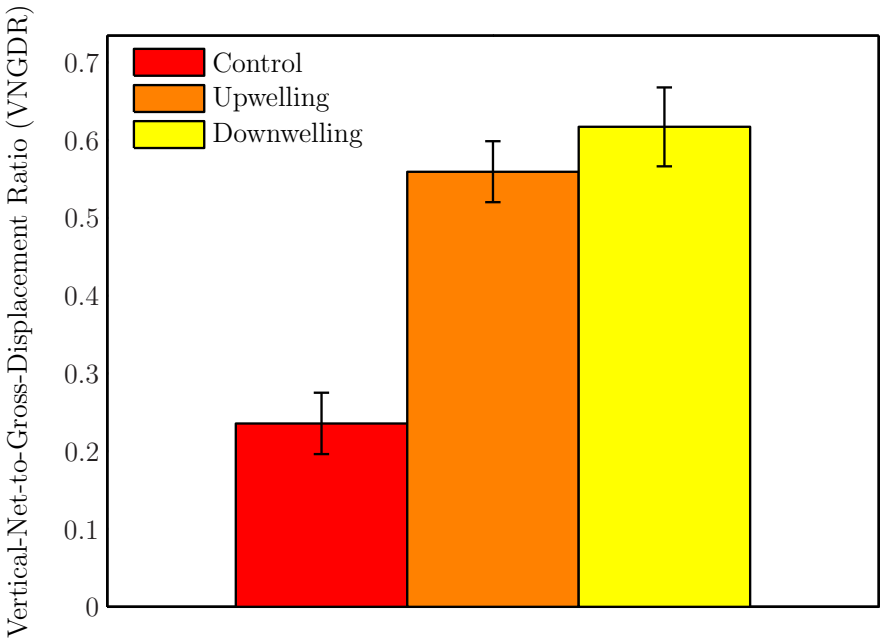

Figure 4.35: Vertical-Net-to-Gross-Displacement Ratio ($VNGDR$) in Various Treatments for *Clausocalanus furcatus*. Error bars span a range of twice the standard error.

in $VNGDR$ under both upwelling and downwelling conditions when compared to control values (p <0.0001 Upwelling; p <0.0001 Downwelling; Table 4.6, Figure 4.35) indicating that the presence of the vertical shear layer causes a preferential alignment of the trajectory parallel to the shear strain rate isocontours (i.e. parallel to the gravity vector).

Again, more information is gained by looking at histograms of $VNGDR$ (Figure 4.36). Phenomena similar to *A. negligens* are seen for *C. furcatus* under both upwelling and downwelling treatments. It is clear that even though on average the $VNGDR$ did increase, there was also a spread of population $VNGDR$ to high ($\rightarrow$ 1, straight vertical trajectories) and low ($\rightarrow$ 0, "U-shaped" or "C-shaped" trajectories) values, with smaller peaks at intermediate values of $VNGDR$. This results in a somewhat bimodal distribution and suggests that significant portions of the population were explicitly exhibiting both depth-keeping behavior (low $VNGDR$ values)

and active vertical advection (high $VNGDR$ values). As for the other calanoid copepod *A. negligens*, the data for *C. furcatus* explicitly shows that not only do vertical shear layers cause a preferential trajectory alignment to the vertical along the shear isocontours (high $VNGDR$ values), but copepods are also resisting large scale vertical advection through depth-keeping behavior (low $VNGDR$ values), at least when gradients of vertical velocity are readily coherent and sensible and other sensory cues are absent.

4.2.2.3 Panopeus herbstii Megalops

P. herbstii megalops showed a direct behavioral response to the vertical shear layers through a statistically significant increase in turn frequency pre-contact versus post-contact with the layer under both upwelling and downwelling conditions (Exposure Effect, $p = 0.002$, Exposure by Layer Effect, $p = 0.75$, Table 4.3, Figure4.37). Interestingly, *P. herbstii* turned more frequently, on average, under downwelling conditions as compared to upwelling (Layer Effect, $p = 0.001$, Table 4.3).

Insignificant layer and exposure effects for relative swimming speed (Layer Effect, $p = 0.68$, Exposure Effect $p = 0.96$, Table 4.2, Figure 4.38) reveal that, on average, swimming speeds under upwelling and downwellings conditions are the same, as they are in the presence or absence of a vertical shear layer. However, importantly, a significant interaction term indicates that the trends in relative swimming speed response are different under upwelling versus downwelling conditions (Exposure by Layer Effect, $p = 0.02$, Table 4.2), namely swimming speeds increased post-contact in the upwelling layer while they decreased post-contact under downwelling conditions. As observed in Figure 4.38, the conflicting trends are masking the significance of the main effects in the statistical analysis.

For *P. herbstii* megalops, the combined effects of an increased turn frequency post-contact with the shear layer (upwelling and downwelling) and either an increase

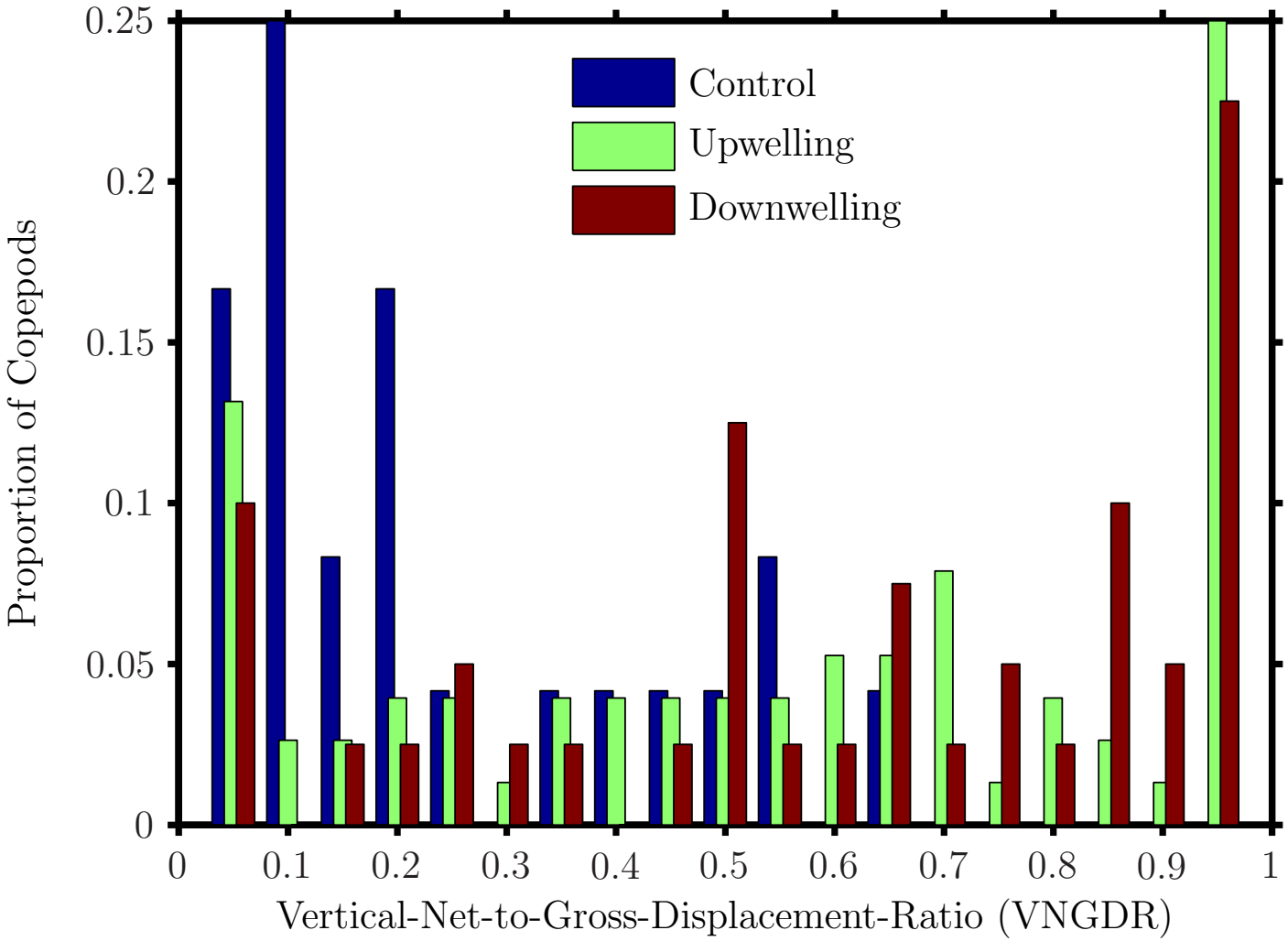

Figure 4.36: VNGDR Response Histograms for Upwelling and Downwelling Shear Layers for *Clausocalanus furcatus*

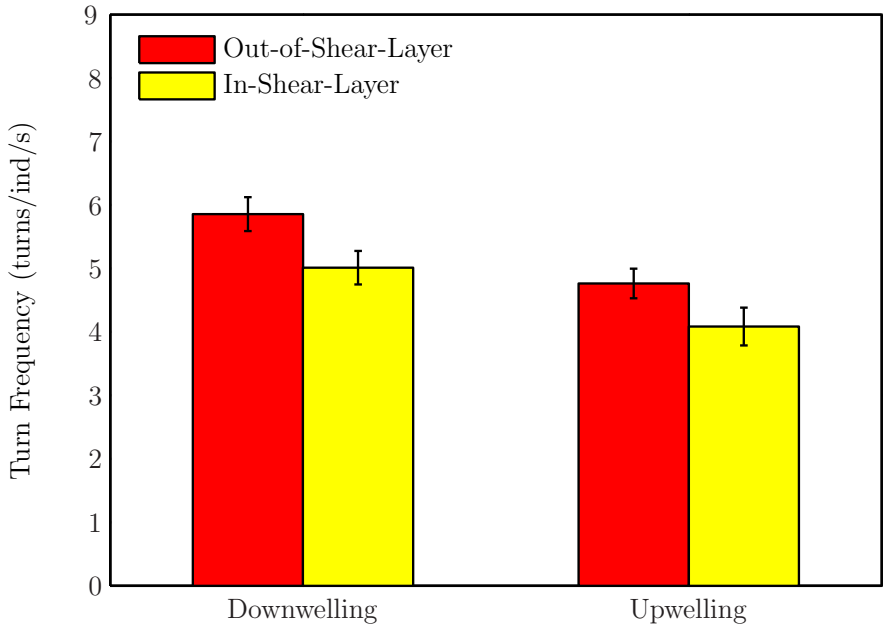

Figure 4.37: Turn Frequency in Upwelling and Downwelling Treatments for *Panopeus herbstii*. Error bars span a range of twice the standard error.

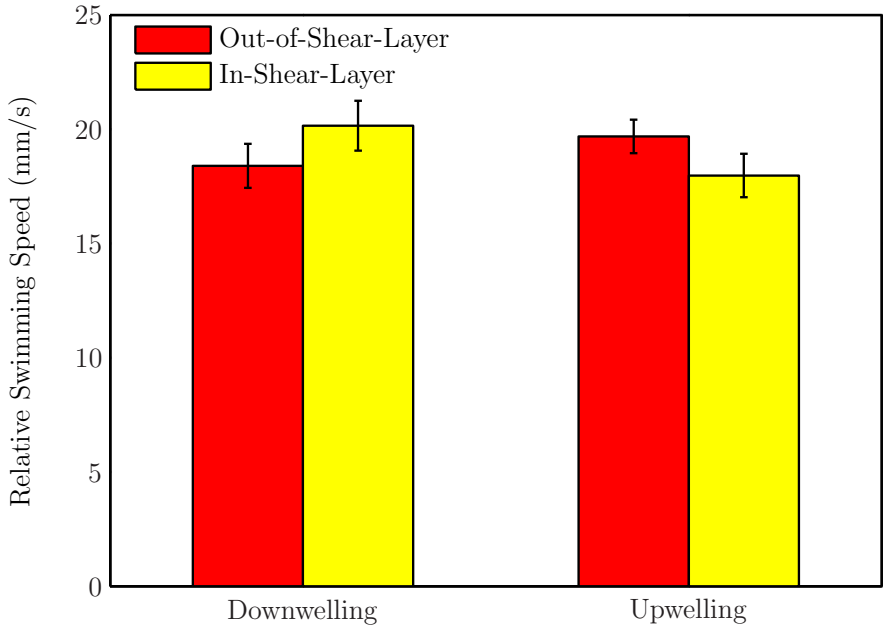

Figure 4.38: Relative Swimming Speed in Upwelling and Downwelling Treatments for *Panopeus herbstii*. Error bars span a range of twice the standard error.

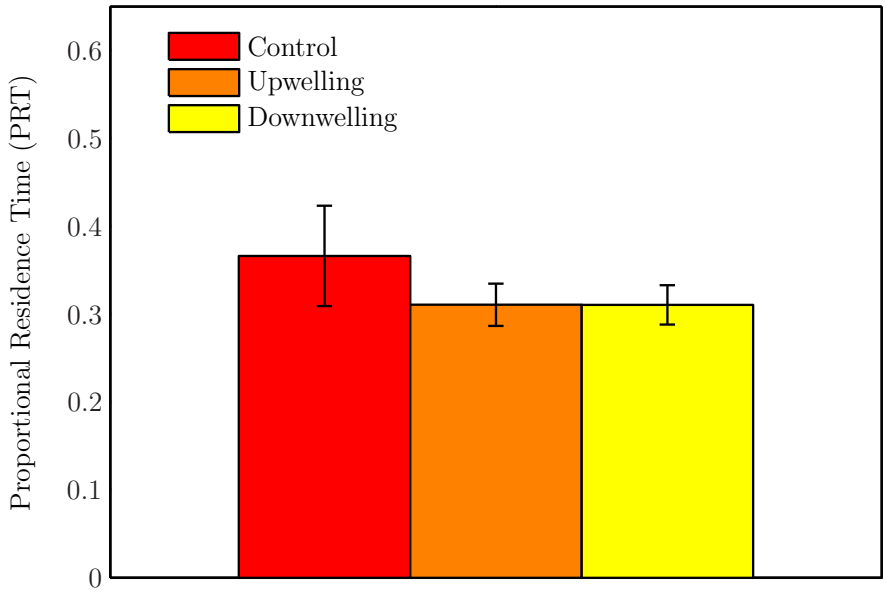

Figure 4.39: Proportional Residence Time (PRT) in Various Treatments for *Panopeus herbstii*. Error bars span a range of twice the standard error.

(upwelling) or decrease (downwelling) in relative swimming speed simply changed the overall heading of the trajectories and resulted in no significant increase in PRT due to the presence of either upwelling or downwelling vertical shear layers (Treatment to Control, $p = 0.94$ Upwelling, $p = 0.97$ Downwelling, Table 4.4, Figure 4.39).

In contrast to both of the calanoid copepods, estuarine *P. herbstii* megalops showed no significant changes in $NGDR$ in response to either upwelling or downwelling shear layers ($p = 0.08$ Upwelling; $p = 0.49$ Downwelling; Table 4.5, Figure 4.40), although the decrease in $NGDR$ under upwelling conditions was significant to a slightly lower confidence level (i.e. $p < 0.1$) indicating that trajectories became more sinuous under the upwelling shear layer treatment.

A significant decrease in $VNGDR$ for upwelling and no change in $VNGDR$ for downwelling compared to control treatments (Treatment to Control, $p = 0.04$ Upwelling, 0.08 Downwelling, Table 4.6, Figure 4.41) indicates that under upwelling conditions path trajectories became more horizontal and sinuous and vertical displacement was more likely to be retraced throughout the course of the trajectory.

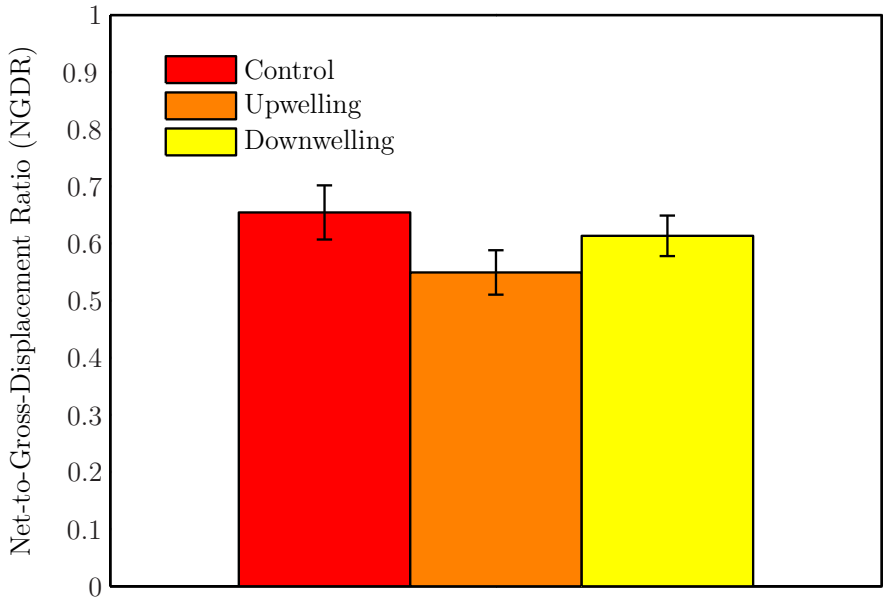

Figure 4.40: Net-to-Gross-Displacement Ratio ($NGDR$) in Various Treatments for *Panopeus herbstii*. Error bars span a range of twice the standard error.

However, again the decrease in $VNGDR$ under downwelling conditions was significant, but to a slightly lower confidence level (i.e. p <0.1), indicating that trajectories similarly became more horizontal and sinuous under the downwelling shear layer treatment but to a lesser extent.

Examination of $VNGDR$ histograms for *P. herbstii* (Figure 4.42) reveals behavioral phenomena similar to that seen for both calanoid copepods in which $VNGDR$ values are weighted toward higher and lower values for shear layer treatments in a somewhat bimodal distribution. However, in contrast to the copepods whose $VNGDR$ histograms under control conditions were skewed towards lower values and not bimodal, the control $VNGDR$ histogram for *P. herbstii* was already somewhat bimodally distributed towards higher and lower values. This suggests that observed changes are likely the simple decreases seen statistically through the ANOVA. Therefore, in contrast to both calanoid copepod species, for *P. herbstii* megalops the presence of vertical shear layers causes a preferential trajectory alignment in the direction of changing shear strain rate (i.e. the gradient direction) and increased depth-keeping

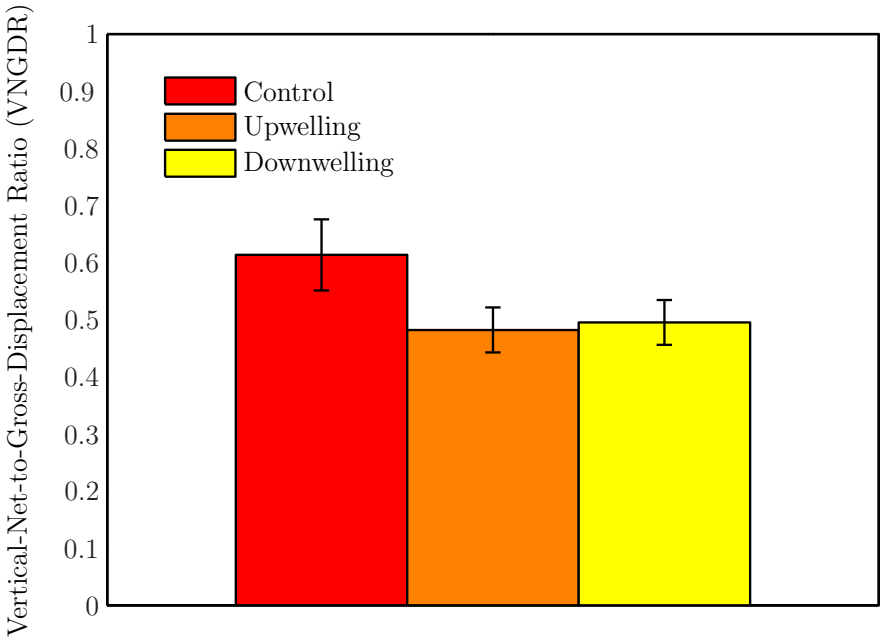

Figure 4.41: Vertical-Net-to-Gross-Displacement Ratio ($VNGDR$) in Various Treatments for *Panopeus herbstii*. Error bars span a range of twice the standard error.

behavior (decreased $VNGDR$ values), possibly in an effort to obtain the maximum amount of information about the hydrodynamic environment by sweeping in the gradient direction (e.g. across a frontal feature) while resisting vertical advection.

4.2.2.4 Neomysis americana

In contrast to the other estuarine zooplankter, *P. herbstii*, the mysid *N. americana* showed a direct behavioral response to the vertical shear layer through a statistically-significant decrease in relative swimming speed pre-contact versus post-contact with the layer (Exposure Effect, $p = 0.03$, Table 4.2, Figure 4.43) under both upwelling and downwelling conditions (Exposure by Layer Effect, $p = 0.68$, Table 4.2). Additionally, relative swimming speeds were on average higher under upwelling conditions versus downwelling (Layer Effect, $p = 0.02$, Table 4.2).

Insignificant exposure and interaction terms for turn frequency (Exposure Effect, $p = 0.17$, Exposure by Layer Effect, $p = 0.78$, Table 4.3, Figure 4.44) reveal that turning behavior was not significantly affected by the presence of either upwelling

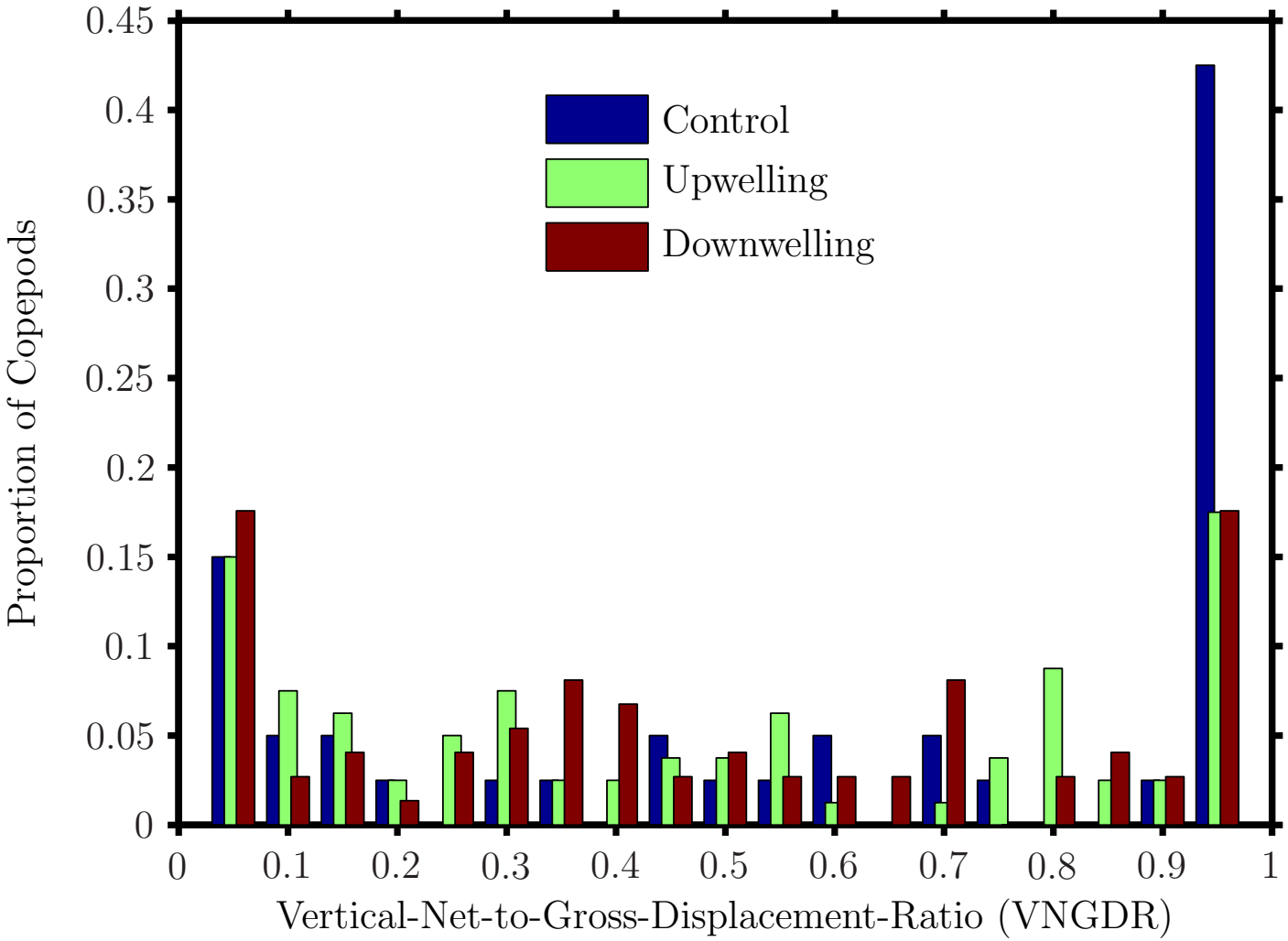

Figure 4.42: Histograms of $VNGDR$ under Various Treatments for *Panopeus herbstii*

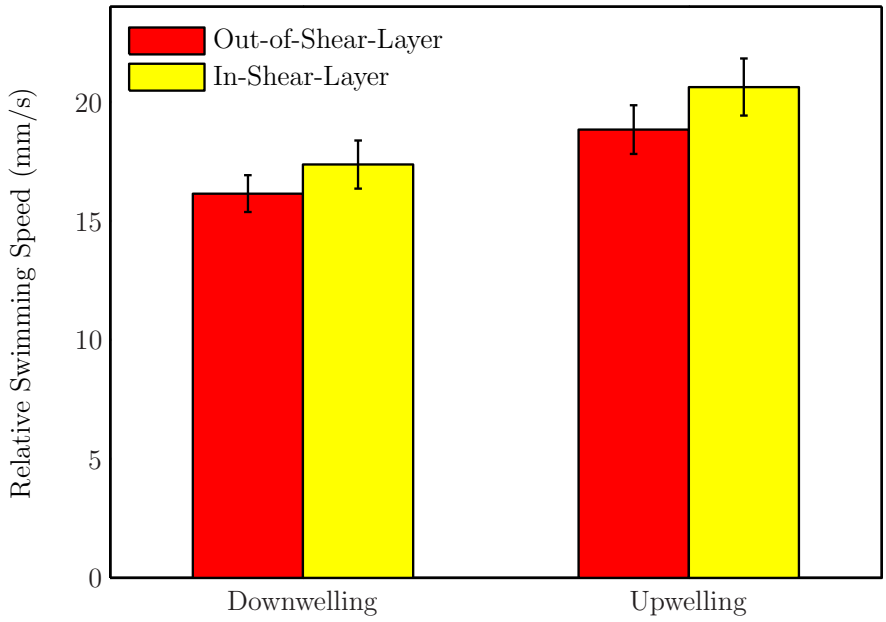

Figure 4.43: Relative Swimming Speed in Upwelling and Downwelling Treatments for *Neomysis americana*. Error bars span a range of twice the standard error.

or downwelling shear layers, although *N. americana* did turn more on average under downwelling conditions as compared to upwelling (Layer Effect, $p = 0.02$, Table 4.3).

For *N. americana*, the combined effects of a decreased relative swimming speed post-contact with the shear layer (both upwelling and downwelling) and no change in turn frequency (both upwelling and downwelling) were sufficient to cause a significant increase in PRT due to the presence of both upwelling and downwelling shear layers (Treatment to Control, $p = 0.02$ Upwelling, $p < 0.0001$ Downwelling, Table 4.4, Figure 4.45).

In contrast to all three previously discussed zooplankton species, *N. americana* is the only species tested whose overall trajectory shape was uninfluenced by the vertical shear layers, as there was no significant change in either $NGDR$ or $VNGDR$ for either upwelling or downwelling (Tables 4.5 and 4.6). However, although not significant there is a decrease in both $NGDR$ and $VNGDR$ under both upwelling and downweillng conditions, similar to the other estuarine species tested, *P. herbstii*.

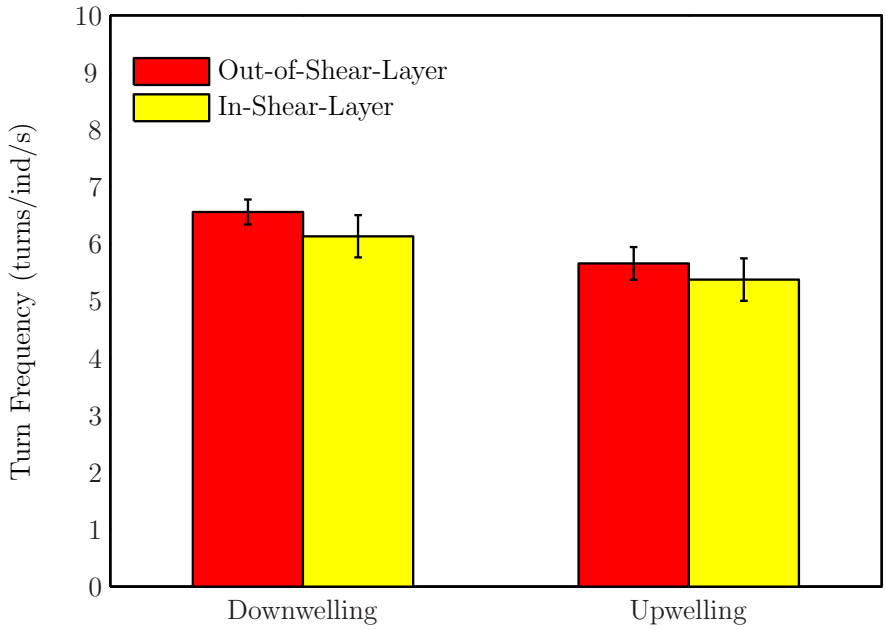

Figure 4.44: Turn Frequency in Upwelling and Downwelling Treatments for *Neomysis americana*. Error bars span a range of twice the standard error.

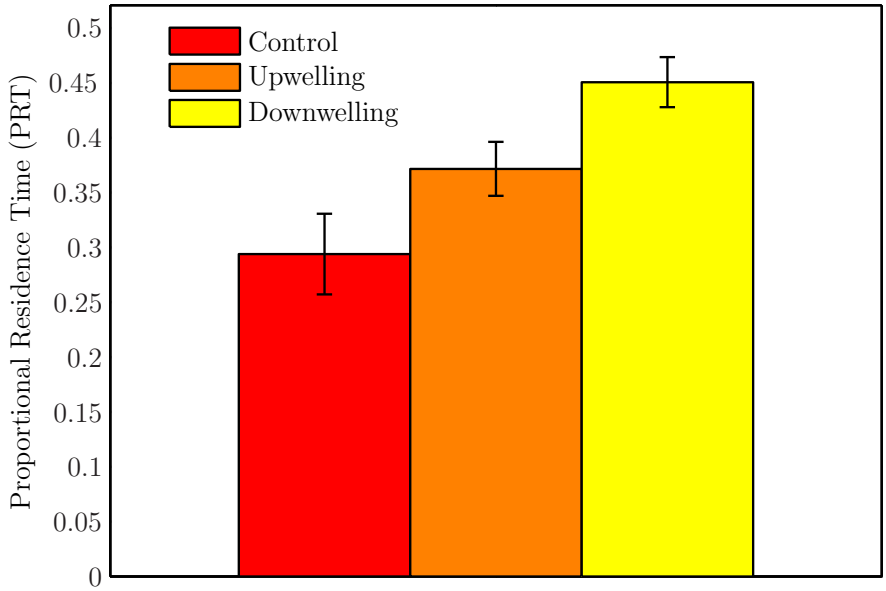

Figure 4.45: Proportional Residence Time (PRT) in Various Treatments for *Neomysis americana*. Error bars span a range of twice the standard error.

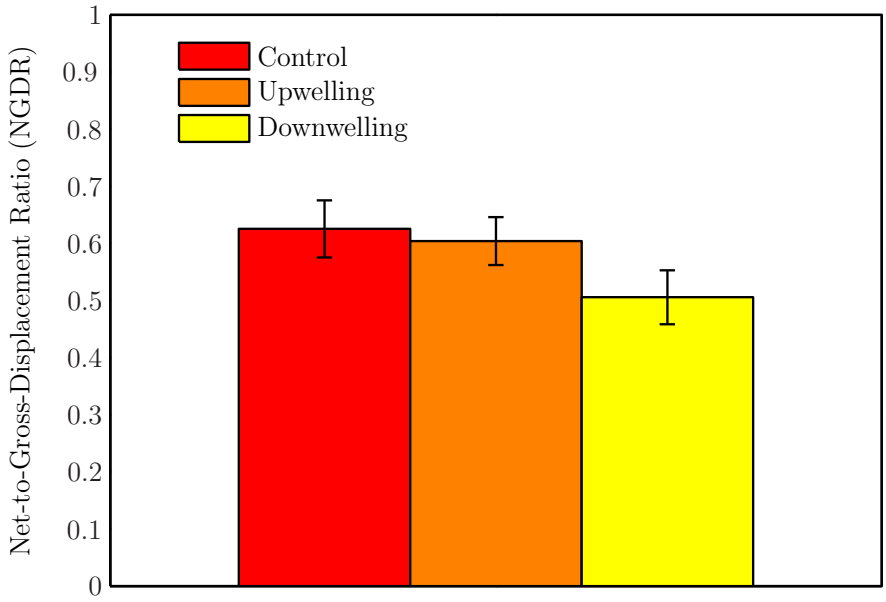

Figure 4.46: Net-to-Gross-Displacement Ratio ($NGDR$) in Various Treatments for *Neomysis americana*. Error bars span a range of twice the standard error.

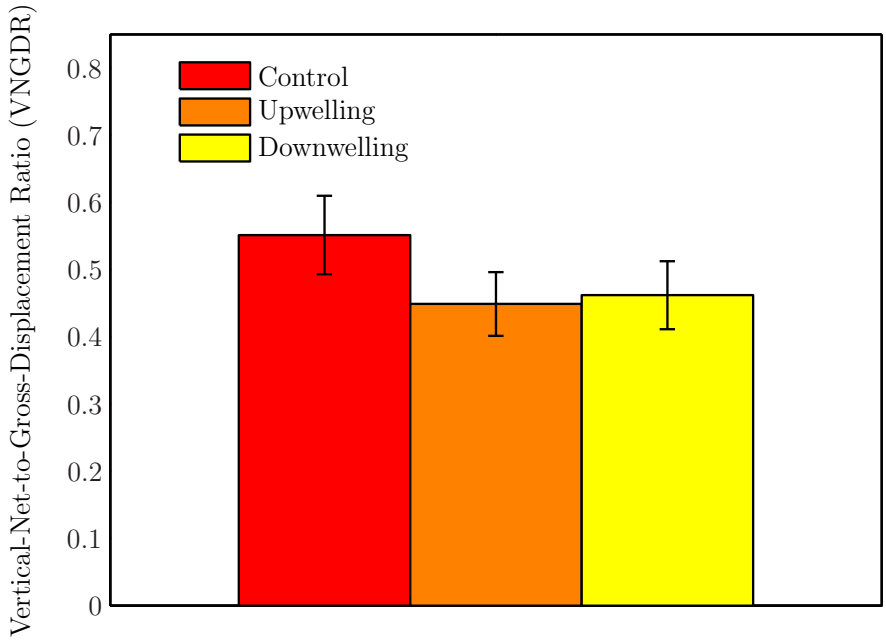

Figure 4.47: Vertical-Net-to-Gross-Displacement Ratio ($VNGDR$) in Various Treatments for *Neomysis americana*. Error bars span a range of twice the standard error.

Interestingly, examination of $VNGDR$ histograms for *N. americana* reveals similar phenomena as observed for both calanoid copepods (Figure 4.48). It is clear that even though statistically the $VNGDR$ did not change, there was a definite spread of population $VNGDR$ to high ($\rightarrow 1$, straight vertical trajectories) and low ($\rightarrow 0$, "U-shaped" or "C-shaped" trajectories) values. This results in a somewhat bimodal distribution and suggests that significant portions of the population exhibit both depth-keeping behavior (low $VNGDR$ values) and active vertical advection (high $VNGDR$ values).

4.2.2.5 Summary of Results

Holistically, a few interesting results stand out. First, all species showed a statistically significant behavioral response to the vertical shear layers through changes in relative swimming speed and/or turn frequency in-layer versus out-of-layer (tropical calanoid copepods) or pre-contact versus post-contact (estuarine crabs megalops and mysid). The combination of behavioral responses leads to significantly increased time spent in the shear layer region for two of the four species (*C. furcatus* and *N. Americana*), which can directly scale up to population-level aggregations on the finescale. For the other two species, increased PRT and population-level aggregations seem likely when considering the data through the lens of the spatial scale of the current behavioral observations as well as the relevant ecological contexts *in situ*, discussed thoroughly in the subsections below. Second, both coral reef copepod species tested, *A. negligens* and *C. furcatus*, showed increasingly vertical and linear swimming trajectories in the presence of finescale upwelling and downwelling layers. In contrast, both estuarine species, *P. herbstii* and *N. americana*, showed increasingly horizontal and sinuous swimming trajectories in the vertical shear layers (although not statistically significant for *N. americana*). As discussed in the subsections below and summarized in Table 4.7, these behavioral consistencies and differences undoubtedly arise as a result of the

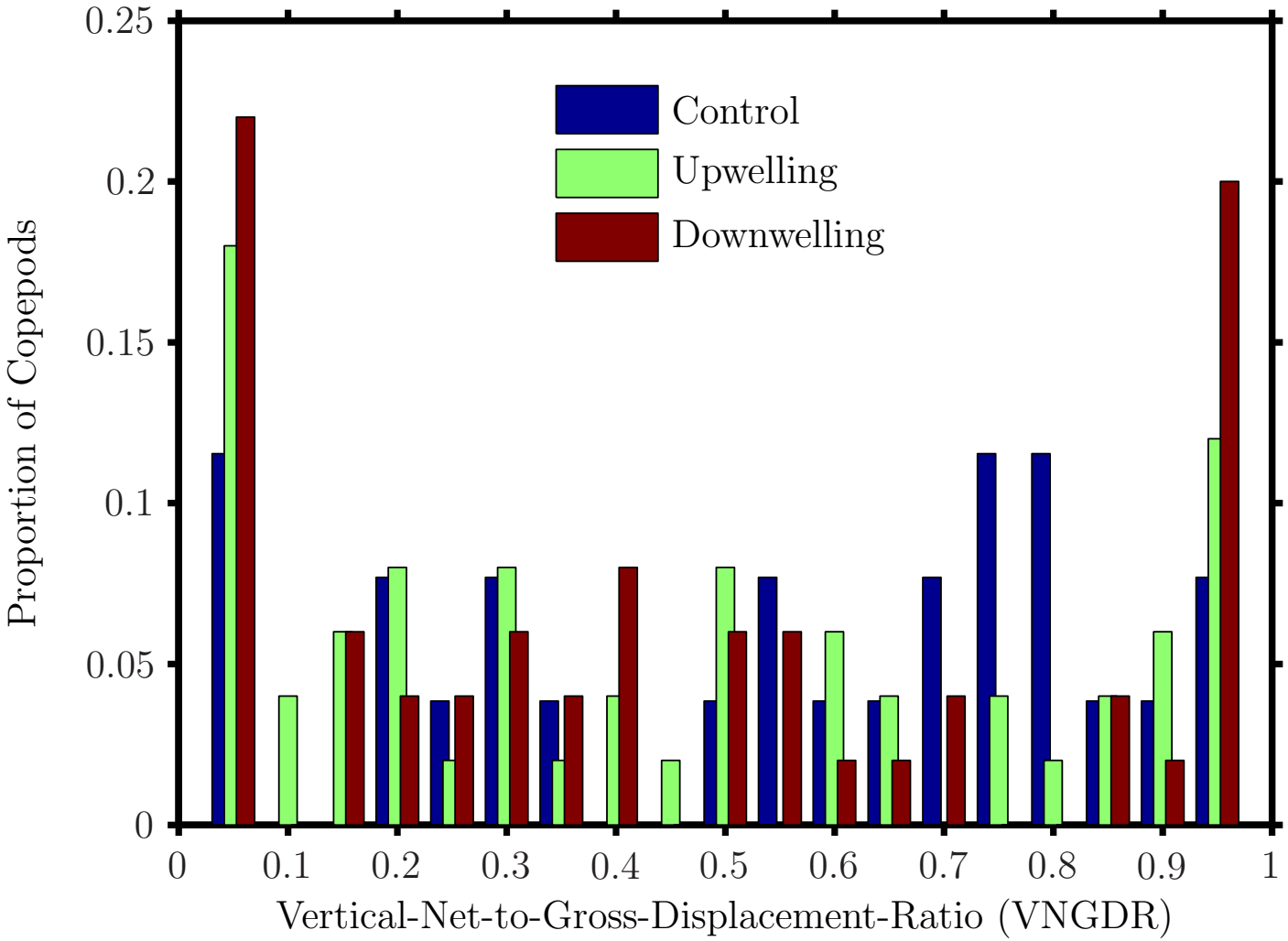

Figure 4.48: Histograms of $VNGDR$ in Various Treatments for *Neomysis americana*

differing hydrodynamic and ecological realities *in situ* and the unique life histories and strategies of the species involved.

4.2.3 Discussion

Interpreting behavioral responses in the proper ecological context for each species is crucial for assessing the full implications of the present study. A few important findings common to all species are discussed briefly below before each species is discussed in its own ecological context.

There is strong, statistically-significant evidence that, in the absence of any other sensory cue, the direction of vertical flow is largely unimportant. For each species tested, behavioral responses to upwelling versus downwelling shear layers are essentially identical (Tables 4.8 - 4.11). The majority of changes in path kinematics are the same for upwelling versus downwelling treatments (Tables 4.8 - 4.11). Further, the way in which changes in path kinematic parameters affected gross path parameters and/or trajectory shape ($NGDR$, $VNGDR$, PRT) is identical under upwelling versus downwelling for each species (Tables 4.8 - 4.11), although for one species (*P. herbstii*) and one parameter ($VNGDR$ decrease under downwelling conditions) the confidence level was slightly lower (p <0.1).

Thus, what is important is the presence of horizontal gradients of vertical velocity, which often demarcate boundaries between water masses of differing hydrographic and/or biochemical conditions at marine fronts. Furthermore, for each species, under both upwelling and downwelling conditions, significant changes (or lack thereof) in PRT (the proportion of time spent in the jet layer) are either increases or no changes (Tables 4.8 - 4.11). Thus, the presence of a vertical shear layer *on the finescale*, regardless of flow direction and in the absence of any other sensory cue, is always an attractive (or neutral) feature that induces behavioral responses in zooplankton from a variety of ecological settings with a variety of morphological and mechanosensory

Table 4.7: Summary of Statistically Significant Behavioral Responses for All Species Tested. ↑ (↓) Indicates a Statistically Significant Increase (Decrease) between Out-of-Layer and In-Layer Values (Copepods) or Pre-contact and Post-contact Values (Crab Larvae, Mysids) of Swimming Speed and Turn Frequency or between Control and Upwelling/Downwelling Values of $VNGDR$, $NGDR$, and PRT. = Indicates No Significant Change.

Species and Flow Condition	Relative Swimming Speed	Turn Frequency	$VNGDR$	$NGDR$	PRT
Acartia negligens					
Upwelling	↑	=	↑	↑	=
Downwelling	↑	↑	↑	↑	=
Clausocalanus furcatus					
Upwelling	↑	↑	↑	↑	↑
Downwelling	=	↑	↑	↑	↑
Panopeus herbstii					
Upwelling	↑	↑	↓	=	=
Downwelling	↑	↑	=	=	=
Neomysis americana					
Upwelling	↓	=	=	=	↑
Downwelling	↓	=	=	=	↑

adaptations. In this study, a vertical shear layer is never an aversive or dispersive sensory cue. Additionally, shear-induced changes in population $VNGDR$ histograms for all species indicate that significant portions of all populations are exhibiting both depth-keeping behavior and active vertical advection under both upwelling and downwelling conditions. As an aggregative cue which often induces depth-keeping behavior, a persistent vertical shear layer is likely a common mechanism which acts to generate patchiness in a variety of coastal marine ecosystems on a variety of spatiotemporal scales.

4.2.3.1 Acartia negligens and Clausocalanus furcatus

For calanoid copepods, the ability to sense and incorporate hydrodynamic (and chemical) information is a matter of life and death. From setting up inconspicuous feeding currents and capturing prey particles efficiently (Paffenhöfer 1998, Kiørboe and Visser 1999, Malkiel et al. 2003, Kiørboe 2011), to predator detection and escape behaviors (Fields and Yen 1997, Fields and Yen 1997, Viitasalo et al. 1998,Holzman and Wainwright 2009), to mate detection (Yen et al. 1998) and foraging (Woodson et al. 2007), life *is* hydrodynamics. For the coral reef-dwelling calanoid copepods *Acartia negligens* and *Clausocalanus furcatus*, life in highly-predacious, high-visibility waters presents some unique challenges.

To better understand the implications of the observed behavioral responses to both upwelling and downwelling shear layers for these copepods, it is important to consider the hydrodynamic and ecological realities *in situ*. The coral reef where these copepods were collected is a vibrant fringing reef in the Gulf of Aqaba, Red Sea. Reef hydrodynamics are largely dominated by longshore tidal flows and cross-shore thermally-driven diel exchange flows (Figure 4.49) between the reef and deep ocean (Monismith et al. 2005). Both free stream flows over the rough bed of the fringing reef generate fully-developed benthic boundary layers that agree well with turbulent

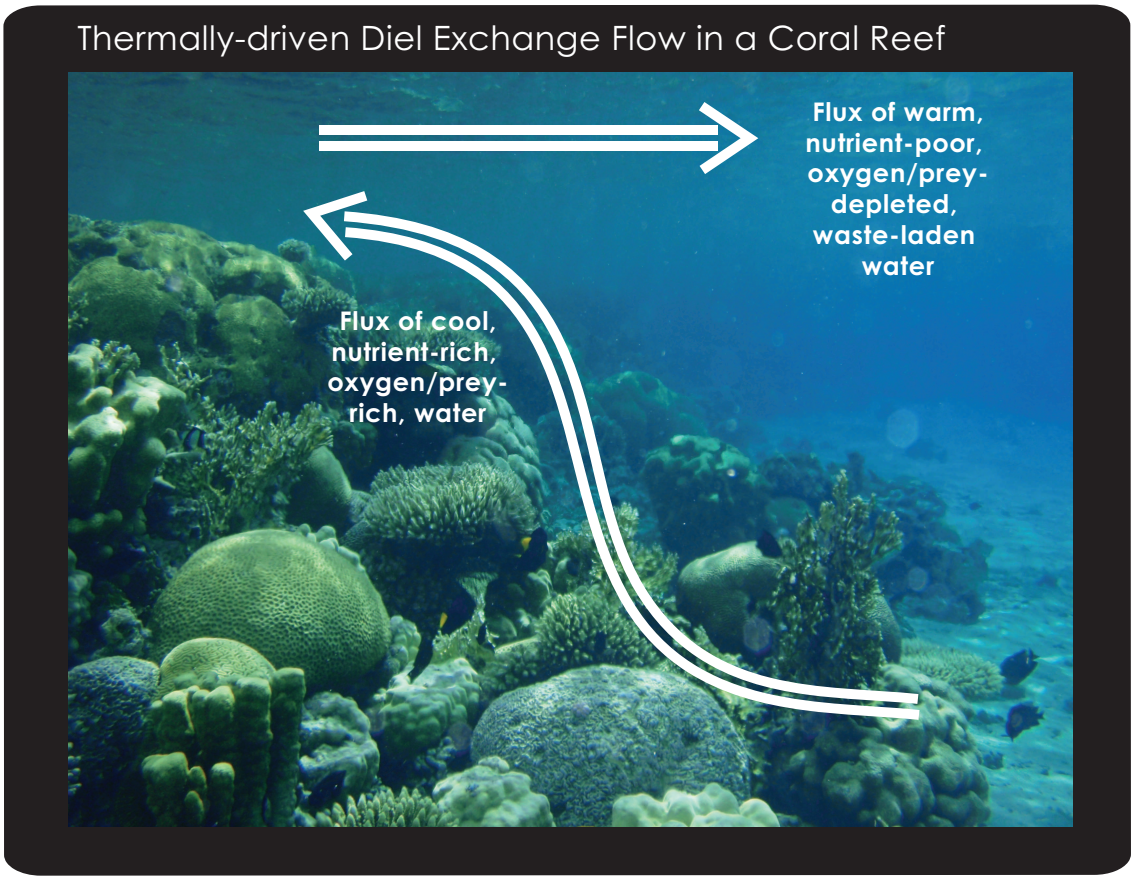

Figure 4.49: Thermally-Driven Diel Exchange Flow Between a Fringing Reef and the Deep Ocean

boundary layer flow theory ((Figure 4.50),Reidbenbach et al. 2006).

The net effect of thermally-driven diel exchange flows is to flush out warm, nutrient-poor, oxygen-and-food-depleted reef waters with cold, nutrient-oxygen-and-food-rich deep, offshore waters. Similarly, just as turbulent boundary layer flows efficiently transport high-momentum fluid vertically towards the bed and low-momentum fluid vertically away from the bed, nutrient-poor, oxygen-and-food-depleted benthic waters are transported vertically into the free stream flow higher in the water column while nutrient-oxygen-and-food-rich free stream waters are transported vertically downwards into the benthic boundary layer near the reef bed where intense productivity and predation act to deplete the near-bed waters.

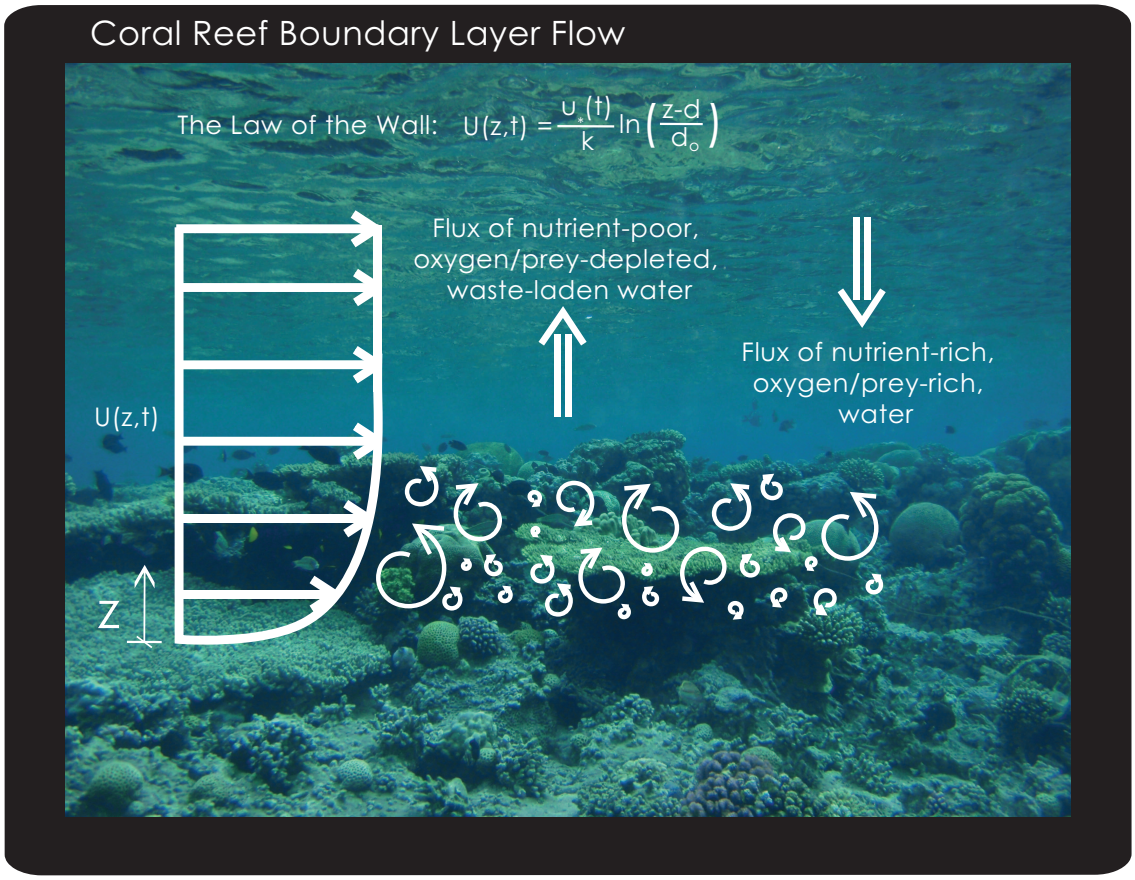

Figure 4.50: Well-developed Turbulent Boundary Layer Flow over a Fringing Reef Bed

Of course reef ecology and productivity are intricately linked to local hydrodynamics which effectively transport passive scalars such as mass (food, dissolved nutrients, dissolved oxygen), heat (temperature), and momentum (drag and lift forces, shear stresses, etc.) which are vital to reef dynamics and livelihood. Indeed, Yahel et al. (Yahel et al. 1998) measured phytoplankton abundances on this fringing reef and found greatly reduced phytoplankton abundances in near-bed waters (1 - 3 m) due to benthic grazing by soft corals. Furthermore, the carbon flux input to near-bed reef waters due to phytoplankton was significantly higher when compared to that due to zooplankton. This suggests that zooplankton (predominantly copepods on this reef) probably reside higher in the water column where they can forage in food-rich waters while avoiding predation pressure. This was later confirmed by Yahel et al. (Yahel et al. 2005) who documented substantial depletion of zooplankton abundances near the reef bed, which was more pronounced nocturnally, probably due to diel vertical migration. Similarly, Holzman et al. (Holzman et al. 2005) found vertical gradients of zooplankton abundances with substantial near-bed depletion in the benthic boundary layer ($\sim 1.5m$), with the strength of the gradient dependent on the swimming ability of the zooplankton species. Gradients were steepest for the strongest swimmers (copepods and polychaetes), suggesting bottom-avoidance behavior through active vertical swimming behavior (Genin et al. 2005). This has given rise to the idea of a vertical gradient of predation pressure (Motro et al. 2005) that strongly influences the vertical distribution of zooplankton in reef water columns. Collectively, these studies indicate that there is an optimal depth at which copepods can forage effectively while avoiding predation pressure from below (zooplanktivourous reef-dwelling fish) and above (zooplankton become very conspicuous high in the water column in high visiblity reef waters). Of course, predation pressure and food availability change on a diel cycle and are intricately linked to diel vertical migratory behaviors observed for many reef-dwelling zooplankton species (Yahel et al. 2005).

The findings of the present study are consistent with copepod behavior that would maximize foraging and mate-finding success while minimizing predation pressure *in situ* in the fringing reef habitat. Namely, observed behavioral responses suggest that in the absence of phototactic cues and in the presence of finescale upwelling and downwelling shear flows, both *Acartia negligens* and *Clausocalanus furcatus* will exploit the information contained in a coherent shear structure to seek out regions of low vertical velocity in order to avoid large net vertical advection. This behavior is indicative of preferential depth-keeping within an optimal range of the water column, consistent with acoustic tracking studies of zooplankton on the reef *in situ* (Genin et al. 2005).

Overall, the hop-sink swimming *Acartia negligens* and the cruise-swimming *Clausocalanus furcatus* each responded almost identically to upwelling and downwelling shear layers in terms of path kinematic parameters (relative swimming speed and turn frequency) (Tables 4.8 and 4.9). For both copepods, changes in relative swimming speed in-layer versus out-of-layer for both upwelling and downwelling layers were always increases, with the exception of *C. furcatus* in the downwelling layer, in which speed remained unchanged (Tables 4.8 and 4.9). This indicates that copepods are typically maintaining swimming speeds higher than ambient vertical flow velocities, a necessary precursor to depth-keeping behavior, at least given a spatiotemporally persistent shear signal. Similarly, for both copepods, changes in turn frequency in-layer versus out-of-layer for both upwelling and downwelling layers were always increases, with the exception of *A. negligens* in the upwelling layer, in which turn frequency remained unchanged (Tables 4.8 and 4.9). Thus, in the absence of phototactic cues, copepod behavioral responses to both upwelling and downwelling shear layers are predominantly *excited* behaviors, rarely *unchanged*, and never *subdued*. Increasing relative swimming speed and increasing turn frequency in response to coherent shear structures allows copepods to effectively sample the surrounding volume and use

the available hydrodynamic information to make decisions which optimize habitat-partitioning and life success.

The one behavioral response that was different for *A. negligens* than *C. furcatus* was proportional residence time (PRT), or the fraction of time spent within the jet versus outside (Tables 4.8 and 4.9). It seems likely that the disparity is easily understood when considering differences in morphology and swimming style between the two copepods. The significantly increased PRT in response to both the upwelling and downwelling shear layers for the cruise-swimming *C. furcatus* (Table 4.9) indicates that, through shear sensing and active behavioral responses, copepods remain in the geometrical area of the shear layer significantly longer than they would remain in the same area in a stagnant flow field. In contrast, PRT remained unchanged (and did *not decrease*) under both upwelling and downwelling conditions for the hop-sink-swimming *A. negligens* (Table 4.8). Cruise-swimming copepods are able to sense and incorporate hydrodynamic information via an array of mechanosensory hairs (setae) along the antennules (Yen et al. [1992], Fields et al. [2002]) *while cruising*. Hop-sinkers can also sense and incorporate hydrodynamic information via an array of setae, however they can only incorporate information effectively *while sinking*, not hopping (see Figure 2.2, e.g. Mauchline [1998]). Thus, the cruise-swimming *C. furcatus* can remain in the upwelling and downwelling shear layers directly (i.e. increased PRT) *while* incorporating information about the shear stress field *and* resisting vertical advection in an optimal depth-keeping effort. For the hop-sinking *A. negligens*, however, incorporating hydrodynamic information while in the upwelling and/or downwelling shear layers would require not hopping, and thus sinking while being advected with the mean flow, which is contrary to its likely goals of maintaining an optimal depth within the water column. This is perhaps a competitive advantage for *C. furcatus*, as copepods (and plankton in general) that are able to sense spatial gradients of fluid velocity can exploit the ambient flow to, for example, swim against

the flow and allow prey to be advected into their feeding spheres (Genin et al. [2005]).

Convincing evidence for individual and population-level depth-keeping behavior is not obvious at first, but is revealed by examining $VNGDR$ histograms. Recall that a $VNGDR$ histogram can be viewed as a spectra of depth-keeping behavior, where low values ($\rightarrow 0$) indicate "U-shaped" or "C-shaped" trajectories with low net vertical transport and thus strong depth-keeping behavior. Similarly, high $VNGDR$ values ($\rightarrow 1$) indicate straight vertical trajectories with high net vertical transport and thus weak depth-keeping behavior, referred to here as active vertical advection. For *A. negligens* and *C. furcatus*, it is clear that even though on average $VNGDR$ did increase, there was also a preferential spread of population $VNGDR$ values towards both low and high values resulting in a bimodal distribution. This suggests that significant portions of the population were explicitly exhibiting both depth-keeping behavior (low $VNGDR$ values) and active vertical advection (high $VNGDR$ values). It is possible, but not *explicitly* shown in the data here, that straight vertical trajectories are simply portions of larger scale "U-shaped" or "C-shaped" trajectories, which would indicate that both are revealing similar depth-keeping behavioral phenomena on different spatial scales. Nonetheless, what is explicitly seen in the data for *A. negligens* and *C. furcatus* is that not only do vertical shear layers cause a preferential trajectory alignment to the vertical along the shear isocontours (increased $VNGDR$ values), but copepods are likely also resisting large scale vertical advection through depth-keeping behavior (population spread to low $VNGDR$ values), at least when gradients of vertical velocity are readily coherent and sensible and other sensory cues are absent. While preferential alignment of trajectories parallel to the shear strain rate iso-contours (the vertical) could act as a physical boundary of ecological significance leading to horizontally patchy distributions given persistent hydrodynamic features, individual copepods resisting large scale net vertical advection in an effort to maintain optimal depth could produce population-level aggregations within a finite

Table 4.8: *Acartia negligens*: Summary of Behavioral Responses to Upwelling and Downwelling Jets. ↑ (↓) Indicates a Statistically Significant Increase (Decrease) between Out-of-Layer and In-Layer Values (Speed, Turn Frequency) or Control and Upwelling/Downwelling Values (VNGDR, PRT). = Indicates No Significant Change. * Indicates a Significant Interaction between Location and Layer Effects (i.e., Layer Trends Are Dependent on Upwelling Versus Downwelling). + Indicates which Value is Significantly Higher, Upwelling or Downwelling, due to Significant Layer Effects.

Flow Condition and Behavior Metrics	Significant Trends
Upwelling	
Speed	↑+
Turn Frequency	=*+
$NGDR$	↑
$VNGDR$	↑
PRT	=
Downwelling	
Speed	↑
Turn Frequency	↑*
$NGDR$	↑
$VNGDR$	↑
PRT	=

region of the water column (as optimized by reduced predation risk and prey/mate availability). These two mechanisms acting in concert could likely act as mechanisms of both horizontal and vertical patchiness *in situ*.

4.2.3.2 Panopeus herbstii Megalops

To appreciate the implications of the observed behavioral responses for *P. herbstii*, it is crucial to understand the hydrodynamic and ecological realities *in situ* in the Wassaw Sound estuary. Additionally, the nature by which larval stage-dependent behavioral responses to physical and chemical cues combine with lower frequency vertical migrations (ontogenetic, diel, and tidal), while being superimposed on local hydrodynamics, to produce complex larval dispersal trajectories must be considered. Interpreting results in the context of the correct larval stage and its stage-dependent

Table 4.9: *Clausocalanus furcatus*: Summary of Behavioral Responses to Upwelling and Downwelling Jets. ↑ (↓) Indicates a Statistically Significant Increase (Decrease) between Out-of-Layer and In-Layer Values (Speed, Turn Frequency) or Control and Upwelling/Downwelling Values (VNGDR, PRT). = Indicates No Significant Change. * Indicates a Significant Interaction between Location and Layer Effects (i.e., Layer Trends Are Dependent on Upwelling Versus Downwelling). + Indicates which Value is Significantly Higher, Upwelling or Downwelling, due to Significant Layer Effects.

Flow Condition and Behavior Metrics	Significant Trends
Upwelling	
Speed	↑*
Turn Frequency	↑
$NGDR$	↑
$VNGDR$	↑
PRT	↑
Downwelling	
Speed	=*
Turn Frequency	↑
$NGDR$	↑
$VNGDR$	↑
PRT	↑

life-strategy will reveal the ecological significance of behavioral responses seen in the data. Indeed, behavioral responses observed here to finescale upwelling and downwelling shear layers show changes in path kinematics (relative swimming speed and turn frequency) and gross path parameters ($VNGDR$) which produce depth-keeping behavior in individuals (consistent with the classical Negative Feedback Model of Sulkin (Sulkin 1984)). These changes in individual behavior would likely produce population-scale aggregations around persistent frontal flow features in the absence of any other dominating sensory cues.

Crab megalops are in the dispersed (pelagic) larval phase directly preceding benthic settlement, and are known to exploit tidal cycles via mechanosensing of local shear strain rate fields to control net horizontal transport in an effort to find optimal settling habitat, the final selection of which is typically chemically-mediated (Forward et al. 2001). Thus, it is in the best interest of megalops to maintain depth at an optimal position in the water column (as modulated by tidal levels) until a favorable cue such as adult habitat substrate, aquatic vegetation, conspecific odors, estuarine water, odor of a related crab species, and/or prey odor presents itself and induces benthic settlement.

The ability to sense spatial gradients of fluid velocity and exploit that information is a fundamental ability *P. herbstii* megalops require in order to navigate the complex estuarine hydrodynamic environment in order to ultimately find suitable settling habitat. Hydrodynamics in much of Wassaw Sound are largely tidally driven (tidal range $\sim 2-3m$) with extended periods of unidirectional flow and low wave action under normal conditions (Smee et al. 2010). Moderate current speeds ($\sim 0.5\ m/s$) and relatively shallow depths ($\sim 10-15m$) ensure that persistent tidally-modulated vertical shear structure is ever present and ideal for Selective Tidal Stream Transport (STST) (e.g. Forward et al. 2001, Forward et al. 2003) and/or habitat portioning by competent pelagic crab larvae. Low freshwater input to the estuary ensures that

the most persistent *horizontal* shear structure is likely to be associated with vertical circulation along estuarine fronts separating water masses of differing hydrographic and biochemical properties (Largier 1993). Thus, for these eminently-settling, chemical cue-seeking *P. herbstii* megalops, depth-keeping and large-scale sweeping around persistent frontal flows provides the potential to sample various chemical cues being advected with the frontal circulation, possibly an energetically-favorable means of optimal site-selection for benthic settlement (e.g Forward et al. 2001).

The trajectories of *P. herbstii* megalops become more horizontal and more sinuous in the presence of persistent vertical shear layers. This conclusion is supported by a significant increase in turn frequency under both upwelling and downwelling conditions and a decrease in $VNGDR$ under both conditions (although to a slightly lower confidence level for downwelling) (Table 4.10). This behavior, coupled with an explicit lack of aggregation *at this scale* (i.e. no change in PRT) (Table 4.10), could indicate a spatial sweeping across a persistent frontal feature, possibly in a foraging or chemical cue seeking-context. The increase in relative swimming speed under upwelling conditions and the decrease under downwelling conditions is not readily explained (Table 4.10). Possible explanations include a direct, excited avoidance of upward vertical advection given that benthic settlement is eminent, or perhaps an excitement to sample upwelled waters for chemical-cues and thus information about potential settlement sites. Collectively, megalopal behavioral responses indicate that not only are they actively incorporating hydrodynamic information into real-time behavior, but they are also operating at a larger spatial scale than the finescale shear layer presented here. This seems logical considering that with high swimming velocities ($\sim 0.5 - 2\ cm/s$) and appendage-based setae they are likely to find themselves in high shear regions before actually sensing the shear signal, especially given spatiotemporally persistent gradients as in the present upwelling and downwelling shear layers.

Recall the brief discussion about $VNGDR$ histograms for *P. herbstii* (Figure 4.42). Behavioral phenomena similar to that seen for both calanoid copepods were observed, in which $VNGDR$ values were weighted toward higher and lower values for shear layer treatments. However, in contrast to the copepods whose $VNGDR$ histograms under control conditions were skewed towards lower values and not bimodal, the control $VNGDR$ histogram for *P. herbstii* was already somewhat bimodally distributed towards higher and lower values. This suggests that observed changes are likely the simple decreases seen statistically through the ANOVA. Therefore, in contrast to both calanoid copepod species, for *P. herbstii* megalops the presence of vertical shear layers likely simply causes a preferential trajectory alignment in the direction of changing shear strain rate (i.e. the gradient direction) and increased depth-keeping behavior (decreased $VNGDR$ values), possibly in an effort to obtain the maximum amount of information about the hydrodynamic environment by sweeping in the gradient direction (e.g. across a frontal feature) while resisting vertical advection. Megalops can resist large scale net vertical advection by traversing "U-shaped" or "C-shaped" trajectories by actively changing path kinematics (swimming speed and turn frequency), at least when gradients of vertical velocity are readily coherent and sensible. Thus, there is a significant tendency for the population to remain in a given portion of the water column when presented with a persistent vertical shear layer, at least in the absence of other sensory cues, such as strong horizontal tidal flows or ambient chemical cues. Knowing that typical estuarine systems feature prominent vertical circulation at discrete frontal features separating water masses of different hydrographic and/or biochemical properties, the megalopal behavior seen here is consistent with the idea of a cue hierarchy by which they sense an initial shear cue which induces increased sinuosity in path trajectories and horizontal sweeping across persistent frontal circulation possibly in hopes of picking up additional chemical cues in a foraging or settlement-substrate-seeking strategy.

Table 4.10: *Panopeus herbstii*: Summary of Behavioral Responses to Upwelling and Downwelling Jets. ↑ (↓) Indicates a Statistically Significant Increase (Decrease) between Pre-contact and Post-contact Values (Speed, Turn Frequency) or Control and Upwelling/Downwelling Values (VNGDR, PRT). = Indicates No Significant Change. * Indicates a Significant Interaction between Location and Layer Effects (i.e., Layer Trends Are Dependent on Upwelling Versus Downwelling). + Indicates which Value is Significantly Higher, Upwelling or Downwelling, due to Significant Layer Effects.

Flow Condition and Behavior Metrics	Significant Trends
Upwelling	
Speed	↑*
Turn Frequency	↑
$VNGDR$	↓
$NGDR$	=
PRT	=
Downwelling	
Speed	↑*
Turn Frequency	↑+
$VNGDR$	=*
$NGDR$	=
PRT	=

4.2.3.3 Neomysis americana

As the most abundant mysid in the Damariscotta River estuary on the coast of Maine, and most other western Atlantic estuaries, *N. americana* serves a crucial role in estuarine and coastal trophic transfer as an emerger (Schiariti et al. 2006, Sato and Jumars 2008). As emergers, these mysids live in close proximity to the surface of the sediment (the hyperbenthos) during the day, but emerge and migrate vertically towards the water surface at night (Whiteley 1948). However, a significant portion of the population is seen to remain at depth, suggesting that *N. americana* is not a true diel vertical migrator (Herman 1963) and that there is a higher frequency behavioral component of its vertical migration. This is most likely due to individual behavioral responses to changes in hydrographic variables (salinity, temperature, tidal flow, turbidity, etc.) on diel, tidal and lunar time scales (that shift seasonally), resulting in a continuous vertical interchange of the population throughout the night, or a vertical spreading of the population (Sato and Jumars 2008). Social behavior (swarming, schooling, shoaling, etc.) acting in concert with individual behavioral responses to discontinuities in the estuarine environment can produce considerable patchiness around persistent estuarine fronts (Mauchline 1980, Ritz 1994). The behavior observed here indicates the active use of cue hierarchies in habitat partitioning, foraging, mate-seeking, and other fundamental life processes.

The Damariscotta River estuary in Maine is a partially-mixed, glacially-carved, drowned river valley with relatively low freshwater discharge from Damariscotta Lake ($1 - 3m^3/s$). Tides are semidiurnal (range $\sim 3m$) and hydrography closely resemble that of nearby coastal waters. Relatively shallow depths ($10 - 15m$) and moderate to low current speeds (maximum $<0.3\ m/s$) ensure persistent shear structure consistent with classical estuarine hydrodynamics. That is, persistent vertical shear structure is likely generated by vertical gradients of tidally-driven, unidirectional horizontal flow while persistent *horizontal* shear structure is likely to be associated with vertical

circulation along estuarine fronts separating water masses of differing hydrographic and/or biochemical properties (Largier 1993, Sato and Jumars 2008). For *N. americana*, employing a cue hierarchy such that the presence of persistent shear strain rate fields can be exploited to locate changing hydrographic (salinity, density, temperature) and biochemical (dissolved oxygen and nutrients, prey) properties likely provides a distinct competitive advantage for habitat partitioning and optimization.

Field studies show that *N. americana* has been observed to aggregate around the Estuarine Transition Zone (ETZ), a region characterized by sharp gradients of salinity, temperature, and dissolved nutrients (Schiariti et al. 2006). At the ETZ, horizontal pressure gradients driven by buoyancy forces associated with temperature and salinity (i.e. density) gradients set up strong recirculation zones that act as retention cells for everything from dissolved nutrients to planktivores (Largier 1993, Winkler et al. 2003, Winkler et al. 2007). Thus, it is clear that *N. americana* actively incorporates sensory cues such as persistent shear structure on the individual level, which on the population level can produce dense aggregations, swarms, schools, and shoals (Clutter 1969, Ritz 1994, Buskey 2000). Mysid behavioral responses to persistent upwelling and downwelling shear layers observed here show not only direct aggregation around frontal flow features but also individual and population-level depth-keeping behavior similar to all other zooplankton species tested. Acting in concert, these effects have the potential to produce considerable patchiness both horizontally and vertically, with profound effects on the structure of estuarine ecosystems such as that in the Damariscotta River estuary.

In the presence of persistent vertical flow structure similar to those encountered *in situ*, *N. americana* decreased relative swimming speed pre-contact versus post-contact with both upwelling and downwelling shear layers, while leaving turn frequency unchanged under both conditions (Table 4.11). The combined effects here of a post-contact decrease in relative swimming speed and no change in turn frequency

resulted in a significant increase in PRT due to the presence of both upwelling and downwelling shear layers (Table 4.11), hence showing explicit shear-induced aggregation around persistent vertical flow structure. Thus, the presence of horizontal gradients of vertical velocity is sufficient here to cause population-scale aggregations of this estuarine emerger, which have been observed around frontal features of the estuarine transition zone in a South American estuary (Schiariti et al. [2006]). Interestingly, in contrast to all three previous species, *N. americana* is the only species tested whose overall trajectory shape was uninfluenced by the vertical shear layers as there was no significant change in $VNGDR$ for either upwelling and downwelling (Table 4.11), although $VNGDR$ did decrease (not significantly) on average for both flow conditions, as it did for the other estuarine species tested *P. herbstii* (Table 4.6).

Once again, individual and population-scale depth-keeping behavior are revealed by examining $VNGDR$ histograms (Figure 4.48), analagous to the previous discussion for both the tropical calanoid copepods. While it is true that statistically $VNGDR$ did not change for *N. americana* under either flow condition, there was a definite preferential spread of population $VNGDR$s to high ($\rightarrow 1$, straight vertical line trajectories) and low ($\rightarrow 0$, "U- or C-shaped" trajectories) values. This results in a bimodal distribution and suggests that significant portions of the population exhibit both depth-keeping behavior (low $VNGDR$ values) and active vertical advection (high $VNGDR$ values), similar to both copepod species. Thus, for *N. americana* not only do vertical shear layers cause explicit population-level aggregation (increased PRT), but they also cause mysids to resist large scale net vertical advection by traversing "U-shaped" or "C-shaped" trajectories (population spread to low $VNGDR$) by actively changing path kinematics (swimming speed and turn frequency), at least when gradients of vertical velocity are readily coherent and sensible. Thus, there is a significant tendency for the population to remain in a given portion of the water column when presented with a persistent vertical shear layer, at least in the absence of other

Table 4.11: *Neomysis americana*: Summary of Behavioral Responses to Upwelling and Downwelling Jets. ↑ (↓) Indicates a Statistically Significant Increase (Decrease) between Pre-contact and Post-contact Values (Speed, Turn Frequency) or Control and Upwelling/Downwelling Values (VNGDR, PRT). = Indicates No Significant Change. * Indicates a Significant Interaction between Location and Layer Effects (i.e., Layer Trends Are Dependent on Upwelling Versus Downwelling). + Indicates which Value is Significantly Higher, Upwelling or Downwelling, due to Significant Layer Effects.

Flow Condition and Behavior Metrics	Significant Trends
Upwelling	
Speed	↓+
Turn Frequency	=
$NGDR$	=
$VNGDR$	=
PRT	↑
Downwelling	
Speed	↓
Turn Frequency	=+
$NGDR$	=
$VNGDR$	=
PRT	↑

sensory cues. Knowing that typical estuarine systems feature prominent vertical circulation at discrete frontal features separating water masses of different hydrographic and/or biochemical properties, mysid behavioral responses seen here are consistent with the idea of a cue hierarchy by which they sense an initial shear cue which induces increased residence time in a persistent flow structure in hopes of gaining more useful information from coincident chemosensory cues and/or high-density resource (food, mate, oxygen, et.c) patches.

CHAPTER V

SUMMARY AND CONCLUSIONS

5.1 Summary

A recirculating flume apparatus with a laminar, planar free jet (the Bickley jet) was used to create finescale gradients of vertical fluid velocity (shear) in both upwelling and downwelling configurations for zooplankton behavioral assays. Planar particle image velocimetry (PIV) was used to fully resolve the velocity (and shear) fields allowing us to fine-tune experimental parameters to match fluid mechanical conditions commonly reported in the field literature. These behavioral assays were designed in an effort to determine the potential for persistent *horizontal* shear associated with vertical flow structure to produce population scale aggregations, or patchiness.

Zooplankton behavioral assays with two tropical calanoid copepods, *Acartia negligens* and *Clausocalanus furcatus*, an estuarine mysid, *Neomysis americana*, and the larvae of an estuarine mud crab, *Panopeus herbstii*, were conducted in control (stagnant), upwelling, and downwelling flow configurations. Results from behavioral analyses reveal species-specific threshold shear strain rates that trigger individual behavioral responses for all zooplankton species tested. Furthermore, results show statistically significant changes in behavior (relative swimming speed and/or turn frequency and/or heading) for all species tested in response to the coherent shear structure. These results show that changes in path kinematics can induce depth-keeping behavior and can significantly increase proportional residence time (PRT = percent time spent in the jet structure). On a population scale, the observed behavior can lead to dense aggregations around persistent flow features, which is consistent with numerous field studies. It is likely that gradients of vertical velocity may act as

an initial mechanosensory cue for zooplankters to optimize habitat partitioning and locate high-density food, nutrient, and mate patches.

5.2 Conclusions

When interpreting behavioral responses to *persistent* shear structure with finite and static spatiotemporal characteristics, it is important to consider all of the following when assessing the full ecological implications of the observed behaviors: zooplankton morphology and energetics, ecological and hydrodynamic realities *in situ*, stage-dependent life goals, and the presence or absence of other sensory cues.

The results of this study indicate that shear-triggered depth-keeping behavior and aggregation around persistent vertical flow structures by individual zooplankters, at a variety of spatiotemporal scales and for a variety of ecological reasons, is likely a ubiquitous behavior among the zooplankton and a possible mechanism that acts to produce considerable patchiness both vertically (by depth-keeping behavior) and horizontally (by aggregation around frontal features) in estuarine and coastal marine ecosystems. It is possible that gradients of vertical velocity may act as an initial mechanosensory cue for zooplankters to optimize habitat partitioning and locate high-density food, nutrient, and mate patches.

Quantifying basic biophysical mechanisms that generate patchy productivity in coastal marine ecosystems is fundamental to developing sustainable tools for fishery conservation. The simplicity of well-designed laboratory studies coupled with *in situ* field data and quantitative tools from experimental fluid mechanics allows us to confidently extrapolate our laboratory findings to the ecosystem-level.

5.3 Future Directions

A large majority of ecologically-relevant vertical flows in coastal marine ecosystems coincide with sharp horizontal gradients in watermass biochemical properties, as in

frontal, Langmuir, and classical upwelling systems. It is possible that gradients of vertical velocity act as an initial mechanosensory cue for a foraging zooplankter to locate high-density food, nutrient, and mate patches coincident with persistent vertical flow structure. Thus, a valuable extrapolation of the present study would be to evaluate the individual and interactive effects of various other physical (temperature, salinity, flow steadiness) and biochemical (organism size, hunger level, phytoplankton patches) factors on zooplankton behavior as in previous experiments from a horizontal flume (Woodson et al. 2005). This information would provide a valuable basis for building individual-based ecosystem models (IBM) to evaluate the potential of species-specific behavioral responses to produce patchniess via population scale aggregations. Individual behavioral responses to sensory cues on the finescale ($< 1\ m$) drive ecological processes in the coastal ocean on the submesoscale ($< 1\ km$). Extrapolating from individual behavior to population scale phenomena helps shed light on the factors regulating the spatiotemporal distribution of marine productivity.

Bibliography

H.U. Abello, S.M. Shellito, L.H. Taylor, and P.A. Jumars. Light-cued emergence and re-entry events in a strongly tidal estaury. *Estuaries*, 28:487–499, 2005.

A. L. Alldredge, T. J. Cowles, S. MacIntyre, J. E. B. Rines, et al. Occurrence and mechanisms of formation of a dramatic thin layer of marine snow in a shallow pacific fjord. *Marine Ecology Progress Series*, 233:1–12, 2002.

D.M. Allen. Maintenance of the mysid crustacean *Neomysis americana* (smith) in closed synthetic seawater systems. *Reprint Ser. 4, Lehigh University, Wetlands Institute*, 1975.

M. Alnahhal and Th. Panidis. The effect of sidewalls on rectangular jets. *Experimental Thermal and Fluid Science*, 33:838–851, 2009.

E. Bagøien and T. Kiørboe. Blind dating mate finding in planktonic copepod. iii. hydromechanical communication in *Acartia tonsa*. *Marine Ecology Progress Series*, 300:129–133, 2005a.

E. Bagøien and T. Kiørboe. Blind dating mate finding in planktonic copepods. i. tracking the pheromone trail of *Centropages typicus*. *Marine Ecology Progress Series*, 300:105–115, 2005b.

K. J. Benoit-Bird, T. J. Cowles, and C. E. Wingard. Edge gradients provide evidence of ecological interactions in planktonic thin layers. *Limnol Oceanogr*, 54:1382–1392, 2009.

K. J. Benoit-Bird, M. A. Moline, C. M. Waluk, and I. C. Robbins. Integrated measurements of acoustical and optical thin layers i: Vertical scales of association. *Continental Shelf Research*, 30:17–28, 2010.

W. G. Bickley. The plane jet. *Philosophical Magazine*, 23:727–731, 1937.

D. A. Birch, W. R. Young, and P. J. S. Franks. Thin layers of plankton: Formation by shear and death by diffusion. *Deep-Sea Research Part I*, 55:277–295, 2008.

A. B. Bochdansky and S. M. Bollens. Relevant Scales in Zooplankton Ecology: Distribution, Feeding, and Reproduction of the Copepod *Acartia Hudsonica* in Response to Thin Layers of the Diatom *Skeletonema Costatum*. *Limnology and Oceanography*, 49:626–636, 2004.

S. M. Bollens, B. W. Frost, and J. R. Cordell. Chemical, mechanical and visual cues in the vertical migration behavior of the marine planktonic copepod *Acartia hudsonica*. *Journal of Plankton Research*, 16:555–564, 1994.

N. D. Boroditch and F. K. Havlena. The biology of mysids acclimated in the reservoirs of the volga river. *Hydrobiologia*, 42:527–539, 1973.

E. J. Buskey. Swimming pattern as an indicator of the roles of copepod sensory systems in the recognition of food. *Marine Biology*, 79:165–175, 1984.

E.J. Buskey. Role of vision in the aggregative behavior of the planktonic mysid *Mysidium columbiae*. *Marine Biology*, 137:257–265, 2000.

O. M. Cheriton, M. A. McManus, D. V. Holliday, C. F. Greenlaw, P. L. Donaghay, and T. J. Cowles. Effects of mesoscale physical processes on thin zooplankton layers at four sites along the west coast of the u.s. *Estuaries and Coasts*, 30:575–590, 2007.

O. M. Cheriton, M. A. McManus, M. T. Stacey, and J. V. Steinbuck. Physical and biological controls on the maintenance and dissipation of a thin phytoplankton layer. *Marine Ecology Progress Series*, 378:55–69, 2009.

F. S. Chia, J. Buckland-Nicks, and C. M. Young. Locomotion of marine invertebrate larvae: A review. *Canadian Journal of Zoology*, 62:1205–1222, 1984.

T. W. Clay, S. M. Bollens, A. B. Bochdansky, and T. R. Ignoffo. The effects of thin layers on the vertical distribution of larval pacific herring, *Clupea pallasi*. *Journal of Experimental Marine Biology and Ecology*, 305:171–189, 2004.

R.I. Clutter. The microdistribution and social behavior of some pelagic shrimps. *Journal of Experimental Marine Biology and Ecology*, 3:125–155, 1969.

E. A. Cowen and S. G. Monismith. A hybrid digital particle tracking velocimetry technique. *Experiments in Fluids*, 22:199–211, 1997.

T. Cowles, R. A. Desiderio, and M. E. Carr. Small-scale planktonic structure: persistence and trophic consequences. *Oceanography*, 11:4–9, 1998.

T. J. Cowles, R. A. Desiderio, and S. Neuer. *In situ* characterization of phytoplankton from vertical profiles of fluorescence emission spectra. *Mar. Biol.*, 115:217–222, 1993.

T. W. Cronin and Jr. R. B. Forward. Vertical migration cycles of crab larvae and their role in larval dispersal. *Bulletin of Marine Science*, 39:192–201, 1986.

Y. Crouau. Primary stages in the sensory mechanism of the setulate sensilla, external mechanoreceptors of a cavernicolous mysidacea. *Biology of Cells*, 44:45–56, 1982.

Y. Crouau. Antenunular mechanosensitivity in a cavernicolous mysid crustacean. *Journal of Crustacean Biology*, 6:158–165, 1986.

Andrade EN da C. The velocity distribution in a liquid-into-liquid jet. part 2: The plane jet. *Proc Phys Soc*, 51:784–793, 1939.

M. H. Daro. Migratory and grazing behavior of copepods and vertical distributions of phytoplankton. *Bull Mar Sci*, 43:710–729, 1988.

L. P. Dasi. *The small-scale structure of passive scalar mixing in turbulent boundary layers*. PhD thesis, Georgia Institute of Technology, Atlanta, GA, 2004.

M. M. Dekshenieks, P. L. Donaghay, J. M. Sullivan, J. E. B. Rines, T. R. Osborn, and M. S. Twardowski. Temporal and spatial occurrence of thin phytoplankton layers in relation to physical processes. *Marine Ecology Progress Series*, 223:61–71, 2001.

R. C. Deo, J. Mi, and G. J. Nathan. The influence of nozzle aspect ratio on plane jets. *Experimental Thermal and Fluid Science*, 31:825–838, 2007a.

R. C. Deo, J. Mi, and G. J. Nathan. The influence of nozzle-exit geometric profile on statistical properties of a turbulent plane jet. *Experimental Thermal and Fluid Science*, 32:545–559, 2007b.

J. B. Derenbach, H. Astheimer, H. P. Hansen, and H. Leach. Vertical microscale distribution of phytoplankton in relation to the thermocline. *Marine Ecology Progress Series*, 1:187–193, 1979.

P. G. Drazin and W. H. Reid. *Hydrodynamic stability*. Cambridge University Press, United Kingdom, 1981.

W. M. Durham, J. O. Kessler, and R. Stocker. Disruption of vertical motility by shear triggers formation of thin phytoplankton layers. *Science*, 323:1067–1070, 2009.

D. B. Eggleston, D. A. Armstrong, W. E. Elis, and W. S. Patton. Estuarine fronts as conduits for larval transport: hydrodynamics and spatial distribution of dungeness crab postlarvae. *Marine Ecology Progress Series*, 164:73–82, 1998.

J. T. Enright and W. M. Hamner. Vertical diurnal migration and endogenous rhythmicity. *Science*, 157:937–941, 1967.

D. M. Fields. Orientation affects the sensitivity of *Acartia tonsa* to fluid mechanical signals. *Marine Biology*, 157:505–514, 2010.

D. M. Fields and J. Yen. The escape behavior of marine copepods in response to a quantifiable fluid mechanical disturbance. *Journal of Plankton Research*, 19: 1289–1304, 1997a.

D. M. Fields and J. Yen. Implications of the feeding current structure of *Euchaeta rimana*, a carnivorous pelagic copepod, on the spatial orientation of their prey. *Journal of Plankton Research*, 19:79–95, 1997b.

D. M. Fields, D. S. Shaeffer, and M. J. Weissburg. Mechanical and neural responses from the mechanosensory hairs on the antennule of *Gaussia princeps*. *Marine Ecology Progress Series*, 227:173–186, 2002.

R. B. Forward. Negative phototaxis in crustacean larvae: Possible functional significance. *J Exp. Mar. Bio. and Eco.*, 16:11–17, 1974.

R. B. Forward. Behavioural responses of crustacean larvae to rates of salinity change. *Biological Bulletin*, 176:229–238, 1989a.

R. B. Forward. Depth regulation of larval marine decapod crustaceans: Test of an hypothesis. *Marine Biology*, 176:229–238, 1989b.

R. B. Forward, R. A. Tankersley, and D. Rittschof. Cues for metamorphosis of brachyuran crabs: An overview. *Amer Zool*, 41:1108–1122, 2001.

R. B. Forward, R. A. Tankersley, and J. M. Welch. Selective tidal-stream transport of the blue crab *Callinectes sapidus*: an overview. *Bulletin of Marine Science*, 72: 347–365, 2003.

R. B. Forward, N. B. Reyns, H. Diaz, J. H. Cohen, and D. B. Eggleston. Endogenous swimming rhythms of juvenile blue crabs, *Callinectes sapidus*, as related to horizontal transport. *Journal of Experimental Marine Biology and Ecology*, 229:63–76, 2004.

P. J. S. Franks. Sink or swim: accumulation of biomass at fronts. *Marine Ecology Progress Series*, 82:1–12, 1992.

P. J. S. Franks. Thin layers of phytoplankton: a model of formation by near-inertial wave shear. *Deep Sea Res I*, 42:75–91, 1995.

S. M. Gallager, H. Yamazaki, and C. S. Davis. Contributions of fine-scale vertical structure and swimming behavior to formation of plankton layers on georges bank. *Marine Ecology Progress Series*, 267:27–43, 2004.

A. Genin, J. S. Jaffe, R. Reef, C. Richter, and P. J. S. Franks. Swimming against the flow: A mechanism of zooplankton aggregation. *Science*, 308:860–862, 2005.

L. Gui and S. T. Wereley. A correlation-based continuous window-shift technique to reduce the peak-locking effect in digital pic image evaluation. *Exp Fluids*, 32: 506–517, 2002.

W. Harder. Reactions of plankton organisms to water stratification. *Limnol Oceanogr*, 13:156–168, 1968.

L. R. Haury, D. E. Kenyon, and Brooks. Experimental evaluation of the avoidance reaction of *Calanus finmarchicus*. *J Plankton Res*, 2:187–202, 1980.

S. S. Herman. Spectral sensitivity and phototaxis in the opposum shrimp *Neomysis americana*. *Biological Bulletin*, 123:562–570, 1962.

S. S. Herman. Vertical migration of the opposum shrimp *Neomysis americana*. *Limnology and Oceanography*, 8:228–238, 1963.

A. E. Hill. A mechanism for horizontal zooplankton transport by vertical migration in tidal currents. *Marine Biology*, 111:485–492, 1991a.

A. E. Hill. Vertical migration in tidal currents. *Marine Ecology Progress Series*, 75: 39–54, 1991b.

R. C. Hobbs and L. W. Botsford. Diel vertical migration and timing of metamorphosis of larvae of the dungeness crab *Cancer magister*.

D. V. Holliday, R. E. Piper, C. F. Greenlaw, and J. K. Dawson. Acoustical sensing of small-scale vertical structures in zooplankton assemblages. *Limnology and Oceanography*, 11:18–23, 1998.

D. V. Holliday, P. L. Donaghay, C. F. Greenlaw, D. E. McGehee, M. M. McManus, J. M. Sullivan, and J. L. Miksis. Advances in defining fine- and micro-scale pattern in marine plankton. *Aquatic Living Resources*, 16:131–136, 2003.

R. Holzman and P. C. Wainwright. How to surprise a copepod: Strike kinematics reduce hydrodynamic disturbance and increase stealth of suction-feeding fish. *Limnol Oceanogr*, 54:2201–2212, 2009.

R. Holzman, M.A. Reidenbach, S.G. Monismith, J. R. Koseff, and A. Genin. Near-bottom depletion of zooplankton over a coral reef ii: Relationships with zooplankton swimming ability. *Coral Reefs*, 24:87–94, 2005.

L. T. Houser and C. E. Epifanio. Impacts of biochemical cues on horizontal swimming behavior of individual crab larvae. *Marine and Freshwater Behaviour and Physiology*, 42:249–264, 2009.

H. J. Hussein. Evidence of local axisymmetry in the small scales of a turbulent planar jet. *Phys Fluids*, 6:2058–2070, 1994.

G. E. Hutchison. The paradox of the plankton. *Am Nat*, 95:137–145, 1961.

T. R. Ignoffo, S. M. Bollens, and A. B. Bochdansky. The effects of thin layers on the vertical distribution of the rotifer, *Brachionus plicatilis*. *Journal of Experimental Marine Biology and Ecology*, 316:167–181, 2005.

J. S. Jaffe, P. J. S. Franks, and A. W. Leising. Simultaneous imaging of phytoplankton and zooplankton distributions. *Oceanography*, 11:24–29, 1998.

G. S. Jamieson and A. C. Phillips. Occurrence of *Cancer spp.* crab megalopae off the west coast of vancouver island, british columbia. *US Fishery Bulletin*, 86:525–542, 1988.

H. Jiang, T. R. Osborn, and C. Meneveau. Chemoreception and the deformation of the active space in freely swimming copepods: A numerical study. *J Plankton Res*, 24:495–510, 2002.

T. Kiørboe. How zooplankton feed: mechanisms, traits and trade-offs. *Biological Reviews*, 86:311–339, 2011.

T. Kiørboe and A. W. Visser. Predator and prey perception in copepods due to hydromechanical signals. *Marine Ecology Progress Series*, 179:81–95, 1999.

T. Kiørboe, E. Saiz, and A. W. Visser. Hydrodynamic signal perception in the copepod *Acartia tonsa*. *Marine Ecology Progress Series*, 179:97–111, 1999.

K. L. Kirk and J. J. Gilbert. Escape behaviour of *Polyathra* in response to artificial flow stimuli. *Bull Mar Sci*, 53:96–105, 1988.

E. S. Kornienko, O. M. Korn, and S. D. Kashenko. Comparative morphology of larvae of coastal crabs (crustacea: Decapoda: Varunidae). *Russian Journal of Marine Biology*, 34:77–93, 2008.

P. K. Kundu and I. M. Cohen. *Fluid Mechanics*. Elsevier Academic Press, 2004.

J. Largier. Estuarine fronts: How important are they? *Estuaries*, 16:1–11, 1993.

D. Lecchini, S. C. Mills, C. Brie, R. Maurin, and B. Banaigs. Ecological determinants and sensory mechanisms in habitat selection of crustacean postlarvae. *Behavioral Ecology*, 17:599–607, 2010.

A. W. Leising. Copepod foraging in patchy habitats and thin layers using a 2-d individual-based model. *Marine Ecology Progress Series*, 216:167–179, 2001.

A. W. Leising and P. J. S. Franks. Copepod vertical distribution within a spatially variable food source: A simple foraging-strategy model. *J Plankton Res*, 22:999–1024, 2000.

A. W. Leising and P. J. S. Franks. Does *Acartia clausi* (copepoda: Calanoida) use an area-restricted search foraging strategy to find food? *Hydrobiologia*, 480:193–207, 2002.

A. W. Leising, J. J. Pierson, S. Cary, and B. W. Frost. Copepod foraging and predation risk within the surface layer during night-time feeding forays. *Journal of Plankton Research*, 27:987–1001, 2005.

D. L. Mackas, H. Sefton, C. B. Miller, and A. Raich. Vertical habitat partitioning by large calanoid copepods in the oceanic sub-arctic pacific during spring. *Progress in Oceanography*, 32:259–294, 1993.

E. Malkiel, J. Sheng, J. Katz, and J. R. Strickler. The three-dimensional flow field generated by a feeding calanoid copepod measured using digital holography. *The Journal of Experimental Biology*, 206:3657–3666, 2003.

J. Mauchline. *The Biology of Mysid and Euphausiids*, volume 18 of *Advances in Marine Biology*. 1980.

J. Mauchline. *The Biology of Calanoid Copepods*. San Diego: Elsevier Academic Press, 1998.

P.A. McLaughlin. *The Comparative Morphology of Recent Crustacea*. W. H. Freeman and Co. San Francisco, 1980.

M. A. McManus, A. L. Alldredge, A. H. Barnard, E. Boss, et al. Characteristics, distribution and persistence of thin layers over a 48 hour period. *Marine Ecology Progress Series*, 261:1–19, 2003.

R. D. Mehta and P. Bradshaw. Design rules for small low speed wind tunnels. *aeronautical Journal*, 83:443–449, 1979.

S. A. Mileikovsky. Speed of active movement of pelagic larvae of marine bottom invertebrates and their ability to regulate their vertical position. *Marine Biology*, 23:11–17, 1973.

M. A. Moline, K. J. Benoit-Bird, I. C. Robbins, M. Schroth-Miller, C. M. Waluk, and B. Zelenke. Integrated measurements of acoustical and optical thin layers ii: Horizontal length scales. *Continental Shelf Research*, 30:29–38, 2010.

S. G. Monismith, A. Genin, M. A. Reidenbach, G. Yahel, and J. R. Koseff. Thermally driven exhanges between a coral reef and the adjoining ocean. *Journal of Physical Oceanography*, 36:1332–1347, 2005.

R. Motro, I. Ayalon, and A. Genin. Near-bottom depletion of zooplankton over coral reefs iii: Vertical gradients of predation pressure. *Coral Reefs*, 24:95–98, 2005.

M. M. Mullin and E. R. Brooks. Some consequences of distributional heterogeneity of phytoplankton and zooplankton. *Limnol Oceanogr*, 21:784–796, 1976.

H. T. Odum and E. P. Odum. Trophic structure and productivity of a windward coral reef community on eniwetok atoll. *Ecol. Mono.*, 25:291–320, 1955.

C. B. Officer. *Physical Oceanography of Estuaries (and Associated Coastal Waters)*. John Wiley and Sons, 1976.

E. J. Olmi. Vertical migration of blue crab *Callinectes sapidus* megalopae: Implications for transport in estuaries. *Marine Ecology Progress Series*, 113:39–54, 1994.

F. S. Ott and R. B. forward Jr. The effect of temperature on phototaxis and geotaxis by larvae of the crab *Rhithropanopeus harrisii* (gould). *Journal of Experimental Marine Biology*, 23:97–107, 1976.

G. A. Paffenhöfer. On the relation of structure, perception and activity in marine planktonic copepods. *Journal of Marine Systems*, 15:457–473, 1998.

T. Peacock, E. Bradley, J. Hertzberg, and Y. Lee. Forcing a planar jet flow using mems. *Experiments in Fluids*, 37:22–28, 2004.

D.S. Pezzack and S. Corey. The life history and distribution of *Neomysis americana* (smith), crustacea, mysidacea. *Canadian Journal of Zoology*, 57:785–793, 1979.

J. J. Pierson, B. W. Frost, D. Thoreson, A. W. Leising, J. R. Postel, and M. Nuwer. Trapping migrating zooplankton. *Limnol Oceanogr: Methods*, 7:334–346, 2009.

S. A. Poulet and G. Ouellet. The role of amino acids in the chemosensory swarming and feeding of marine copepods. *J Plankton Res*, 4:341–361, 1982.

H. Queiroga. Vertical migration and selective tidal stream transport in the megalopa of the crab *Carcinus maenas*. *Hydrobiologia*, 375/376:137–149, 1998.

H. Queiroga and J. Blanton. Interactions between behaviour and physical forcing in the control of horizontal transport of decapod crustacean larvae. *Advances in Marine Biology*, 47:107–214, 2005.

M. Raffel, C. Wilbert, and J. Kompenhans. *Particle Image Velocimetry: A Practical Guide*. Berlin: Springer, 1998.

M. A. Reidbenbach, S. G. Monismith, J. R. Koseff, G. Yahel, and A. Genin. Boundary layer turbulence and flow structure over a fringing coral reef. *Limnology and Oceanography*, 51:1956–1968, 2006.

A. Revuelta, A. L. Sanchez, and A. Linan. The virtual origin as a first-order correction for the far-field description of laminar jets. *Phys Fluids*, 14:1821–1824, 2002.

A. L. Rice. Observations on the effects of changes of hydrostatic pressure on the behavior of some marine animals. *Journal of the Marine Biological Association of the United Kingdom*, 44:163–175, 1964.

D.A. Ritz. Social aggregation in pelagic invertebrates. *Advances in Marine Biology*, 30:155–216, 1994.

S.D. Roast, J. Widdows, and M.B. Jones. The position maintenance behavior of *Neomysis integer* (peracarida: Mysidacea) in response to current velocity, substratum, and salinity. *Journal of Experimental Marine Biology and Ecology*, 220:25–45, 1998.

L.G. Rudstam, K. Danielsson, S. Hansson, and S. Johansson. Diel vertical migration and feeding patterns of *Mysis mixta* (crustacea, mysidacea) in the baltic sea. *Marine Biology*, 101:43–52, 1989.

J. P. Ryan, M. A. McManus, J. D. Paduan, and F. P. Chavez. Phytoplankton thin layers caused by shear in frontal zones of a coastal upwelling system. *Mar Ecol Prog Ser*, 354:21–34, 2008.

W. Santana, G. Pohle, and F. Marques. Larval development of *Apiomithrax violaceus* (a. milne edwards, 1868) (decapoda: Brachyura: Majoidea: Pisidae) reared in laboratory conditions, and a review of larval characters of pisidae. *Journal of Natural History*, 38:1773–1797, 2004.

H. Sato. The stability and transition of a two-dimensional jet. *J Fluid Mech*, 7:53–80, 1960.

H. Sato and F. Sakao. An experimental investigation of the instability of a two-dimensional jet at low reynolds numbers. *J Fluid Mech*, 20:337–352, 1964.

M. Sato and P.A. Jumars. Seasonal and vertical variations in emergence behavior of *Neomysis americana*. *Limnology and Oceanography*, 53:1665–1677, 2008.

A. Schiariti, A.D. Berasategui, D.A. Giberto, R.A. Guerrero, E.M. Acha, and H.W. Mianzan. Living in the front: *Neomysis americana* (mysidacea) in the rio de la plata estuary, argentina-uruguay. *Marine Biology*, 149:483–489, 2006.

H. Schlichting. Laminare strahlausbreitung. *ZAMM*, xiii:260–263, 1933.

A. L. Shanks. Vertical migration and cross-shelf dispersal of larval *Cancer spp.* and *Randallia ornata* (crustacea:brachyura) off the coast of southern california. *Marine Biology*, 92:189–199, 1986.

D. L. Smee, M. C. Ferner, and M. J. Weissburg. Hydrodynamic sensory stressors produce nonlinear predation patterns. *Ecology*, 91:1391–1400, 2010.

M. T. Stacey, M. A. McManus, and J. V. Steinbuck. Convergences and divergences and thin layer formation and maintenance. *Limnol Oceanogr*, 52:1523–1532, 2007.

J. V. Steinbuck, M. T. Stacey, M. A. McManus, O. M. Cheriton, and J. P. Ryan. Observations of turbulent mixing in a phytoplankton thin layer: Implications for formation, maintenance, and breakdown. *Limnol Oceanogr*, 54:1353–1368, 2009.

J. R. Strickler and G. Balazsi. Planktonic copepods reacting selectively to hydrodynamic disturbances. *Phil Trans R Soc*, 362:1947–1958, 2007.

S. D. Sulkin. The influence of light in the depth regulation of crab larvae. *Biol Bull*, 148:33–343, 1975.

S. D. Sulkin. Behavioral basis of depth regulation in the larvae of brachyuran crabs. *Marine Ecology Progress Series*, 15:181–205, 1984.

S. D. Sulkin, I. Phillips, and W. van Heukelem. On the locomotory rhythm of brachyuran crab larvae and its significance in vertical migration. *Marine Ecology Progress Series*, 1:331–335, 1979.

S. D. Sulkin, W. van Heukelem, P. Kelly, and L. van Heukelem. The behavioral basis of larval recruitment in the crab *Callinectes sapidus* rathbun: a laboratory investigation of ontogenetic changes in geotaxis and barokinesis. *Biol Bull*, 159: 402–417, 1980.

J. M. Sullivan et al. Layered organization in the coastal ocean: An introduction to planktonic thin layers and the loco project. *Continental Shelf Research*, 30:1–6, 2010.

M. M. Sutor, T. J. Cowles, W. T. Peterson, and S. D. Pierce. Acoustic observations of finescale zooplankton distributions in the oregon upwelling region. *Deep Sea Research*, 52:109–121, 2005.

R. A. Tankersley, L. M. McKelvey, and R. B. Forward Jr. Responses of estuarine crab megalopae to pressure, salinity and light: Implications for flood-tide transport. *Marine Biology*, 122:391–400, 1995.

T. Tatsumi and T. Kakutani. The stability of a two-dimensional laminar jet. *J Fluid Mech*, 4:261–75, 1958.

N. Tinbergen, M. Impekoven, and D. Franck. An experiment on spacing-out as a defense against predation. *Behavior*, 28:307–321, 1967.

P. Tiselius. Behavior of *Acartia tonsa* in patchy food environments. *Limnol Oceanogr*, 37:1640–1651, 1992.

P. Tiselius and P. R. Jonsson. Foraging behavior of six calanoid copepods: observations and hydrodynamic analysis. *MEPS*, 168:119–126, 1990.

J. Titelman. Swimming and escape behavior of copepod nauplii: implications for predator-prey interactions among copepods. *Marine Ecology Progress Series*, 213: 203–213, 2001.

J. Titelman and T. Kiørboe. Motility of copepods nauplii and implications for food encounter. *Marine Ecology Progress Series*, 247:123–135, 2003.

J. H. Tumlinson, W. J. Lewis, and L. E. M. Vet. How parasitic wasps find their hosts. *Sci Am*, 268:100–106, 1993.

J. L. Turner and W. Heubach. Ecological studies of the sacremento-san joaquin estuary. distribution and concentration of *Neomysis awatschensis* in the sacremento-san joaquin delta. *California Fish and Game*, 133:105–112, 1966.

L. Velo-Suarez, L. Fernand, P. Gentien, and B. Reguera. Hydrodynamic conditions associated with the formation, maintenance and dissipation of a phytoplankton thin layer in a coastal upwelling system. *Continental Shelf Research*, 30:193–202, 2010.

L. E. M. Vet. From chemical to population ecology: Infochemical use in an evolutionary context. *J Chem Ecol*, 25:31–49, 1999.

M. Viitasalo, T. Kiørboe, J. Flinkman, L. W. Pedersen, and A. W. Visser. Predation vulnerability of planktonic copepods: consequences of predator foraging strategies and prey sensory abilities. *Marine Ecology Progress Series*, 175:129–142, 1998.

J. M. Welch, R. B. Forward Jr., and P. A. Howd. Behavioural responses of blue crab *Callinectes sapidus* larvae to turbulence: implications for selective tidal stream transport. *MEPS*, 179:135–143, 1999.

S. T. Wereley and C. D. Meinhart. Second-order accurate particle image velocimetry. *Exp Fluids*, 31:258–268, 2001.

G. C. Whiteley. The distribution of larger planktonic crustacea on georges bank. *Ecological Monographs*, 1948.

A.B. Williams, T.E. Bowman, and D.M. Damkaer. Distribution, variation, and supplemental description of the opossum shrimp *Neomysis americana* (crustacea: Mysidacea). *Fishery Bulletin*, 1973.

G. Winkler, J.J. Dodson andN. Bertrand, D. Thivierge, and W.F. Vincent. Trophic coupling across the st. lawrence river estuarine transition zone. *Marine Ecology Progress Series*, 2003.

G. Winkler, C. Martineau, J.J. Dodson, W.F. Vincent, and L.E. Johnson. Trophic dynamics of two sympatric mysid species in estuarine transition zone. *Marine Ecology Progress Series*, 2007.

C. B. Woodson. *Thin layers: Physical and chemical cues contributing to observed copepod aggregations*. PhD thesis, Georgia Institute of Technology, Atlanta, GA, 2005.

C. B. Woodson, D. R. Webster, M. J. Weissburg, and J. Yen. Response of copepods to physical gradients associated with structure in the ocean. *Limnology and Oceanography*, 2005.

C. B. Woodson, D. R. Webster, M. J. Weissburg, and J. Yen. Cue hierarchy and foraging in calanoid copepods: ecological implications of oceanographic structure. *Marine Ecology Progress Series*, 2007.

G. Yahel, A. F. Post, K. Fabricius, D. Marie, D. Vaulot, and A. Genin. Phytoplankton distribution and grazing near coral reefs. *Limnology and Oceanography*, 1998.

R. Yahel, G. Yahel, T. Berman, J. S. Jaffe, and A. Genin. Diel pattern with abrupt crepuscular changes of zooplankton over a coral reef. *Limnol. Ocean.*, 2005a.

R. Yahel, G. Yahel, and A. Genin. Near-bottom depletion of zooplankton over coral reefs i: Diurnal dynamics and size distribution. *Coral Reefs*, 2005b.

J. Yen and D. M. Fields. Escape responses of *Acartia hudsonica* (copepoda) nauplii from the flow field of *Temora longicornis* (copepoda). *Archive Hydrobiol*, 36:123–134, 1992.

J. Yen, P. H. Lenz, D. V. Gassie, and D. K. Hartline. Mechanoreception in marine copepods: electrophysiological studies on the first antennae. *Journal of Plankton Research*, 1992.

J. Yen, M. J. Weissburg, and M. H. Doall. The fluid physics of signal perception by mate-tracking copepods. *Philosophical Transactions of the Royal Society of London*, 1998.

C. M. Young. *Ecology of Marine Invertebrate Larvae*, chapter Behaviour and locomotion during the dispersal phase of larval life, pages 249–277. CRC Press, Boca Raton, FL, 1995.

G. Zagursky and R.J. Feller. Macrophyte detritus in the winter diet of the estuarine mysid *Neomysis americana*. *Estuaries*, 1985.

J. H. Zar. *Biostatistical Analysis*. Upper Saddle Hall, NJ: Prentice Hall, 4 edition, 1999.